UNIVERSITY OF CALIFORNIA

IRVINE

A Search for Advanced Fields in Electromagnetic Radiation

A dissertation submitted in partial satisfaction of the requirements for the degree Doctor of Philosophy in Physics

by

Jeffrey David Schmidt

Committee in charge:

Professor Riley Newman, Chair

Professor Frederick Reines

Professor Jonas Schultz

1980

The dissertation of Jeffrey David Schmidt is approved, and is acceptable in quality and form for publication on microfilm:

Committee Chair

University of California, Irvine

1980

DEDICATION

To my parents.

CONTENTS

List of Tables viii

List of Figures ix

Acknowledgments xii

Vita xiv

Abstract xv

Chapter 1. Introduction

1.1 A Hierarchy of Paradigms 1

1.2 The Retarded and Advanced Solutions of Maxwell's Equations 2

1.3 A Role for the Absorber 5

1.4 The Cosmological Connection 6

Chapter 2. Discussion of the Absorber Theory of Radiation

2.1 Introduction 11

2.2 Assumptions of Absorber Theory 12

2.3 Complete Absorption, A Self-consistent Pure Retarded Solution 12

2.4 Spherical Waves 17

2.5 Complete Absorption, A Self-consistent Pure Advanced Solution 18

2.6 Incomplete Absorption, Self-consistent Solutions 22

2.7 Experiment 30

2.8 The Necessity of a Deliberate Search . . 35

Chapter 3. Advanced Effects: A Logical Paradox? 37

Chapter 4. Design of the Experiment 52

Chapter 5. The Apparatus and its Operation

5.1 Elements of the Block Diagram 59

5.2 Phantom Structure in the Advanced Time Region Noise 63

5.3 Transmitter Triggering and Reception. . . 64

5.4 Linearity of the System 68

5.5 The Computer Controlled Sequence 69

5.6 Microwave Lenses 72

Chapter 6. Data Collection and Results of the Experiment

6.1 Data Collection 80

6.2 Treatment of the Data 82

6.3 Results of the Experiment 86

6.4 Structure of the Log Graphs 95

Chapter 7. The Noise Calculation

7.1 Introduction 99

7.2 The Theoretical Noise Temperature 99

7.3 Antenna Noise 103

7.4 Receiving Line Noise 104

7.5 Mixer-Preamplifier Noise 105

7.6 Amplifier Noise 106

7.7 The Observed Noise Temperature 107

Chapter 8. Phase Drift Due to Variations in Temperature

8.1 Introduction 112

8.2 Retarded and Advanced Phase Drifts . . . 113

8.3 Losses in Integrated Retarded and Advanced Power Due to Phase Drifts . . . 121

8.4 Consideration of the Phase Data and Determination of the Optimal Choice of Data to Integrate 125

8.5 The Extraction of Phase Information from the Data 130

Chapter 9. The Atmospheric Trajectory and Attenuation of the Microwave Signal

9.1 The Trajectory and Atmospheric Attenuation of a Microwave Signal Projected from a Mountain Top 133

9.2 The Index of Refraction as a Function of Position in the Atmosphere 134

9.3 The Trajectory of the Microwave Beam Thru the Atmosphere 136

9.4 Absorption of the Microwave Signal by the Atmosphere 145

Chapter 10. Review 150

References 155

Appendix A. Some Calculations in the Absorber Theory of Radiation

A.1 Introduction 157

A.2 Fields From an Oscillating Sheet of Charge 160

A.3 Symmetric Absorber Placement 166

A.4 Energy Flow 176

A.5 Asymmetric Absorber Placement 181

Appendix B. A Note in the Absorber Theory of Radiation 192

LIST OF TABLES

Table		Page
1.	Results of the Experiment	89
2.	Integrated Data for the "Without Lenses" Experimental Configuration	97
3.	Integrated Data for the "With Lenses" Experimental Configuration	98
4.	Power Gain and Noise Temperature of Each Receiver Element	108
5.	Results of Phase Drift Calculations	122
6.	Results Which Indicate the Choice of Data to Minimize r	131

LIST OF FIGURES

Figure		Page
1.	Complete absorption; the full retarded self-consistent solution	14
2.	Complete absorption; the full advanced self-consistent solution	19
3.	Complete absorption in all but one direction; a self-consistent solution featuring advanced and retarded action . .	24
4.	Placement of antennas in experiment indicating correspondence to theoretical configuration of Figure 3 . .	32
5.	Pellet, shutter, and charges	38
6.	Effects of advanced velocity	41
7.	Two possible causes which are paradoxical. .	44
8.	Graph of the logically consistent solution	46
9.	The logically consistent solution	49
10.	Outline of the apparatus	53
11.	Expected response of the receiver to a microwave pulse from the transmitter; definition of time regions	55
12.	Block diagram of the apparatus	60
13.	Mixer function in the receiver	65
14.	Linearity of the transmitter-receiver system	70
15.	Definition of plano-convex lens profile parameters	74

Figure		Page
16.	Definition of parameters for calculation of the theoretical gain of the lens system	77
17.	Sketch showing form of received amplitude with time	84
18.	Graph of the results of the lensless experiment	91
19.	Graph of the results of the experiment using lenses	93
20.	The effective input noise temperature of each element of the receiver system . .	101
21.	Microwave paths pertinent to phase drifts. .	114
22.	Phase (of 77 ns delay bin) versus starting time of run. With lenses	126
23.	Phase (of 69 ns delay bin) versus starting time of run. Without lenses	128
24.	Definition of parameters for various calculations	140
A-1.	Absorber placement for two calculations . .	158
A-2.	Assignment of variables in the integration to find the vector potential of an oscillating sheet of charge. Charge is in the x-y plane	161
A-3.	Simplification of the vector potential integral as made possible by symmetry . .	164
A-4.	Symmetric placement of absorber material . .	167
A-5.	Induced current sheets such as dz contribute to E(z), the field at z	170
A-6.	Induced current sheet dz contributes to field at z	182

Figure | Page

A-7. Fraction, f, of outer face effect versus absorber thickness, $k\Delta$ ($k\Delta$ is the number of radians corresponding to the number of free-space wavelengths in the thickness, modulo π radians), for large absorber thickness. Curves are shown for five source sheet - absorber separations. $\alpha = 4$ 188

A-8. Fraction, f, of outer face effect versus absorber thickness, $k\Delta$ ($k\Delta$ is the number of radians corresponding to the number of free-space wavelengths in the thickness, modulo π radians), for large absorber thickness. Curves are shown for five source sheet - absorber separations. $\alpha = 50$. 190

ACKNOWLEDGMENTS

The nature of the experiments a scientist undertakes reflects the nature of the human relations he wants in his work. Riley Newman has initiated some quite unusual experiments with very fundamental conceptual or scientific implications, experiments which are relatively small in scale and relatively free from technological motivation. His very act of testing things which most scientists take for granted constitutes somewhat of an unspoken challenge to accepted scientific doctrine.

It is not surprising that one who makes such a personal challenge to routine science is also one who works with people in a way which tends to hold the line against the unfortunate work relationships which have become accepted as the norm in "big physics." Riley demonstrates the possibility that dedication both to one's work and to human considerations need not diminish the importance of either. An ambitious work schedule can also allow time for discussing problems at almost any moment. His style embodies principles that are increasingly rare, and that stand out against the competitiveness, the pressure to produce even at the expense of understanding, the

alienation characteristic of physics as it has developed since the Second World War. It has been a pleasure to have had Riley Newman as an advisor and as a co-worker on this experiment.

I also wish to acknowledge the assistance in this work given by two other UCI faculty members: Professor Frederick Reines, for the important and continuous support he gave to the idea that this experiment should be done; and Professor Jonas Schultz for the valuable contributions made during many consultations including a review of this manuscript.

I wish to thank Bob Spero for his assistance with this experiment, at both UC Irvine and Lick Observatory.

The friendly accomodation provided by people at Lick Observatory for the experiment and experimenters during the two weeks of operation and data collection there is appreciated.

Arlene Sanders did the graphics; I am grateful for the careful attention she gave to make sure things were done accurately and in the clearest of the many possible ways.

I wish to thank Myra Handsaker for her work preparing this manuscript as well as for typing it. Her support throughout this period has been invaluable.

This work was paid for out of Department of Energy Contract Number DE-AT 03-76-ER-71019.

VITA

	Born, Los Angeles, California
1968	B.S., Physics University of California Los Angeles
1973 - 1974	Teaching Assistant Department of Physics California State University Los Angeles
1974	M.S., Physics California State University Los Angeles
1975 - 1977	Teaching Assistant Department of Physics University of California Irvine
1976	M.A., Physics University of California Irvine
1978 - 1980	Research Assistant Department of Physics University of California Irvine

FIELDS OF STUDY

Major Field: Physics

ABSTRACT OF THE DISSERTATION

A Search for Advanced Fields
in Electromagnetic Radiation

by

Jeffrey David Schmidt
Doctor of Philosophy in Physics
University of California, Irvine, 1980
Professor Riley Newman, Chair

We have conducted an experiment to search for an advanced component of electromagnetic radiation, as suggested by the time symmetry of Maxwell's equations. A dipole transmitting antenna was driven periodically with 10.2 GHz microwave pulses of 12 ns duration and 4 watt instantaneous power. A receiving dipole antenna at a distance r = 10m away was instrumented to search for power above noise received in a time gate at a time r/c prior to transmission of each pulse. Data were integrated over 10^7 pulses. The experiment was performed at Lick Observatory, atop Mt. Hamilton, CA, to enable placement of the antennas so that a line connecting them, when extended to infinity in both directions, encounters

no local complete absorber. Defining R to be the ratio of signal power in the "advanced" time gate to power received in a corresponding "retarded" gate at time r/c after pulse transmission, we obtain a limit: $R < 10^{-11.5}$ (90% confidence). Runs were also made using dielectric microwave lenses placed to focus an advanced radiation component, yielding a more theory-dependent result: $R < 10^{-14.0}$. These results have cosmological implications within the Wheeler-Feynman absorber theory of radiation.

Chapter 1

INTRODUCTION

1.1 A HIERARCHY OF PARADIGMS

Maxwell's equations provide an accurate description of electromagnetic phenomena. They have survived a century of experimental tests and usage.

Although these equations are fundamentally time-symmetric it is a striking fact of common experience that only the retarded solutions are observed: electromagnetic signals move forward in time. The advanced solutions to Maxwell's equations which move backwards in time are as mathematically valid as the retarded solutions but as of yet have not been observed.

Thus we have a time-symmetric theory which has quite fruitfully guided the work of researchers over a long period of time. Such a well established framework within which researchers carry on their work is known as a "paradigm" in the language of T. S. Kuhn (1970).

In spite of the strength of the electromagnetic paradigm researchers are directed away from serious examination of the time-symmetric advanced solution by an even more entrenched paradigm, causality. Although it is not clear that advanced effects would necessarily violate the deterministic connection of effects to causes, they definitely would violate the normal time-ordering of cause and effect.

Nevertheless, the time-symmetric solutions have been discussed by some authors (surveyed by Pegg, 1975). Much of the discussion has sprung from a time-symmetric theory which incorporates the absorber into the mechanism of radiation and yields, for certain absorber configurations, normally observed retarded radiation. This theory predicts advanced effects for certain other absorber configurations.

It was our purpose to experimentally search for these advanced effects and, in the case of their absence, to place an upper limit on their amplitude.

1.2 THE RETARDED AND ADVANCED SOLUTIONS OF MAXWELL'S EQUATIONS

Maxwell's equations in a medium of unit dielectric constant and magnetic permeability are

$$\vec{\nabla}\cdot\vec{E} = 4\pi\rho \qquad \vec{\nabla}\cdot\vec{B} = 0$$

$$\vec{\nabla} \times \vec{E} = -\frac{1}{c}\frac{\partial\vec{B}}{\partial t} \qquad \vec{\nabla}\times\vec{B} = \frac{1}{c}\frac{\partial\vec{E}}{\partial t} + \frac{4\pi}{c}\vec{J}.$$

$\vec{E}$ and $\vec{B}$ can be written in terms of potentials:

$$\vec{B} = \vec{\nabla} \times \vec{A}$$

$$\vec{E} = -\vec{\nabla}\phi - \frac{1}{c}\frac{\partial\vec{A}}{\partial t} \quad .$$

The Maxwell's equations can be written in terms of ϕ and $\vec{A}$.

$\vec{B}$ and $\vec{E}$ remain unchanged under certain transformations of $\vec{A}$ and ϕ which uncouple the differential equations. The choice of $\vec{A}$ and ϕ such that $(\vec{\nabla}\cdot\vec{A} + \frac{1}{c}\frac{\partial\phi}{\partial t}) = 0$, the Lorentz condition, leads to the following solution of Maxwell's equations:

$$\vec{A}_{\mu\,\substack{\text{ret.}\\ \text{adv.}}}(\vec{x},t) = \frac{1}{c}\int_t\int_\tau \frac{J_\mu(\vec{x}',t')}{R'}\,\delta(t'\pm\frac{R'}{c} - t)d^3x'dt'$$

$$\phi_{\substack{\text{ret.}\\ \text{adv.}}}(\vec{x},t) = \frac{1}{c}\int_t\int_\tau \frac{\rho(\vec{x}',t')}{R'}\,\delta(t' \pm \frac{R'}{c} - t)\; d^3x'dt' \;,$$

where $R' = |\vec{x} - \vec{x}'|$.

Here "retarded" indicates solutions at time t based on integration over currents and charges as they were configured at times given by $(t' + \frac{R'}{c} - t) = 0$ or $t' = (t - \frac{R'}{c})$, that is, at earlier times. Conforming with the usual notion of causality, contributions to the potential at $(\vec{x}, t)$ are retarded by their propagation time $\frac{R'}{c}$ and thus at time t reflect the charge and current distribution at the earlier time $t - \frac{R'}{c}$.

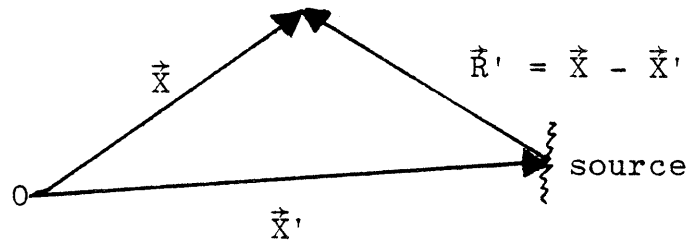

The "advanced" solutions at time t are based on charge and current distributions at times $t' = t + \frac{R'}{c}$, that is, at later times. Although these fields go against usual notions of causality they are mathematically equally acceptable solutions of Maxwell's equations.

Any linear combination of retarded and advanced solutions, a(retarded field) + b(advanced field), where a + b = 1, is also a solution to Maxwell's equations.

Time symmetric solutions in which an accelerated charge gives rise to a field given by half the retarded plus half the advanced solutions to Maxwell's equations, allow development of a theory of direct interparticle action in

which charged particle equations of motion are free of self-action terms. In the Fokker formulation (Fokker, 1929a, 1929b, 1932), an example of a time symmetric theory, the field of a particle itself does not enter into its own equation of motion. "Runaway" solutions or the need for a compensating "pre-acceleration" are thereby avoided (Hoyle and Narlikar, 1974, p. 16, Eq. 27 vs. p. 31, Eq. 10). However, a serious problem remains—the requisite advanced half of the time symmetric solutions are not consistent with normal experience.

1.3 A ROLE FOR THE ABSORBER

This problem was resolved by Wheeler and Feynman in their 1945 paper "Interaction with the Absorber as the Mechanism of Radiation" (Wheeler and Feynman, 1945) (referred to herein as the absorber theory of radiation). They argue that even if we assume that all accelerated charges emit half retarded and half advanced radiation, charges in the absorber respond to this radiation in such a way that there are various self-consistent solutions for the <u>net</u> radiation present. Most significantly, in the case of complete absorption, one such self-consistent solution is the normally encountered purely retarded one. The mechanism by which the absorber contributes to the net radiation will be covered in the next chapter.

Other solutions are equally valid from the point of view of Wheeler-Feynman electrodynamics, including solutions going against the time-ordering of events implicit in usual notions of causality: a purely advanced solution, for example. Wheeler and Feynman suggest that for thermodynamic reasons nature does not choose the available self-consistent advanced solutions. The argument is that advanced activity at the absorber involves spontaneous emission by the absorber, a process going against the thermodynamic arrow of time and of infinitesimal probability.

1.4 THE COSMOLOGICAL CONNECTION

So far, our discussion of the absorber theory of radiation is based on a static Euclidean universe which eventually absorbs all radiation. According to Wheeler-Feynman it is only when the absorption is complete that advanced radiation is everywhere cancelled by the advanced response of the absorber and the net radiation is retarded.

However, if the distribution of matter in the universe or the evolutionary structure of the universe is such that absorption of electromagnetic radiation from a particular source is not complete, then the net radiation from that source would include a presumably detectable advanced component. Conversely, the result of an

experimental search (such as ours) for advanced radiation from an appropriately placed source has cosmological implications within the framework of the Wheeler-Feynman theory.

Hogarth (1962) pointed out the significance of the fact that retarded and advanced radiation encounter the absorber at different times. If the absorber is at cosmological distances, advanced and retarded components may encounter it in vastly different stages of development: the advanced component in its distant past configuration, the retarded component in its distant future.

In the Wheeler-Feynman theory an electromagnetic source gives rise to retarded and advanced fields. In the case of complete absorber, a purely retarded solution is self-consistent because its own interaction with the absorber gives rise to advanced and retarded fields whose advanced part cancels the advanced field of the source (prior to the instant of radiation) and brings up to full strength the retarded field of the source (after the instant of radiation). A parallel line of reasoning shows that a purely advanced solution is also self-consistent in the case of complete absorption.

Hogarth noted that in these descriptions the retarded or advanced solutions come about through their respective interactions with the absorber. Thus self-consistent full retarded solutions require a universe which acts

as a complete <u>future</u> absorber of radiation and full advanced solutions require a universe providing complete <u>past</u> absorption. (This is prior to any thermodynamic considerations.)

Various cosmological models can be examined for their future and past absorption properties and catagorized (based on the assumed validity of the absorber theory of radiation) as allowing or not allowing purely retarded or purely advanced electrodynamics.

The Friedmann cosmological model is based on application of Einstein's field equations, $R_{\mu\nu} - \frac{1}{2}g_{\mu\nu}R = 8\pi G T_{\mu\nu}$, to an assumed homogeneous and isotropic (but not static) universe.

There are two basically different situations in this model depending on whether the universe has an average density of matter less than or greater than that sufficient to stop its expansion. They are respectively known as the $k = -1$ and $k = +1$ Friedmann models, where k is a parameter in the Friedmann model metric. These correspond to universes which are spatially open and closed and have negative and positive spatial curvature, respectively. There is a third case, $k = 0$, which corresponds to a barely open universe.

According to Hoyle and Narlikar (1974, pages 41-48), in an open (or barely open) universe the Friedmann model provides complete absorption only in the past and therefore allows a fully advanced electrodynamics but not a fully retarded one. Furthermore, the closed universe Friedmann model features complete absorption in both the past and future and thus allows both a fully advanced and a fully retarded electrodynamics, ruling out neither.

A static uniform universe of infinite extent, filled homogeneously with stars, completely absorbs radiation in the past and future and thus also rules out neither purely advanced nor purely retarded electrodynamics (Hoyle and Narlikar, 1974, page 47).

Steady state cosmology is based on a model of the universe which features continual creation of matter uniformly throughout space at a rate which maintains constant average density in spite of cosmological expansion.

Hoyle and Narlikar (1974, pages 45-47) and Hogarth (1962, page 370) calculate complete future electromagnetic absorption and incomplete past absorption in the steady state model. Therefore, they conclude, in the absorber theory of radiation fully retarded but not fully advanced solutions are self-consistent.

Davies (1974, pages 145, 149) notes that there is complete future absorption, and thus self-consistent retarded solutions, in matter-conserving models in which the radius expands as $t^{1/3}$ or slower. (Strictly speaking, it is the parameter R(t) in the Robertson-Walker metric (Davies, 1974, page 82),

$$ds^2 = dt^2 - \frac{R^2(t)}{(1 + \frac{1}{4}kr^2)^2} (dr^2 + r^2 d\Omega^2),$$

which must satisfy this condition. This metric is based on a universe which is, on a large scale, homogeneous and isotropic and in uniform motion.)

Chapter 2

DISCUSSION OF THE ABSORBER THEORY OF RADIATION

2.1 INTRODUCTION

The Wheeler-Feynman absorber theory of radiation invokes advanced and retarded potentials in a time-symmetric way such that with appropriate boundary conditions there is a solution which reproduces observed purely retarded electrodynamics. The theory came about during a quest to develop an electrodynamics free from interaction of the electron with itself and from the associated infinite energies (Feynman, 1966). Although this was accomplished by QED the absorber theory of radiation has remained an attractive theory of classical electrodynamics because of its fundamental time-symmetry and because of its potential for relating the electrodynamic arrow of time to the thermodynamic and/or cosmological arrows of time. Several authors have developed the theory and its relation to the past and future history of the universe. In this chapter we describe the Wheeler-Feynman absorber theory of radiation and its role in our experiment.

2.2 ASSUMPTIONS OF ABSORBER THEORY

The theory is a time-symmetric electrodynamics based on the following four postulates (Wheeler and Feynman, 1945, page 160):

1. An accelerated point charge in otherwise charge-free space does not radiate electromagnetic energy.
2. The fields which act on a given particle arise only from other particles.
3. These fields are represented by one-half the retarded plus one-half the advanced Liénard-Wiechert solutions of Maxwell's equations.
4. Sufficiently many particles are present to absorb completely the radiation given off by the source.

There are many configurations of fields in time which are self-consistent with these four postulates. One of these solutions, described in the next section, reproduces all of the results of the purely retarded theory.

2.3 COMPLETE ABSORPTION, A SELF-CONSISTENT PURE RETARDED SOLUTION

To better illustrate the nature of self-consistent solutions in the Wheeler-Feynman absorber theory of radiation we consider the radiation due to a single charge

totally surrounded by complete absorber. We will describe (with reference to Figure 1) the mechanism by which a fully retarded solution is self-consistent in the case of complete absorption.

There is no preferred point in time at which to begin the analysis. Let us start by assuming that although individual charges (q in our example) each give rise to half retarded ($\frac{1}{2}R_q$) and half advanced ($\frac{1}{2}A'_q$) fields when they are disturbed (accelerated), the <u>net</u> result of disturbing our single charge is a full retarded field (R) which propagates from the charge to the surrounding absorber. This net result (R) acts to disturb charges (b_i) in the absorber, charges which give rise to half retarded and half advanced fields. These fields are of proper amplitude and phase such that inside the absorber the net result is a wave which is attenuated with depth: this is the absorption mechanism even in a conventional analysis in which only retarded fields are involved. In the Wheeler-Feynman scheme, since the half advanced part moves out (from b_i) backward in time it has a much earlier existence away from the absorber. The path of this half advanced part of the response of the absorber to the full retarded field (R) is most understandably followed with time moving forward. From this perspective the half advanced response of the absorber sweeps across space,

Figure 1. Complete absorption; the full retarded self-consistent solution.

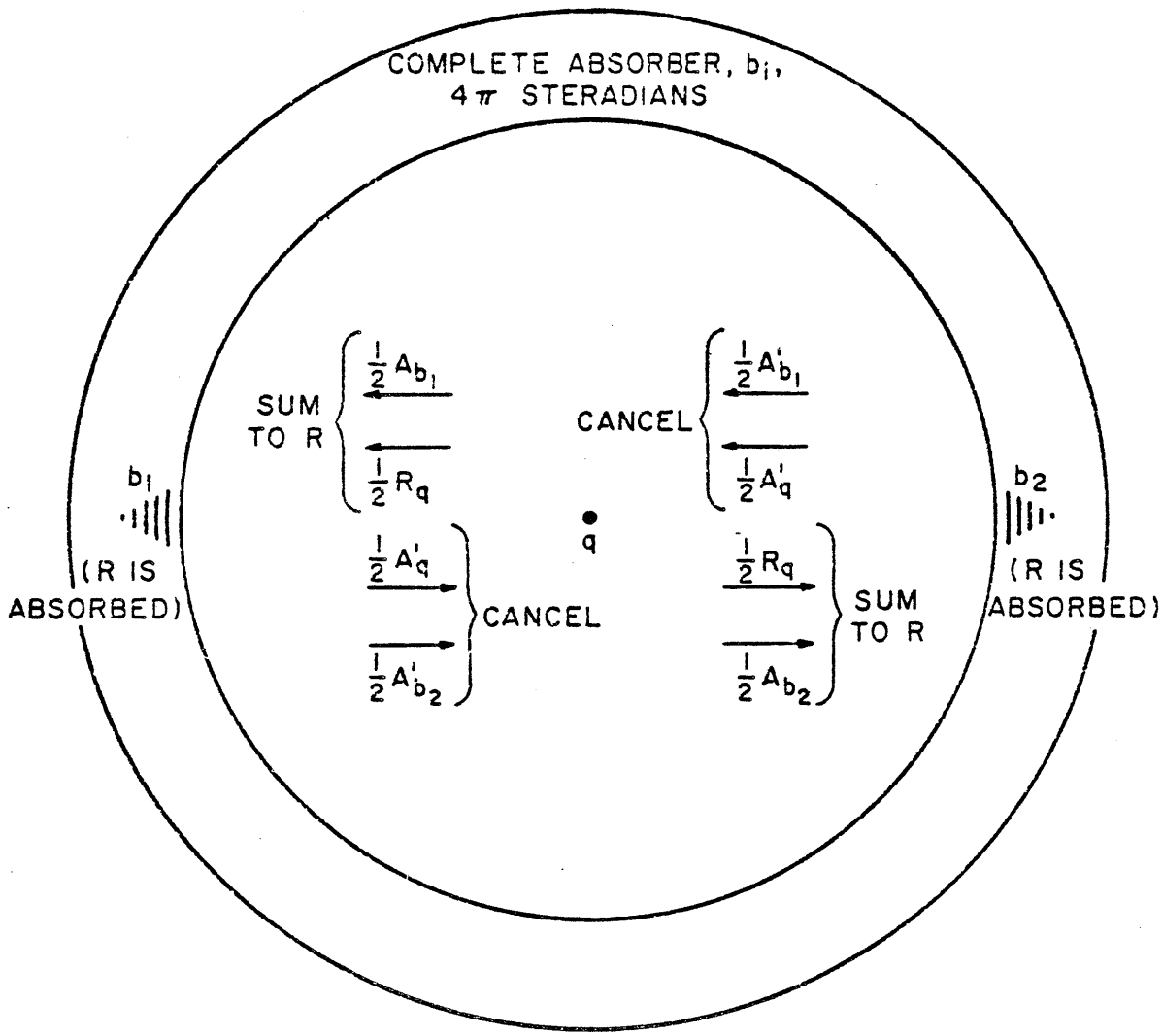

Notes:

1. b_i represent charges of the absorber.
2. R and A represent retarded and advanced fields respectively. Subscripts indicate responsible charges.
3. Primes mark fields in existence before the acceleration of charge q; unprimed, after.
4. Arrows show propagation directions with time moving forward: arrows pointing toward q represent spherical waves collapsing onto q; arrows pointing away from q represent spherical waves diverging from q.

from beyond the original charge (q), toward the absorber. Since this half advanced field passes the original charge (q) at the moment of acceleration, it is moving toward the charge before acceleration (labeled $\frac{1}{2}A'_{b_i}$) and away afterwards (labeled $\frac{1}{2}A_{b_i}$).

Thus before acceleration the half advanced response of the absorber ($\frac{1}{2}A'_{b_i}$) moves toward the charge along with the half advanced field ($\frac{1}{2}A'_q$) from the charge itself. Wheeler and Feynman show that interference between the two is destructive so that there are no radiation fields in advance of the disturbance of the charge (q).

After acceleration the half advanced response of the absorber ($\frac{1}{2}A_{b_i}$) is moving away from the charge (q), continuing on its way to the absorber (b_i), but now moves along with the half retarded field ($\frac{1}{2}R_q$) from the charge itself. Wheeler and Feynman show that interference between these two fields is constructive, combining to form the full retarded field (R) originally assumed.

Thus the original assumption of a full strength retarded wave to which the absorber is to respond is justified in the sense that a self-consistent picture of fields and moving charges emerges. This self-consistent full retarded solution in the absorber theory of radiation is seen to consist equally of retarded radiation ($\frac{1}{2}R_q$) from the accelerated charge (q) and advanced radiation ($\frac{1}{2}A_{b_i}$) from the response of the absorber.

2.4 SPHERICAL WAVES

How can the interference described above be complete when the interfering waves are converging toward different points? Consider for example the participants in the destructive interference of advanced waves which occurs before the acceleration of the charge. The half advanced radiation ($\frac{1}{2}A'_q$) of the accelerated charge is a spherical wave converging onto the charge (q) itself. The half advanced response of the absorber ($\frac{1}{2}A'_{b_i}$) consists of spherical waves converging onto each of the responding charges (b_i) in the absorber. Each of these spherical waves converging onto points in the absorber passes through the charge (q) at the same time (the moment of acceleration) regardless of the shape of the absorber. (A spherically shaped absorber is used in the figures for convenience.) Prior to that time these waves ($\frac{1}{2}A'_{b_i}$) are approaching the charge (q) <u>from all directions</u>, the superposition of wavefronts appearing as a spherical wavefront converging <u>onto the charge (q)</u>. Thus in advance of the moment of acceleration the half advanced response of the absorber ($\frac{1}{2}A'_{b_i}$) is a wave with the same (spherical) shape, motion, and focus on the charge (q) as the half advanced wave ($\frac{1}{2}A'_q$) from the charge itself. This fulfills the geometrical prerequisites for their total interference, in this case destructive.

Similarly, after the moment of acceleration, the advanced response of the absorber ($\frac{1}{2}A_{b_i}$) is moving away from the charge (q) in all directions, appearing as a spherical wave diverging from the charge. This wave has the same shape, motion, and focus as the half retarded wave ($\frac{1}{2}R_q$) from the charge itself. As previously mentioned, these waves interfere constructively and form the full retarded wave.

2.5 COMPLETE ABSORPTION, A SELF-CONSISTENT PURE ADVANCED SOLUTION

We have described how in the case of complete absorption a full retarded solution is self-consistent. A full advanced solution, or any normalized linear combination of retarded and advanced, is also self-consistent in this case. We now describe the self-consistency of a full advanced solution (with reference to Figure 2). The description parallels that for the full retarded solution.

An accelerated charge (q) gives rise to half retarded ($\frac{1}{2}R_q$) and half advanced ($\frac{1}{2}A'_q$) waves. The net result, assumed to be a full advanced wave (A'), propagates backward in time from the charge (q) to the absorber (b_i) where it is attenuated as it is absorbed. Viewed with time moving forward we would see this advanced wave (A)

Figure 2. Complete absorption; the full advanced self-consistent solution.

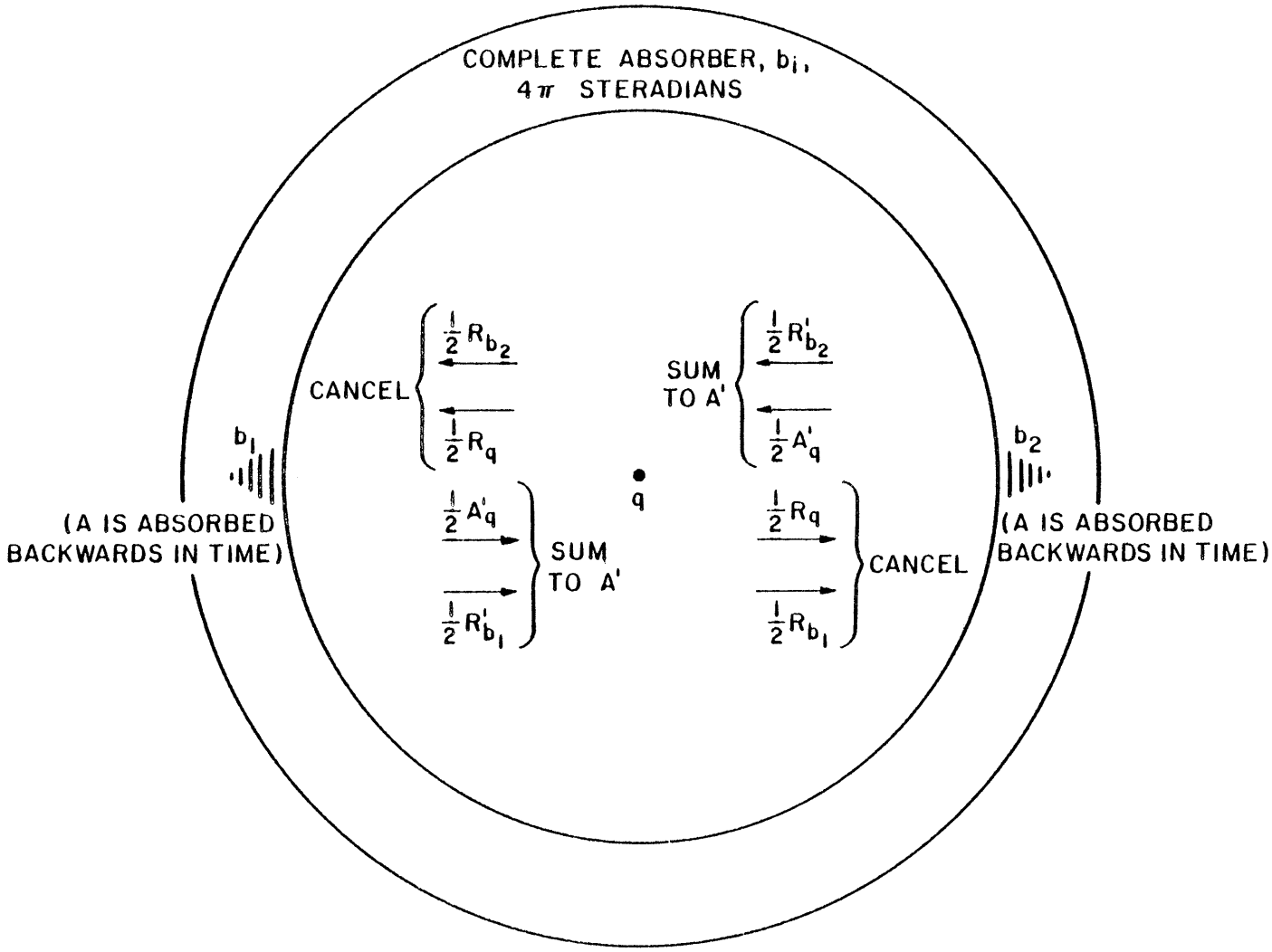
COMPLETE ABSORBER, b_i,
4π STERADIANS
CANCEL
$\frac{1}{2}R_{b_2}$
$\frac{1}{2}R_q$
SUM TO A'
$\frac{1}{2}R'_{b_2}$
$\frac{1}{2}A'_q$
b_1
(A IS ABSORBED BACKWARDS IN TIME)
$\frac{1}{2}A'_q$
$\frac{1}{2}R'_{b_1}$
SUM TO A'
q
$\frac{1}{2}R_q$
$\frac{1}{2}R_{b_1}$
CANCEL
b_2
(A IS ABSORBED BACKWARDS IN TIME)

building up in, and emerging from, the absorber (b_i), making its way toward the charge (q), and arriving there at the moment of acceleration. Charges (b_i) in the absorber are disturbed by the incoming (backward in time) full advanced wave (A') and give rise to a half retarded and half advanced response which attenuates the incoming advanced wave (A') in the absorber (the absorption process). Outside of the absorber the half retarded response of the absorber ($\frac{1}{2}R'_{b_i}$) moves toward the charge (q) (forward in time) along with the half advanced field of the charge itself ($\frac{1}{2}A'_q$). These two fields add to form the full advanced field (A') which we assumed to be the net result of disturbing our charge (q). The half retarded response of the absorber ($\frac{1}{2}R'_{b_i}$) passes the charge at the time of acceleration and then (labeled $\frac{1}{2}R_{b_i}$) goes beyond it, moving away (from q) along with the half retarded field ($\frac{1}{2}R_q$) of the charge (q) itself, exactly cancelling it. In summary, there is no net radiation after the acceleration of the charge (q). Our assumption that full amplitude advanced radiation (A') exists before the charge is disturbed turns out to be self-consistent. This radiation is seen to consist equally of advanced radiation ($\frac{1}{2}A'_q$) from the accelerated charge (q) and retarded radiation ($\frac{1}{2}R'_{b_i}$) from the response of the absorber.

In the case of complete absorber the choice between the purely retarded, the purely advanced, and normalized linear combinations of these self-consistent solutions cannot be made on electrodynamic grounds alone. Thermodynamic arguments are usually used to rule out advanced solutions.

In the examples given above we saw that the advanced field of the absorber is always at the charge just at the moment of the charge's acceleration. Wheeler and Feynman show that this advanced response of the absorber provides the fields necessary to exactly account for the radiation reaction force on the charge which is appropriate in each case. Thus in the absorber theory of radiation the reaction fields experienced by an accelerated charge are nicely accounted for as being due entirely to <u>other</u> charges (in this case charges of the absorber). The postulate that the fields which act on a given particle arise only from other particles simplifies the derivation of important results.

2.6 INCOMPLETE ABSORPTION, SELF-CONSISTENT SOLUTIONS

To the extent that the postulate of complete absorption may not be completely true, the absorber theory of radiation predicts the possibility of advanced action. In the case of incomplete absorption there are

an infinity of self-consistent solutions (Wheeler and Feynman, 1945, page 176). As an example we will describe (with reference to Figure 3) a self-consistent solution in the case of an absorber which is incomplete in one direction (Wheeler and Feynman, 1945, Page 174). Our discussion follows that of Wheeler and Feynman.

An accelerated charge (q) gives rise to half retarded ($\frac{1}{2}R_q$) and half advanced ($\frac{1}{2}A'_q$) waves. We will show the self-consistency of an assumed net result wherein the inner face of the absorber opposite the opening is hit with a full amplitude advanced wave (A') <u>and</u> with a full amplitude retarded wave (R). This assumed solution is motivated by the absence in the opening of absorber which could give rise to fields which cancel advanced waves. In the absorber theory, incomplete absorption necessitates the existence of advanced action (Wheeler and Feynman, 1945, page 175).

Charges (b_i) in the absorber opposite the opening are accelerated by the incoming (backward in time) full advanced wave (A') and give rise to a half retarded and half advanced response which attenuates the incoming advanced wave (A') in the absorber (the absorption process). Inside the cavity surrounded by the absorber the half retarded response of the absorber ($\frac{1}{2}R'_{b_i}$) moves toward the charge (q) (forward in time) along with the half advanced

Figure 3. Complete absorption in all but one direction; a self-consistent solution featuring advanced and retarded action.

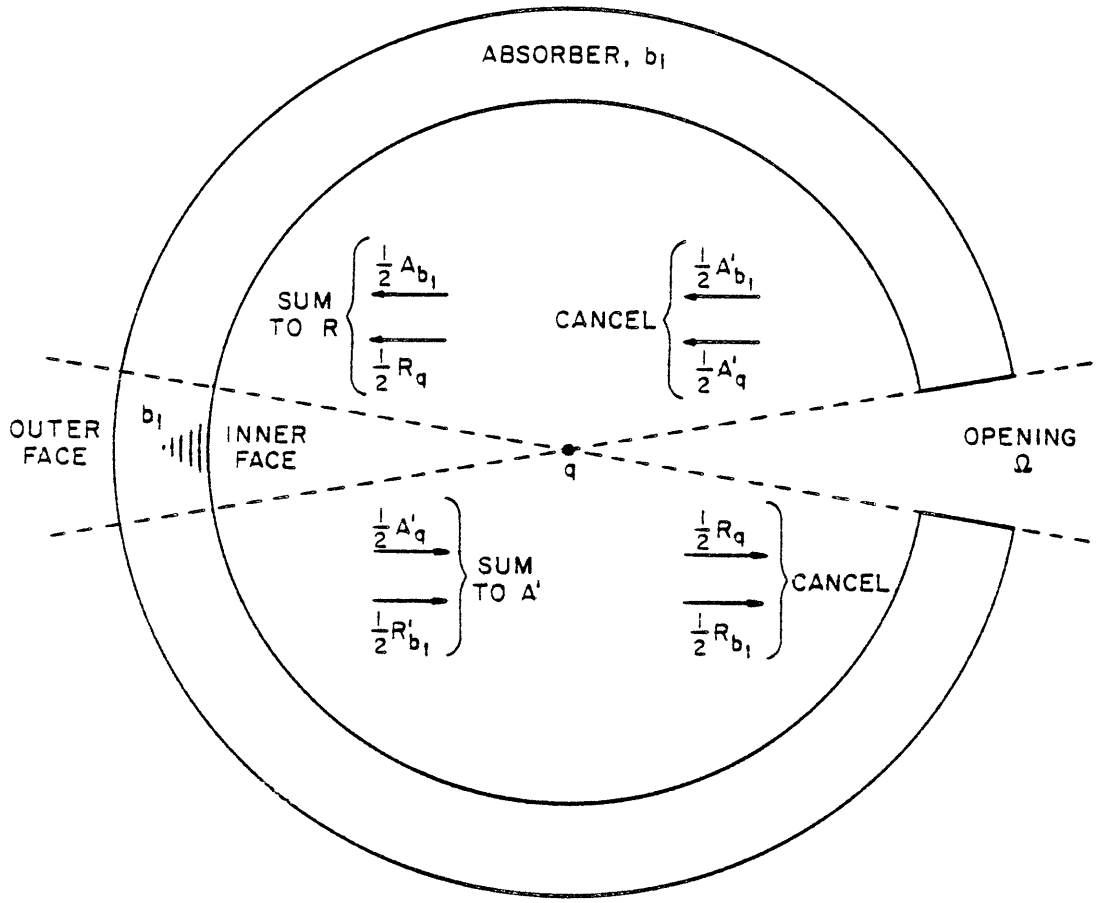

Notes:

1. Dashed lines mark cone of opening.
2. All indicated fields are in cone of opening. Fields elsewhere are given by normalized linear combination of solutions illustrated in Figures 1 and 2.

field of the charge itself ($\frac{1}{2}A'_q$). These two fields add to form the full advanced field (A'), part of our assumed self-consistent solution. The half retarded response of the absorber ($\frac{1}{2}R'_{b_i}$) passes the charge (q) at the time of acceleration and then (labeled $\frac{1}{2}R_{b_i}$) goes beyond it, moving away (from q) along with the half retarded field ($\frac{1}{2}R_q$) of the charge (q) itself, exactly cancelling it.

Subsequently, charges in the absorber are again disturbed, this time along its entire inner face by the full retarded part (R) of our assumed self-consistent solution. These disturbed absorber charges give rise to half retarded and half advanced fields which are of proper phase and amplitude to cancel in the absorber the incoming full retarded wave (the absorption process).

However, the half advanced part of this response of the absorber moves backward in time out from the absorber. If we view this earlier existence with time moving forward we see it moving across space, entering the opening, passing the charge (q), and moving on toward the inner face absorber opposite the opening. While moving toward the charge (q), the absorber's half advanced response ($\frac{1}{2}A'_{b_i}$) to the full retarded wave (R) moves together with, and cancels, the half advanced wave ($\frac{1}{2}A'_q$) from the charge (q) itself. After passing the charge (q) the

half advanced response of the absorber (labeled $\frac{1}{2}A_{b_i}$) moves away from the charge (q) together with the half retarded field ($\frac{1}{2}R_q$) of the charge (q). These two fields combine to form the full strength retarded field assumed earlier.

Thus the assumed solution is self-consistent. Due to the incomplete absorption, advanced effects as well as retarded appear. Note that no fields, retarded or advanced, escape thru the opening in a direction where there is no absorption.

This is not the only self-consistent solution to the absorber configuration just considered. Another solution is described by Wheeler and Feynman (1945, pages 173, 175, 176) and by Davies (1974, pages 149-152) as follows. An incident full strength advanced field converging toward the charge (q) strikes the <u>outer face</u> of the absorber opposite the opening and is absorbed there. A full retarded field is absorbed along the entire inner face of the absorber, except the opening. There are no advanced effects inside the cavity formed by absorber. A full retarded field propagates out through the opening. This field is equivalent to a continuation, as a diverging retarded wave now, of the incident converging advanced wave (Wheeler and Feynman, 1945, page 176). All of the energy lost by the radiating charge (q) appears in the

absorber: some on its outer face opposite the opening (an advanced effect) and the rest along its entire inner face (a retarded effect).

Wheeler and Feynman make no attempt to choose between solutions placing the advanced action on the inner face of the absorber and those placing the advanced action on the absorber's outer face (Wheeler and Feynman, 1945, page 176). In fact, there are an infinity of other possibilities. The general case involves a fraction f of outer face advanced effect and (1-f) of inner face advanced effect. We define Ω as the solid angle of the opening and E_s as the total energy emitted by our source charge when that charge is <u>completely</u> surrounded by absorber and forced to follow a specified trajectory. Then an energy $fE_s(\frac{\Omega}{4\pi})$ will be deposited on the outer face of the absorber opposite the opening as an advanced effect, an energy $(1-f)E_s(\frac{\Omega}{4\pi})$ will be emitted by the inner face of the absorber opposite the opening as an advanced effect, and an energy $E_s(1 - \frac{\Omega}{4\pi})$ will be deposited around the entire inner face of the absorber as a full strength retarded effect. The algebraic sum of these energies is a fraction, $[1 - (1-f)\frac{2\Omega}{4\pi}]$, of E_s. (A discussion by Wheeler and Feynman (1945, page 174) enables comparison in the f = 0 case). The source charge experiences this

fraction of the full radiation reaction force (the full force being what it would experience in the case of identical motion but completely absorbing surroundings).

Thus the radiation reaction force experienced by the charge (q) is dependent upon f, upon the outer face and/or inner face location of the advanced effects. The solution (f = 0) with all advanced action on the absorber's inner face opposite the opening has less than full radiation reaction because of the action (on q) of fields from inner face charges set into motion by the advanced part (A') of the solution (Wheeler and Feynman, 1945, page 174). On the other hand, the solution (f = 1) with all advanced action on the absorber's outer face opposite the opening has no net advanced fields inside the absorber cavity where the charge (q) is located and provides full radiation reaction force (Davies, 1974, page 150; Wheeler and Feynman, 1945, page 175).

Note that "outer face" advanced effects involve the deposition of energy into the absorber whereas "inner face" advanced effects involve the spontaneous emission of energy from the absorber (Davies, 1974, pages 144-145, 150-151). The "outer face" advanced solution, then, is not subject to the statistical mechanical criticism.

2.7 EXPERIMENT

This ambiguity in the expected radiation reaction force has been used (Davies, 1975, pages 278-279) to criticize an experiment by Partridge (1973), who looked for a transmitter's diminished power requirements in an absorber configuration similar to that of our examples (Figure 3). Even if there was an advanced field, it may not have reached his source antenna.

Partridge monitored the power drawn by a microwave transmitter as its radiation was alternately directed skyward and into absorbing material. The skyward direction carries the possibility of incomplete absorption (depending on cosmological considerations) and therefore of advanced fields at the transmitter which could reduce its power requirements. However, there are two potential problems here. First, if the advanced action associated with this experimental configuration is of the sort which occurs on the absorber's "outer face" (as discussed earlier) then the advanced effects would occur on the side of the earth opposite the transmitter, not at the transmitter itself. In this case, discussed at the end of Section 2.5, the transmitter would experience full radiation reaction force. Thus the Partridge experiment

was at best sensitive to "inner face" advanced effects. Second, even sensitivity to those effects is questionable. Although such inner face advanced effects result in a reduced radiation reaction force on each radiating charge in the transmitter's transmitting element, it is not clear what, if any, effect this would have on the total power consumed by the transmitter electronics. In any case, using apparatus capable of detecting a power asymmetry of 1 part in 10^8 Partridge measured no effect.

Our experiment was designed to remove the ambiguity by replacing any earthbased absorber opposite the opening with a receiving antenna (see Figure 4). This antenna is, of course, an absorber, but one which can be monitored for advanced effects on either side. Although the receiver electronics may respond differently to "inner face" advanced effects and "outer face" advanced effects, with this set-up neither will be blocked by other absorber. With this set-up it is only the case of $f = \frac{1}{2}$ for which we expect no detectable advanced signal power. In this case the outer and inner faces of the absorber (antenna) respectively gain and lose equal amounts of electromagnetic energy in the advanced time period.

Our source and receiving antennas, simple half-wave dipoles, were positioned so that the line (1) connecting them, when extended infinitely in either direction,

Figure 4. Placement of antennas in experiment indicating correspondence to theoretical configuration of Figure 3.

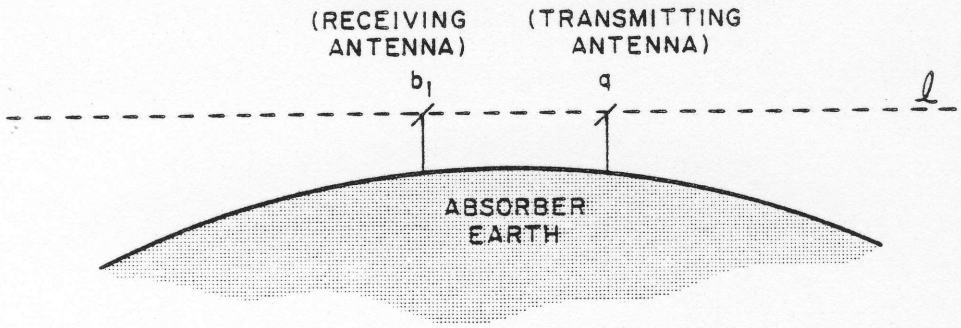
(RECEIVING ANTENNA)
(TRANSMITTING ANTENNA)
b_1
a
ℓ
ABSORBER EARTH

encountered no earth-based absorber such as buildings or mountains. To accomplish this the experiment was done on a mountain top. The source antenna transmitted pulses of 10 GHz microwave radiation and the receiving antenna, 9.7 m away, was monitored for advanced effects.

It should be noted that although our set-up was clearly designed to maximize the likelihood of detection of advanced effects within the Wheeler-Feynman absorber theory of radiation, it constituted a more general search for advanced effects—the time region which we monitored for advanced effects is indicated by Maxwell's equations. The Partridge experiment was more closely tied to the absorber theory of radiation.

The details of our experiment will be discussed in later chapters.

We used microwaves in our experiment. This choice had certain advantages over visible radiation. It enabled us to use bare conductor transmitting and receiving elements which, unlike photomultiplier tubes, have no absorber as backing. It also enabled us to carry out all of our equipment design and calculations in the classical paradigm (rather than the quantum mechanical), consistent with the Wheeler-Feynman theory. Finally, our 10.243 GHz frequency is thought to be appropriate for transmission

through intergalactic space as it avoids absorption lines of various molecules which may be present there (Sagan, 1973, pages 282-285, 314-315; Shklovskii and Sagan, 1966, pages 64-67, 380-381, 388-389). Partridge (1973) estimates only 1% absorption through our galaxy and less than 5% absorption to cosmological distances in this frequency region.

2.8 THE NECESSITY OF A DELIBERATE SEARCH

One may ask whether advanced effects, if they do exist, would have already been observed in the course of human experience. The presence of local absorber, whose response would cancel advanced effects, is rarely avoided inadvertently. In earth-based radio or light communications the line connecting transmitter and receiver, when extended in both directions, almost always intersects absorber. Even if this were not the case there are two reasons why advanced effects might not be seen without a deliberate search. First, the advanced signal arrives in such close time proximity to the retarded signal as to require a deliberate effort to distinguish the two. Second, the intensity of the advanced signal, as a fraction of the retarded, is given by the fractional absence of ultimate absorption. So, in the case of partial

absorption, any advanced signal would appear attenuated and might require deliberate signal processing techniques (integration) to detect.

Finally, one must never forget the power with which paradigms direct the work of scientists (Kuhn, 1970). Anomalies encountered in work peripheral to an experiment tend to be discounted unless they interfere with the goal of the experiment.

All of these considerations argue for a deliberate search for advanced effects.

Chapter 3

ADVANCED EFFECTS: A LOGICAL PARADOX?

Do advanced effects lead to logically inconsistent, impossible, physical situations? Can the advanced effects of an event be harnessed to cancel the event before it occurs? We will outline here an argument given by Wheeler and Feynman (1949), based on the presumed absence of discontinuities in nature, which shows systems involving advanced effects to be just as deterministic as Newtonian mechanics. They consider the behavior of a system which is simple because human action is not involved but contains all the essential elements of the general paradox.

A pellet is moving toward point X on the arm of a shutter (Figure 5) which is free to rotate about a pivot without friction. There is no gravity. The pellet is due to pass the corner (S) of the shutter at 5:59 p.m. and strike X at 6:00 p.m. If it does so, charge A attached to the arm will be accelerated and will emit retarded and advanced radiation. Charge B, residing 5 light-hours

Figure 5. Pellet, shutter, and charges.

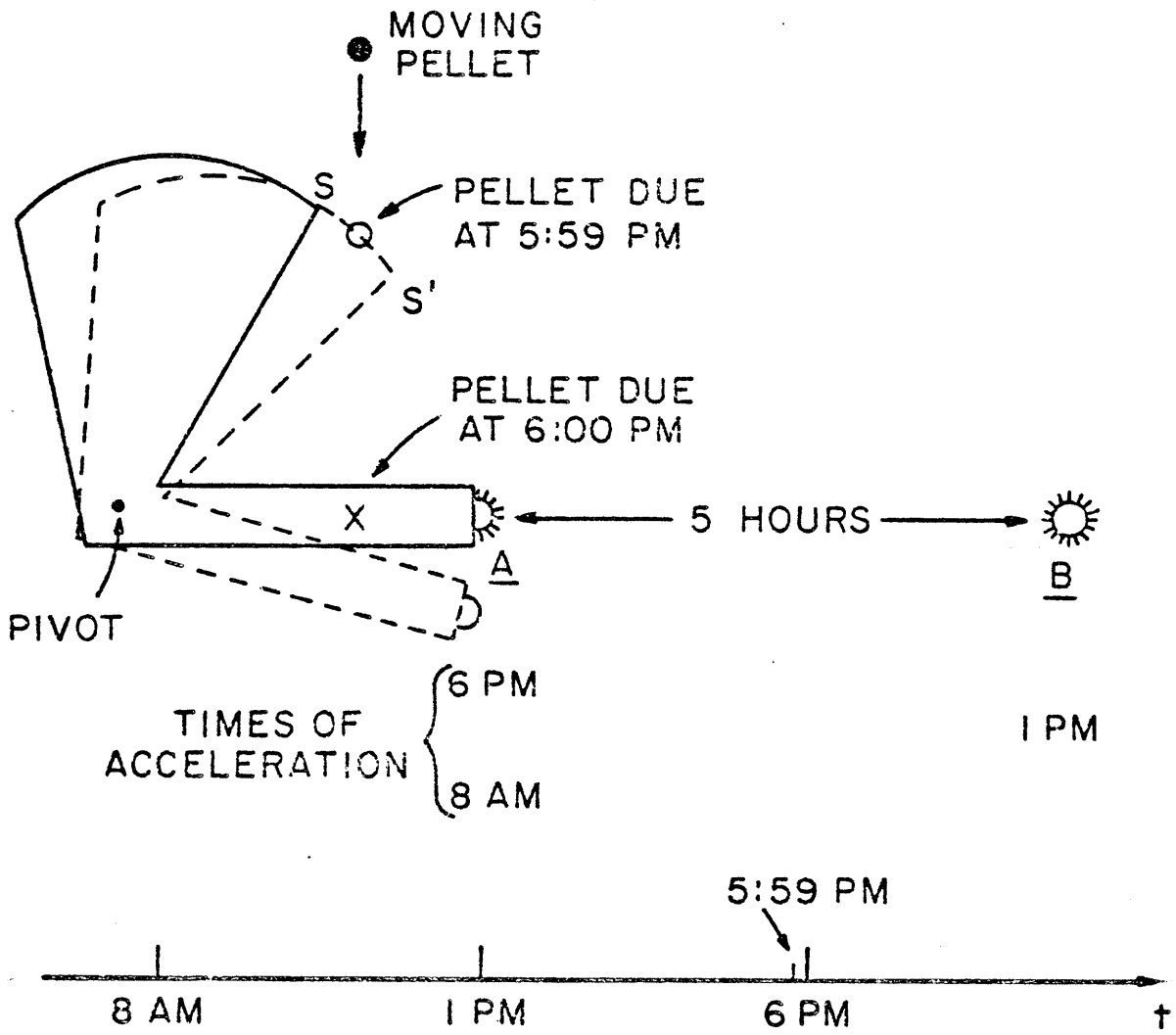
MOVING PELLET
S
Q
PELLET DUE AT 5:59 PM
S'
PELLET DUE AT 6:00 PM
X
5 HOURS
A
B
PIVOT
TIMES OF ACCELERATION
6 PM
8 AM
1 PM
5:59 PM
8 AM
1 PM
6 PM
t

away, will accelerate at 1:00 p.m. under the advanced radiation from A (and again at 11:00 p.m. due to A's retarded radiation). The advanced radiation from B's acceleration arrives back at A at 8:00 a.m. and gives A an impulse in spite of having suffered much attenuation due to the distances involved. This impulse imparts to the shutter a small clockwise (angular) speed which by the end of the 8:00 a.m. - 5:59 p.m. day has displaced the shutter, in effect closing it.

The question is this: What happens at 6:00 p.m.; does the pellet strike X?

If it does strike X, then the associated advanced action closes the shutter during the day, blocking the pellet. Thus, paradoxically, the pellet does not strike X.

If the pellet does not strike X then there is no acceleration of the charges and therefore no advanced action to close the shutter and block the pellet. Thus, paradoxically, the pellet must strike X.

Following Wheeler and Feynman we analyze the situation graphically. In Figure 6 we plot the linear relationship between the shutter's speed during the day (8:00 a.m. - 5:59 p.m.) and its total displacement by the end of the day (5:59 p.m.). We have noted that sufficient total

Figure 6. Effects of advanced velocity.

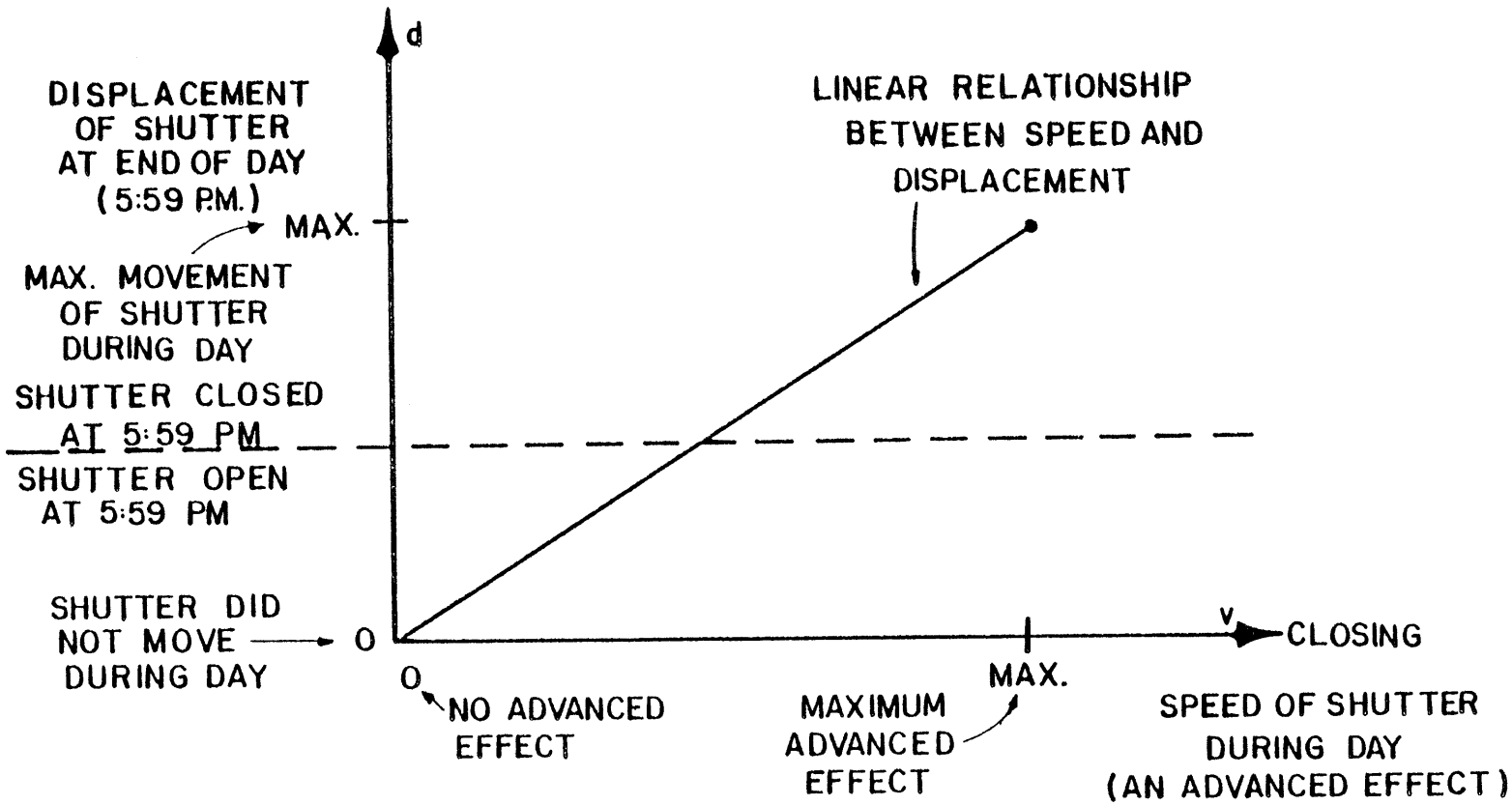
d
DISPLACEMENT OF SHUTTER AT END OF DAY (5:59 P.M.)
MAX.
MAX. MOVEMENT OF SHUTTER DURING DAY
SHUTTER CLOSED AT 5:59 PM
SHUTTER OPEN AT 5:59 PM
SHUTTER DID NOT MOVE DURING DAY
O
LINEAR RELATIONSHIP BETWEEN SPEED AND DISPLACEMENT
v
CLOSING
O
NO ADVANCED EFFECT
MAX.
MAXIMUM ADVANCED EFFECT
SPEED OF SHUTTER DURING DAY (AN ADVANCED EFFECT)

displacement closes the shutter. Thus we have graphed what we call possible effects of advanced shutter velocity.

We want now to place the causes of advanced shutter velocity, defined as the possible shutter positions at 5:59 p.m., in graph positions associated with their corresponding effects. First, "open at 5:59 p.m." means the pellet hits X and we get maximum advanced velocity. In Figure 7 we graph this cause at maximum advanced shutter velocity in the region of "open" final displacement. Similarly "closed at 5:59 p.m." is graphed as the cause of zero advanced shutter velocity in the region of "closed" final displacement. Each of these two graphings is obviously paradoxical. For example, shutter "open at 5:59 p.m." is graphed as the cause of maximum advanced closing speed 8:00 a.m. - 5:59 p.m.

The paradox is due to our implicit assumption that only two final shutter positions exist, open or closed, and that the movement from one to another is discontinuous. However, if we take a physical point of view wherein forces in nature vary continuously, then there is a continuum of possible final shutter positions, causing a continuum of advanced closing speeds during the day. This is shown in Figure 8.

Figure 7. Two possible causes which are paradoxical.

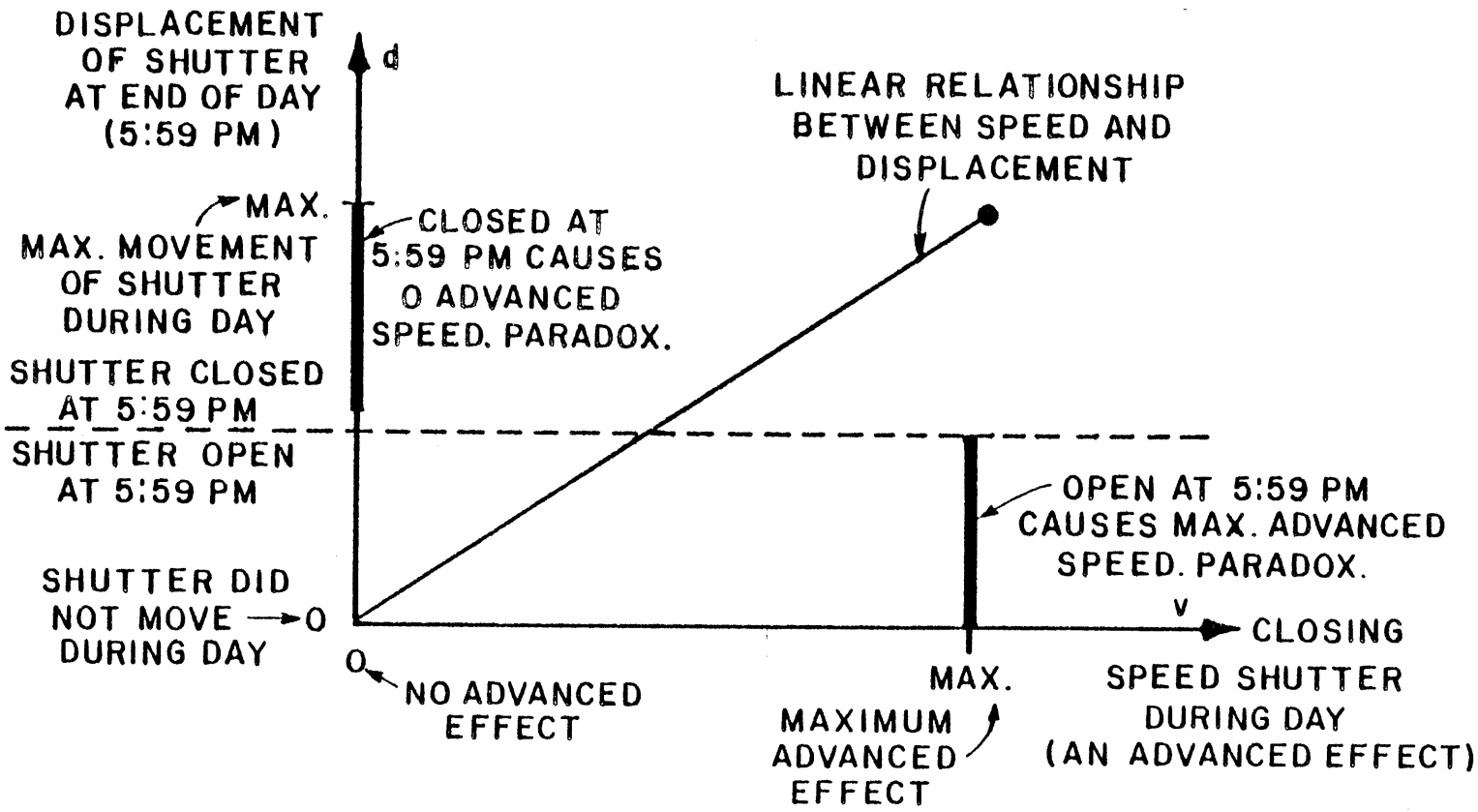
DISPLACEMENT OF SHUTTER AT END OF DAY (5:59 PM)
d
MAX.
MAX. MOVEMENT OF SHUTTER DURING DAY
CLOSED AT 5:59 PM CAUSES 0 ADVANCED SPEED. PARADOX.
LINEAR RELATIONSHIP BETWEEN SPEED AND DISPLACEMENT
SHUTTER CLOSED AT 5:59 PM
SHUTTER OPEN AT 5:59 PM
OPEN AT 5:59 PM CAUSES MAX. ADVANCED SPEED. PARADOX.
SHUTTER DID NOT MOVE DURING DAY
0
0
NO ADVANCED EFFECT
v
CLOSING SPEED SHUTTER DURING DAY (AN ADVANCED EFFECT)
MAX.
MAXIMUM ADVANCED EFFECT

Figure 8. Graph of the logically consistent solution.

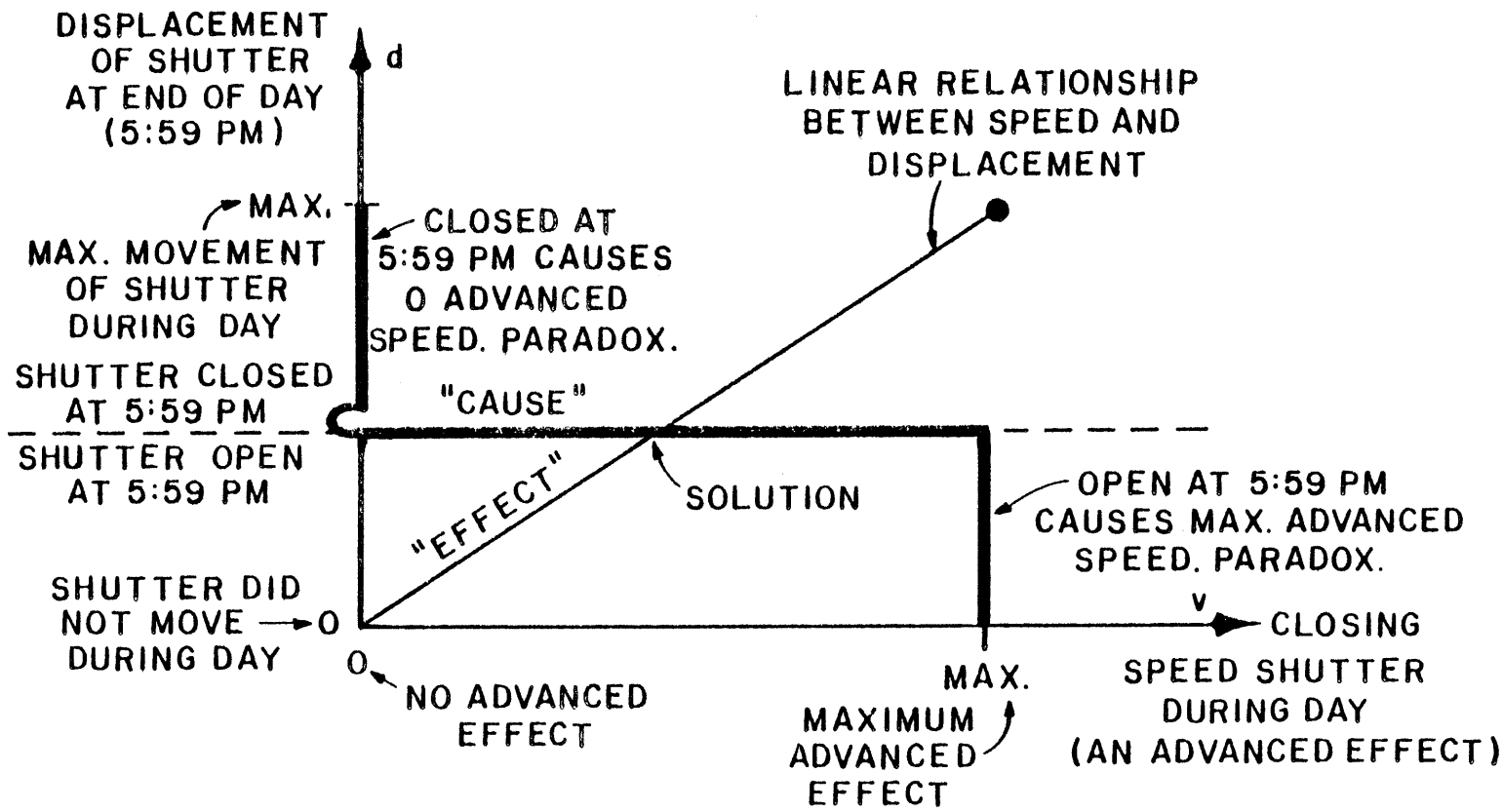
DISPLACEMENT OF SHUTTER AT END OF DAY (5:59 PM)
d
MAX.
MAX. MOVEMENT OF SHUTTER DURING DAY
CLOSED AT 5:59 PM CAUSES 0 ADVANCED SPEED. PARADOX.
SHUTTER CLOSED AT 5:59 PM
SHUTTER OPEN AT 5:59 PM
"CAUSE"
"EFFECT"
SOLUTION
LINEAR RELATIONSHIP BETWEEN SPEED AND DISPLACEMENT
OPEN AT 5:59 PM CAUSES MAX. ADVANCED SPEED. PARADOX.
SHUTTER DID NOT MOVE DURING DAY
0
0
NO ADVANCED EFFECT
v
CLOSING SPEED SHUTTER DURING DAY (AN ADVANCED EFFECT)
MAX.
MAXIMUM ADVANCED EFFECT

A logically consistent solution is then available. Its description has no preferred starting point: The shutter is partially closed at 5:59 p.m.; the pellet strikes a glancing blow, giving the shutter a partial acceleration; the partial acceleration of charges yields a partial advanced velocity which partially closes the shutter by 5:59 p.m. This is illustrated in Figure 9.

This solution is the intersection of the curve representing the effect of the shutter's future on its past ("cause") with the curve representing the effect of the shutter's past on its future ("effect"). There is no time ordering "cause then effect." "Cause" and "Effect" become arbitrarily assignable terms. However, the solution in our example is unique so that advanced effects are as "deterministic" as retarded effects.

One can disagree with Wheeler and Feynman's claim that the example of the shutter contains all the essential elements of the general paradox. Mechanisms involving human participation or devices designed to move abruptly between positions, for example, may require more elaborate analysis.

Quantum mechanical arguments can be raised against the assumption of continuity of force in nature. Within the quantum mechanical paradigm could charge A respond

Figure 9. The logically consistent solution.

THE LOGICALLY CONSISTENT SOLUTION

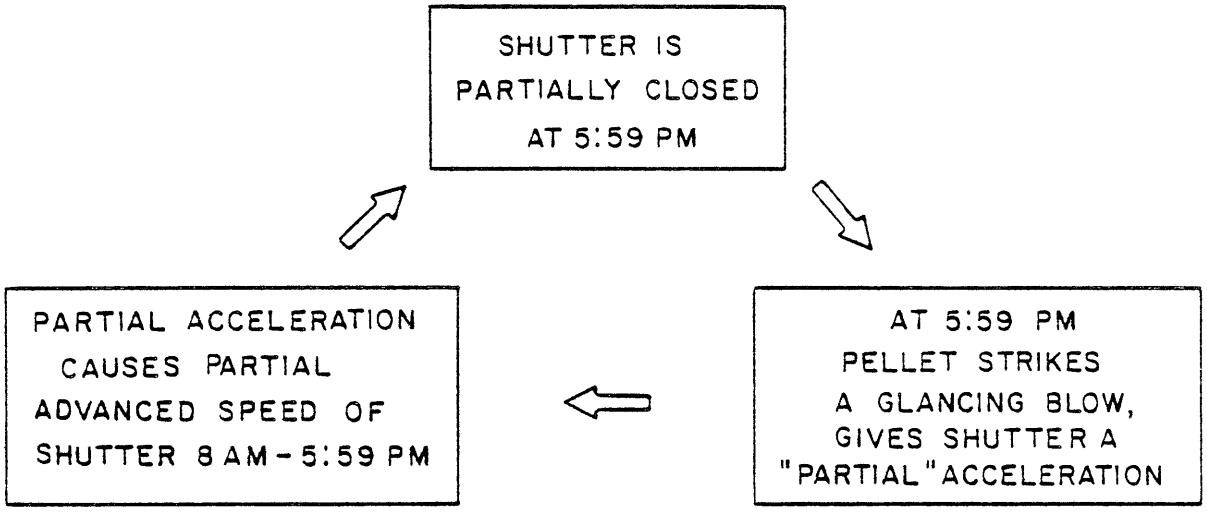

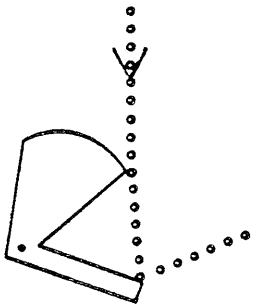

to a partial blow with the exact partial amplitude necessary if it does not have a continuum of possible responses available? How would we describe the motion of the pellet and shutter? Would logically consistent solutions be available for nature? There are many questions for further investigation.

Chapter 4

DESIGN OF THE EXPERIMENT

Our search for advanced effects was carried out with a microwave transmitter and receiver whose antenna design and positioning were, as previously described, motivated by the absorber theory of radiation.

Microwave pulses were sent out by the transmitter which was under computer control (see Figure 10). Figure 11 shows the expected time-response of the receiver to these microwave pulses. It is this response which we examined for advanced effects.

In Figure 11 we have noted that the retarded signal is delayed, as expected, by the transmitter to receiver transit time and arrives at the receiver a time $\frac{r}{c}$ after transmission. Thus any advanced signal would precede the retarded signal by $\frac{2r}{c}$, which in our experiment was 65 ns. In the discussion which follows we will refer to various time regions as indicated in Figure 11.

Figure 10. Outline of the apparatus.

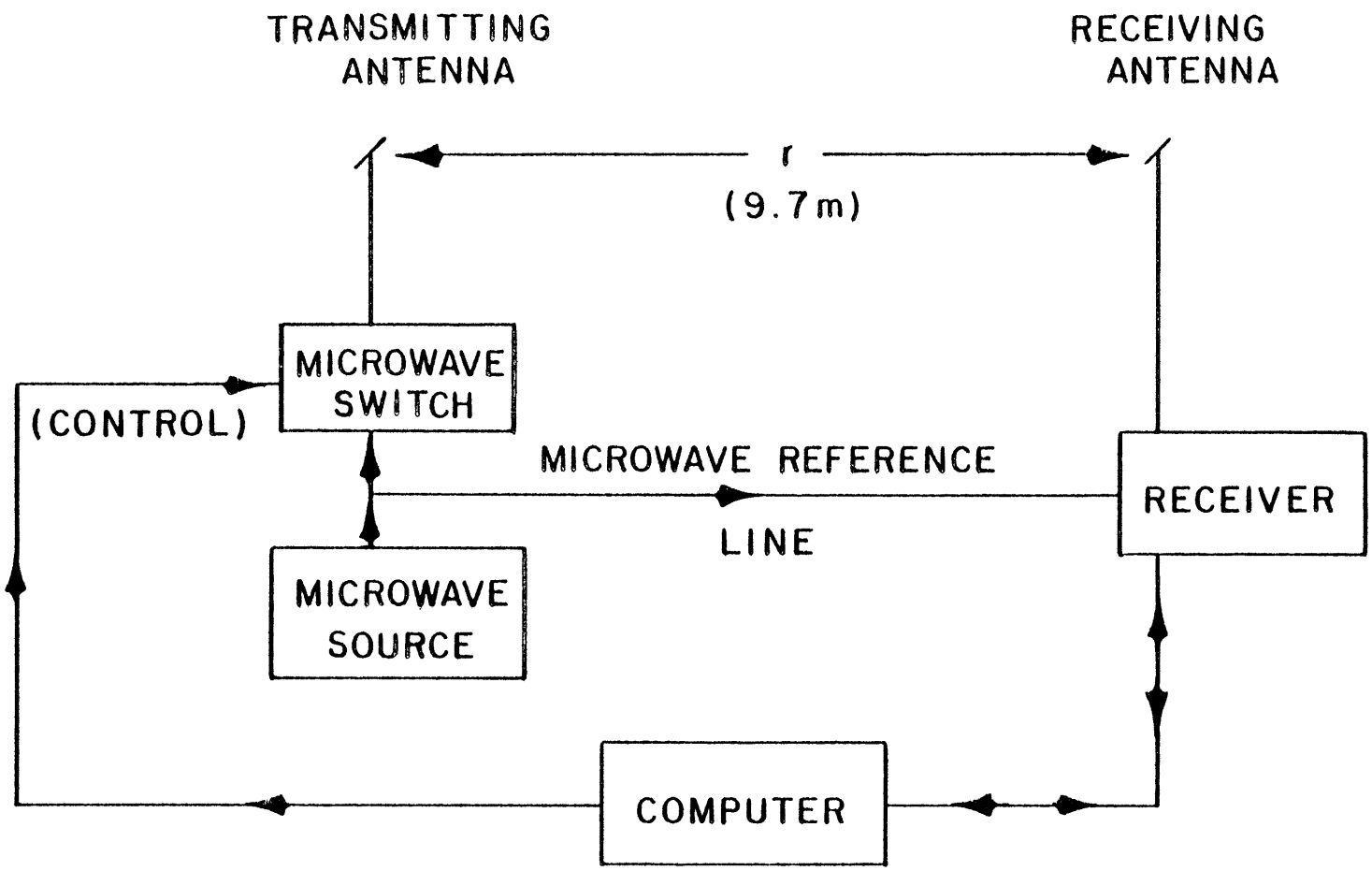
TRANSMITTING ANTENNA
RECEIVING ANTENNA
r
(9.7m)
MICROWAVE SWITCH
(CONTROL)
MICROWAVE REFERENCE LINE
RECEIVER
MICROWAVE SOURCE
COMPUTER

Figure 11. Sketch of expected response of the receiver to a microwave pulse from the transmitter; definition of time regions.

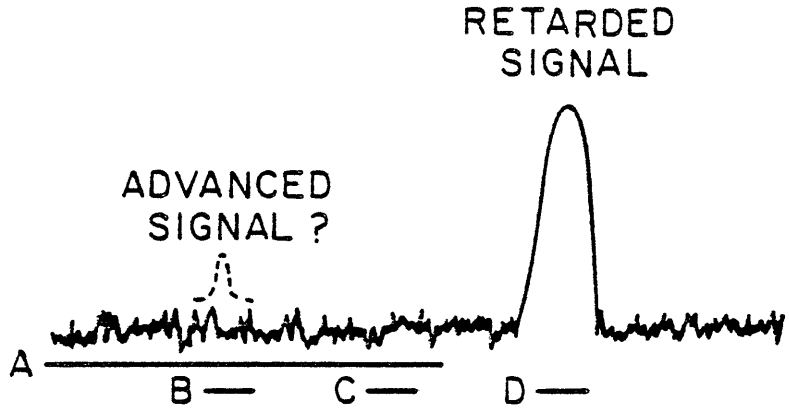

A: ADVANCED TIME-REGION
B: ADVANCED SIGNAL TIME-REGION
C: TIME OF TRANSMITTER PULSE
D: RETARDED SIGNAL TIME-REGION

Our experiment, in principle, consisted of comparing the amplitude measured in the advanced signal time-region with that in the retarded signal time-region to determine the ratio of advanced to retarded power:

$$\frac{P_{adv}}{P_{ret}} = \left(\frac{\text{advanced signal amplitude}}{\text{retarded signal amplitude}}\right)^2 .$$

In practice, however, a non-zero amplitude will be measured in the advanced signal time-region even in the absence of an advanced signal. This amplitude is due to noise, the existence of which constrained the result of our experiment to be, at worst, an <u>upper limit</u> on $\frac{P_{adv}}{P_{ret}}$. In order to reduce the effect of noise we sampled the advanced signal time-region many times and averaged the results.

Use of a microwave reference line to bring phase information to the receiver greatly improved the receiver's signal to noise capability, as will be discussed later.

The receiver output had a non-zero DC level. Because of this pedestal our most sensitive test for the existence of an advanced signal was a comparison of

the amplitude in the advanced signal time-region with that elsewhere in the advanced time region. To reduce the effects of drifts in the pedestal each of the various time regions were sampled frequently.

Steps were taken to reduce the effects of systematic sources of amplitude in the advanced time-region. These were both physical and/mathematical and will be described later.

Finally, there was little possibility of distant objects reflecting significant amounts of retarded microwave signal from one transmitted pulse back into the advanced time-region associated with the next transmitted pulse. The time between pulses, 128 μs, was large from the standpoint of this effect. Furthermore such radar signals off of randomly shaped objects like mountains lose power as $\frac{1}{(\text{range})^4}$.

Our experiment was carried out by varying, in 256 1ns increments, the time of the transmitter pulses relative to the time of receiver gating. The 256 time settings were scanned thru repeatedly, the results were integrated, and the resulting 256 data points were used to construct the graph whose form is represented by Figure 11.

Chapter 5

THE APPARATUS AND ITS OPERATION

5.1 ELEMENTS OF THE BLOCK DIAGRAM

A detailed block diagram of the experimental apparatus is given in Figure 12. The nature and purpose of most apparatus elements require no explanation beyond their identification in the figure. Many serve pulse shaping functions.

Our X-band travelling wave tube amplifier had a specified operating rage of 8.0 GHz to 12.4 GHz and output power capability of 10 watts. We measured its gain to be 45 db.

The microwave source is a Gunn diode oscillator, temperature stabilized against frequency drift. We operated it at a frequency measured to be 10.243 GHz, a free space wavelength of 29.2 mm. The power of the source was specified as 70 mW. We measured it to be 52 mW ± 10%. About half of this power flowed from the

Figure 12. Block diagram of the apparatus.

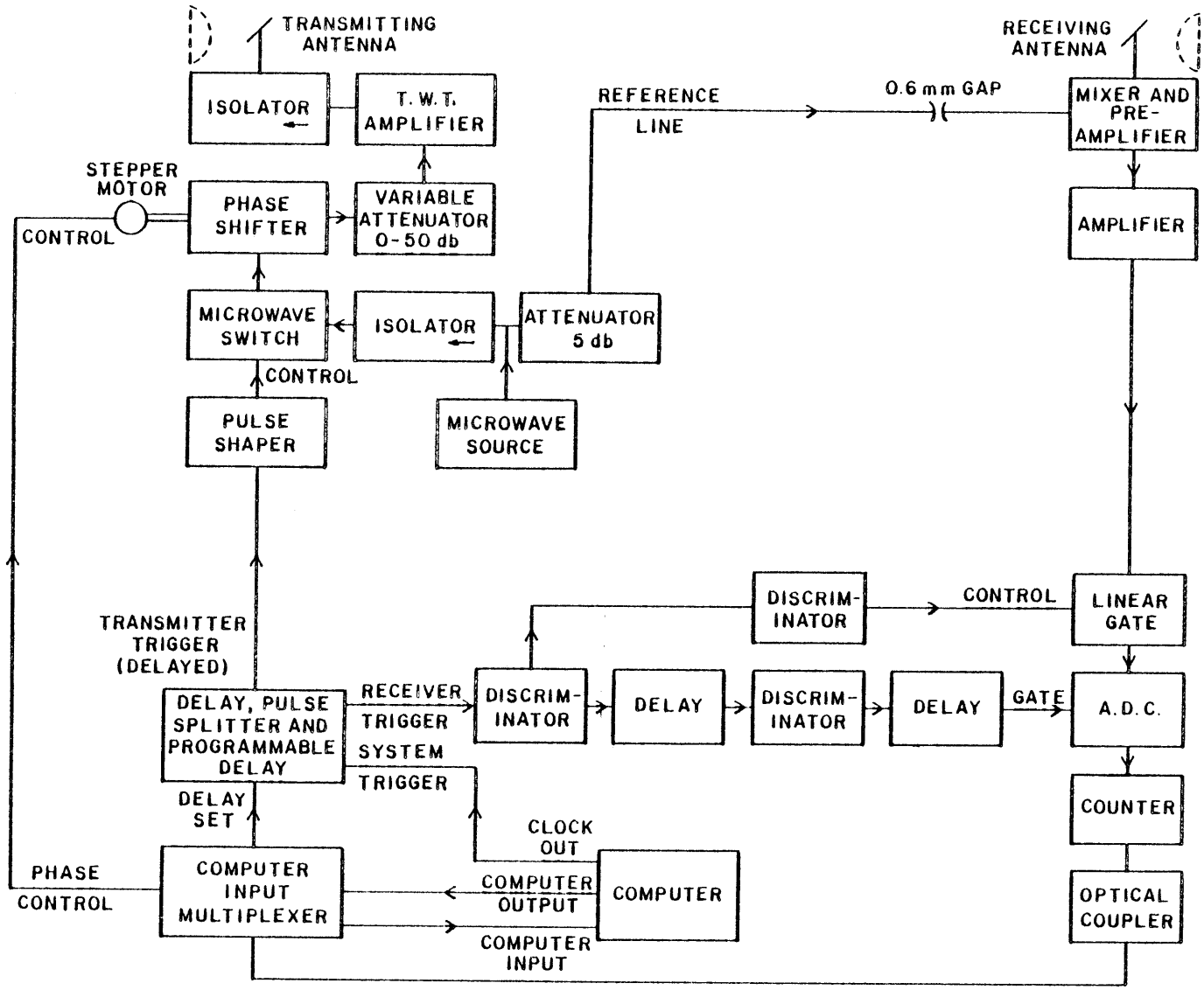
TRANSMITTING ANTENNA
ISOLATOR
T. W. T. AMPLIFIER
STEPPER MOTOR
PHASE SHIFTER
VARIABLE ATTENUATOR 0-50 db
CONTROL
MICROWAVE SWITCH
ISOLATOR
ATTENUATOR 5 db
CONTROL
PULSE SHAPER
MICROWAVE SOURCE
REFERENCE LINE
0.6 mm GAP
RECEIVING ANTENNA
MIXER AND PRE-AMPLIFIER
AMPLIFIER
DISCRIM-INATOR
CONTROL
LINEAR GATE
TRANSMITTER TRIGGER (DELAYED)
DELAY, PULSE SPLITTER AND PROGRAMMABLE DELAY
RECEIVER TRIGGER
SYSTEM TRIGGER
DISCRIM-INATOR
DELAY
DISCRIM-INATOR
DELAY
GATE
A.D.C.
COUNTER
DELAY SET
CLOCK OUT
PHASE CONTROL
COMPUTER INPUT MULTIPLEXER
COMPUTER OUTPUT
COMPUTER
COMPUTER INPUT
OPTICAL COUPLER

microwave source into the isolator, the other half into the attenuator at the beginning of the reference line.

The variable attenuator was set at 20 db during data collection runs in order to operate the TWT amplifier near, but not into, its saturation region. The instantaneous TWT amplifier output power then was measured to be about 4 watts. Under these conditions the receiver was driven to saturation, so that a measurement of the detected "peak retarded power" could not be made. In order to determine the retarded power detected by the receiving antenna, runs were made with the transmitted power reduced by a factor of 1000. This was accomplished by setting the variable attenuator at 50 db during these "calibration runs" so that the receiver would not saturate in the time region of the retarded peak.

The antennas were simple horizontal half wavelength dipoles, placed about 9.7 m apart. The voltage standing wave ratio (VSWR) of each antenna, a measure of its efficiency in radiating power delivered to it, was measured with the aid of a slotted waveguide section and probe. The antenna elements were adjusted to minimize reflection. After final adjustment the ratio of transmitted to reflected power was about 9.

The phase shifter was advanced by a stepper motor under computer control.

The microwave switch has specifications of 85 db minimum attenuation in the "off" mode and 2.6 db maximum attenuation in the "on" mode for 10 GHz microwaves.

The pulse-splitter and programmable delay would, upon receipt of the system trigger pulse from the computer, send out two pulses, one to trigger the transmitter and one to trigger the receiver. The transmitter trigger pulse was delayed by a time preset by the computer. Available delays ranged from 0 to 255 ns. This made it possible to vary under computer control the time at which the signal at the receiving antenna is sampled by the receiver, relative to the time that the transmitter is pulsed. Constant delays in the receiver trigger line were chosen to insure that use of at least part (the lower quarter) of the 0 to 255 ns transmitter trigger delay range resulted in receiver coverage of the retarded peak of the transmitted microwave pulse. The delay in this line was carried out in two steps with pulse shaping in between. The discriminators, E.G. & G. Model T121/NL, served to shape pulses in amplitude and duration.

5.2 PHANTOM STRUCTURE IN THE ADVANCED TIME REGION NOISE

A problem with the electronics was the presence of structure in the receiver noise at times just before the

expected receipt of the microwave pulse. This structure persisted even when the microwave source was off.

The source of the problem was found to be radiation from the computer associated with its execution of individual program instructions immediately after its emission of the system trigger pulse. The nature of the radiation reflected the particular programmable-delay setting being maintained at the time by the computer. The radiation was picked up by the receiver's ground.

This source of structure in the advanced time region noise was eliminated by inserting a 70 μs delay between the system trigger and the pulse splitter. This delayed transmitter and receiver triggering until completion of the computer program steps responsible for the difficulty.

5.3 TRANSMITTER TRIGGERING AND RECEPTION

The transmitter trigger pulse opens the microwave switch briefly, sending to the TWT amplifier a microwave pulse of 12 ns approximate width, with rise and fall time under 5 ns. Note that the 9.7 m antenna separation was about 2½ times the microwave pulse length.

The mixer received its phase information thru a reference line (see Figure 13) which delivered a power of about 9 mW from the microwave source.

Figure 13. Mixer function in the receiver.

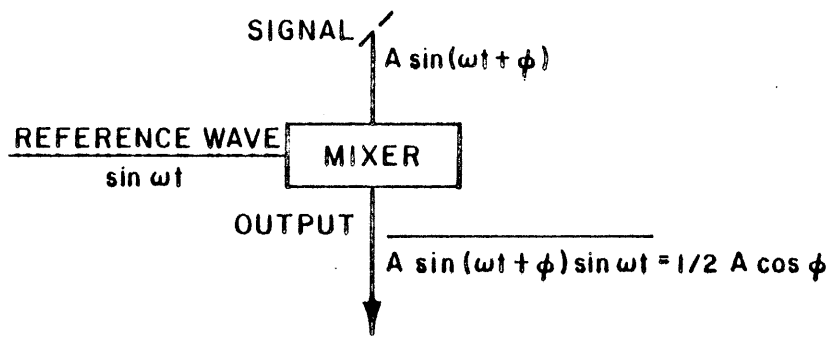

PHASE OF SIGNAL	OUTPUT
ϕ	$1/2\ A \cos \phi$
$(\phi + 180°)$	$-1/2\ A \cos \phi$
$(\phi + 90°)$	$-1/2\ A \sin \phi$
$(\phi + 90°) + 180°$	$1/2\ A \sin \phi$

The time averaged output of such a mixer and reference-wave set-up is a measure of the signal amplitude. If t represents the integrating (pulse accumulation) time, then we can write,

$$\text{(integrated signal amplitude)} \sim t$$
$$\text{(integrated noise amplitude)} \sim \sqrt{t}$$

so that the ratio of signal to noise power increases as $\left(\frac{t}{\sqrt{t}}\right)^2 = t$.

Without the reference wave we would be integrating signal and noise <u>powers</u> rather than amplitudes so that the signal power to noise power ratio would increase only as $\sqrt{t}$ rather than t as in our set-up.

The reference line waveguide was deliberately made longer than the antenna separation in order to delay any disturbance in the reference wave associated with transmitter triggering. Such a disturbance might otherwise mimic an advanced effect. For the same reason a small gap was maintained in the reference line waveguide near the receiver. This gap improved electrical separation of the transmitter and receiver by removing a possible ground loop path.

The linear gate served to protect the ADC from the large retarded signals which arrive during its processing of samples from the advanced time region. While the ADC has its own internal gate for this function, it was considered desirable to add this extra level of protection to insure that the ADC was sensitive only to the signal received during its gating time. The linear gate was set to open about 205 ns before the ADC gate opened and to close about 10 ns after the ADC gate closed. The linear gate has a specified opening and closing time of 2.5 ns.

The ADC integrates its input signal over a time defined by the width of its gating pulse, 7 ns. The result of this integration determines the number of 25 ns pulses sent out to the computer-read counter. The ADC output responded in a linear and bipolar fashion to its input signal level, with a zero input signal level corresponding to a non-zero number of output pulses.

The TWT input pulse was tested for drift in timing relative to the ADC gating pulse. The drift was less than 1 ns/day.

5.4 LINEARITY OF THE SYSTEM

The linearity of the entire transmitter-receiver system was tested by running it for about 7 minutes at

each of an increasing series of TWT amplifier input line attenuations. Each integrated received amplitude is plotted in Figure 14 against the associated transmitter attenuation. The point at about 85 db which is conspicuously off the graph represents possible failure to advance the attenuator by its 10 db intended increment.

In order to get better statistics at the highest transmitter attenuation, a much longer (about 9 hour) run was carried out in addition to the 7 minute run. The resulting data point is slightly off the line due, possibly, to drifts in the TWT gain which were associated with such long runs. Frequent sampling of various time regions minimized the effects of drifts.

5.5 THE COMPUTER CONTROLLED SEQUENCE

The computer controlled various apparatus elements in a sequence described as follows.

After setting initial phase and delay parameters, the computer generated 256 master trigger pulses, at 128 μsec intervals. Each trigger pulse was split to trigger the transmitter and gate the receiver with relative timing determined by the delay parameter. After each sequence of 256 pulses the computer read and cleared the ADC counter, and changed the delay setting

Figure 14. Linearity of the transmitter-receiver system.

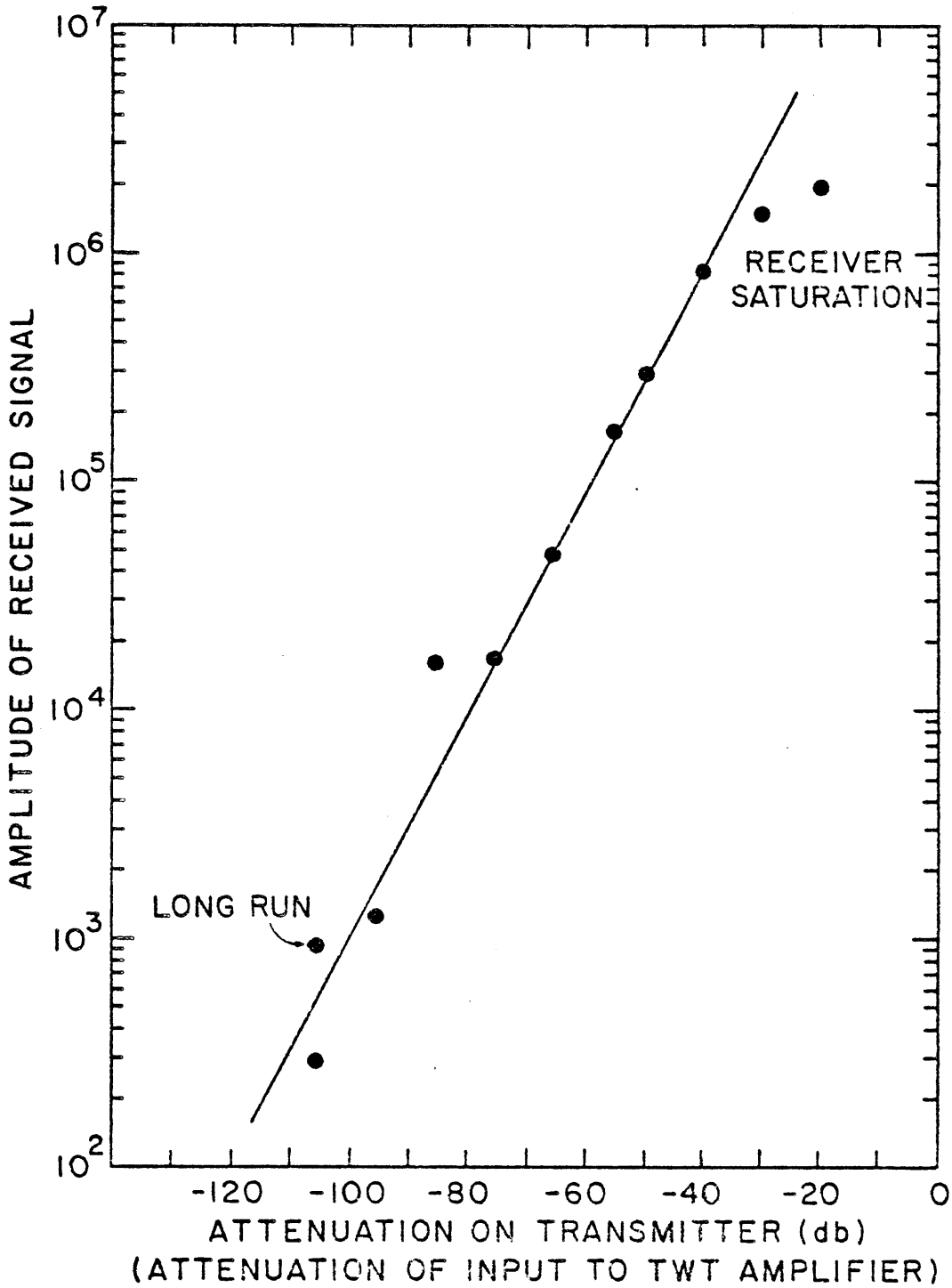
AMPLITUDE OF RECEIVED SIGNAL
10^7
10^6
10^5
10^4
10^3
10^2
RECEIVER SATURATION
LONG RUN
-120
-100
-80
-60
-40
-20
0
ATTENUATION ON TRANSMITTER (db)
(ATTENUATION OF INPUT TO TWT AMPLIFIER)

by 1 ns. After a total of 64 x 256 x 256 pulses, representing 64 scans of the delay time setting thru its range of 256 ns, the computer reset the phase setting and repeated the above cycle. The counter readings for the various delay settings constituted the raw data for the experiment.

5.6 MICROWAVE LENSES

In what amounts to a second experiment, data was collected with microwave lenses mounted as shown, in a position intended to focus advanced radiation.

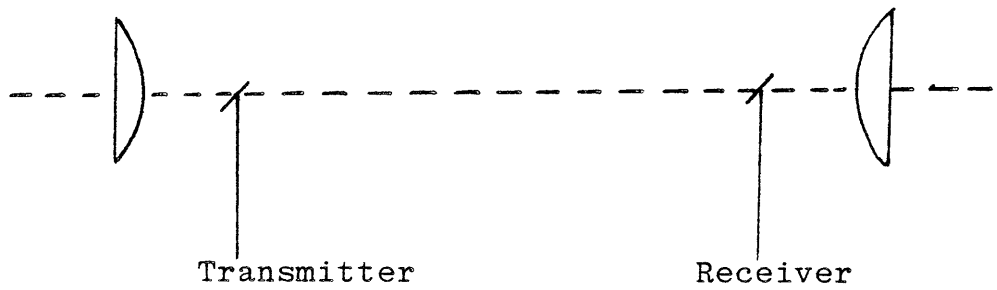

Retarded radiation from the transmitting antenna will be beamed away (to the left in the diagram) as a plane wave by the nearby lens, diverging only due to the effects of diffraction. Recalling our discussion of the absorber theory of radiation (see Chapter 2, Figures 3 and 4), this lens, in effect, increases the fraction of the transmitter's retarded radiation which falls within the cone of

possibly incomplete eventual absorption. The advanced radiation in this cone is increased in equal proportion. Finally, viewed forward in time, this advanced radiation converging from infinity onto the transmitting antenna will pass thru the receiving antenna's lens.

The lenses were made from "Eccofoam 625D" (Emerson and Cuming, Inc.), an artificial dielectric with dielectric constant, $K = 6$. We require that plane waves incident from the left (see Figure 15) arrive in phase at the origin: $nt + f = n(t + f - r\cos\Theta) + r$. This gives the equation for the lens profile:

$$r = \frac{(n - 1)\, f}{n \cos\Theta - 1} ,$$

where n, the index of refraction of the lens material, is given by $n = \sqrt{K}$.

f is fixed by the values of d and t, which are 12 inches and 1 inch respectively. f is found by writing r and Θ at point P in terms of d, f, and t and using the results in the profile equation given above. Then,

$$f = \frac{d^2 - 4(n^2 - 1)t^2}{8(n-1)t} .$$

Figure 15. Definition of plano-convex lens profile parameters.

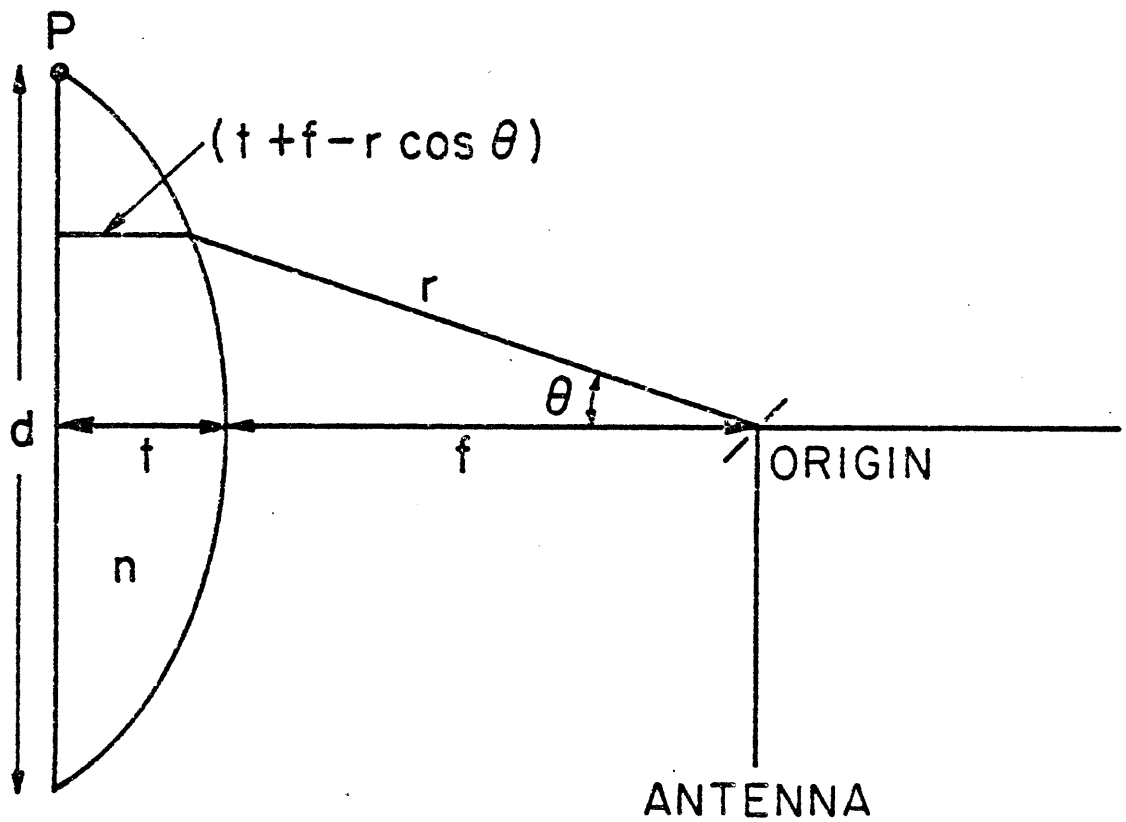
P
(t + f − r cos θ)
r
θ
d
t
f
ORIGIN
n
ANTENNA

In rectangular coordinates the profile equation is

$$y = \sqrt{n - 1} \quad \sqrt{(n+1)x^2 - 2nfx + (n-1)f^2} \ .$$

With $n = \sqrt{6}$, $f = 10.69$ inches and

$$y = \sqrt{5x^2 - 31 \sqrt{6}\ x + 240.25} \qquad \text{(inches)}.$$

The lenses were ground using this equation. It is a hyperbola and gives a lens causing no aberration of non para-axial rays.

The gain of the lenses was tested with the lenses in the retarded position.

Geometrically, the theoretical power gain of the lenses is approximately $\left(\frac{\Theta'}{\Theta}\right)^2$ (see Figure 16). Θ is related to the diameter of the antenna's effective receiving area, $A = \frac{\lambda^2}{4\pi}$, and the antenna separation, ℓ, by $\ell\Theta = \sqrt{\frac{4A}{\pi}}$. Θ' is given by $(f + t)\Theta' \approx d$ so that

$$\left(\frac{\Theta'}{\Theta}\right)^2 = \left[\frac{\pi d \ell}{(f+t)\lambda}\right]^2 = 61 \text{ db}.$$

Figure 16. Definition of parameters for calculation of the theoretical gain of the lens system.

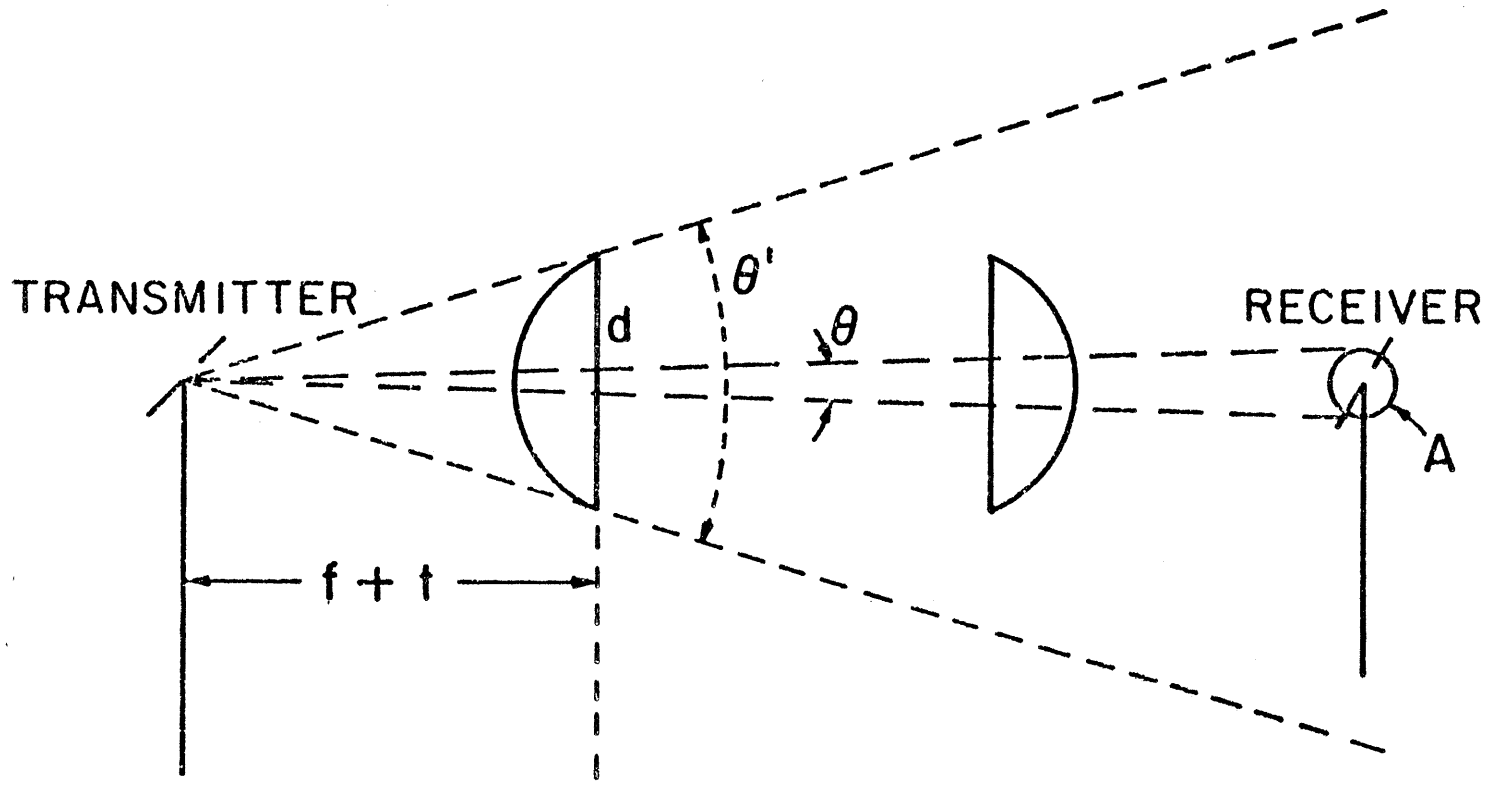
TRANSMITTER
d
θ'
θ
RECEIVER
A
f + t

Diffraction, however, limits the effectiveness of the lens system. The radiation captured by the transmitting lens will not all be beamed directly toward the receiving lens, but will spread out from the axis over a diffraction angle given by $1.22 \frac{\lambda}{d} = 0.12$ radian. The receiving lens subtends an angle from the transmitting lens of only $\frac{d}{\text{(lens separation)}} = 0.034$ radian, and therefore captures a fraction of the power given by $\left[\frac{0.034}{2 \times 0.12}\right]^2 = 0.020 = -17$ db. Furthermore, diffraction limits the fraction of this captured radiation which will finally arrive within the receiving antenna's effective area, A. The fraction captured by A is

$$\left\{ \sqrt{\frac{4A}{\pi}} \div \left[2 \left(\frac{1.22\lambda}{d}\right)(f + t) \right] \right\}^2 = -17.5 \text{ db.}$$

The 61 db geometrical gain, corrected for the 17 db and 17.5 db diffraction losses, gives the expected power gain of the lens system, 26.5 db.

The gain was measured to be 25.9 db. The discrepancy may be due to non-ideal lens shape or placement.

Chapter 6

DATA COLLECTION AND RESULTS OF THE EXPERIMENT

6.1 DATA COLLECTION

The receiving antenna was placed 9.7 m from the transmitting antenna. Therefore it was expected that any advanced signal would be received $\frac{2(9.7\ \text{m})}{3 \times 10^8\ \text{m/s}} = 65$ ns before the retarded signal.

The receiver was monitored at regular 128 μsec intervals while the associated transmitter triggerings were delayed by various times ranging up to 255 ns. The transmitter triggering delays were advanced in 1 ns increments by a programmable delay-line under computer control (see block diagram, Chapter 5, Figure 12). (The delay settings for the time region of greatest interest were calibrated with a 100 ps/channel multi-channel analyzer.) Thus the receiver was monitored at a spectrum of times, including times when the retarded signal was at its antenna as well as times up to about

190 ns earlier. This advanced region, in particular the time region around 65 ns before the retarded signal, was examined for advanced effects.

"Monitoring the receiver" for a given transmitter triggering delay setting was part of a sequence of events initiated by the system trigger pulse from the computer (see block diagram, Chapter 5, Figure 12). In the receiver section of the apparatus this included gating the ADC with a 7 ns pulse. The ADC then output a train of pulses to a counter (see block diagram, Chapter 5, Figure 12). The number of pulses in the train was directly proportional to the signal amplitude out of the receiver amplifier, integrated over the 7 ns gating time.

Without changing the transmitter trigger delay setting, the system was triggered 256 times with the results accumulated by the counter. The counter was then read and cleared by the computer. The reading was stored in a bin identified by the delay-setting time and was a measure of the signal amplitude received at a particular time relative to the retarded pulse.

This process was repeated for each of the 256 transmitter triggering delay settings.

Thus after one "sweep" of all the delay settings the ADC has been gated 256 x 256 times and the computer has stored 256 numbers, one for each delay setting.

The 256 numbers are incremented by each sweep thru the delay settings. After 64 sweeps, called one "run", the phase shifter (see block diagram, Chapter 5, Figure 12) was changed by 180° and another run was done.

6.2 TREATMENT OF THE DATA

The results of the two runs (two sets of 256 numbers) are <u>subtracted</u> in order that only contributions to the amplitude due to microwaves originating after the phase shifter survive (see block diagram, Chapter 5, Figure 12). This is because the 180° phase shift reverses the sign of the amplitude on the microwave signals received. This procedure, though, subtracts away the systematic effects of other sources of ADC input such as might be associated with the delay-setting electronics.

In addition to the run_{ϕ} and $run_{\phi+180^{\circ}}$ described above we carried out another pair of runs, $run_{(\phi+90^{\circ})}$ and $run_{(\phi+90^{\circ})} + 180^{\circ}$. The corresponding elements within this pair were also subtracted.

The results of the two subtractions can be used to find the phase (ϕ) and amplitude (A) of the signal.

If we define:

$$A_i \cos\phi_i \equiv [\text{run}\,\phi]_i - [\text{run}_{\phi+180^o}]_i \tag{6.1}$$

and $$A_i \sin\phi_i \equiv [\text{run}_{(\phi+90^o)}]_i - [\text{run}_{(\phi+90^o)+180^o}]_i \tag{6.2}$$

where i = 0,...,255.

then $$A_i = \sqrt{(A_i \cos\phi_i)^2 + (A_i \sin\phi_i)^2}$$

and $$-\phi_i = \tan^{-1}\left[\frac{A_i \sin\phi_i}{A_i \cos\phi_i}\right].$$ (See Chapter 5, Figure 13).

Graphically, the amplitudes take the form shown in Figure 17.

We call the set of four runs at different phases a "quadrature set".

Data was recorded for 24 such four-run sets. Each run required about 13 min 51 seconds for completion. The total number of ADC gatings was 3×2^{27} or about 4.0×10^8.

These data are integrated as follows: in each of the 24 quadrature sets the two subtractions are carried out as indicated above (Equations 6.1 and 6.2).

Figure 17. Sketch showing form of received amplitude with time.

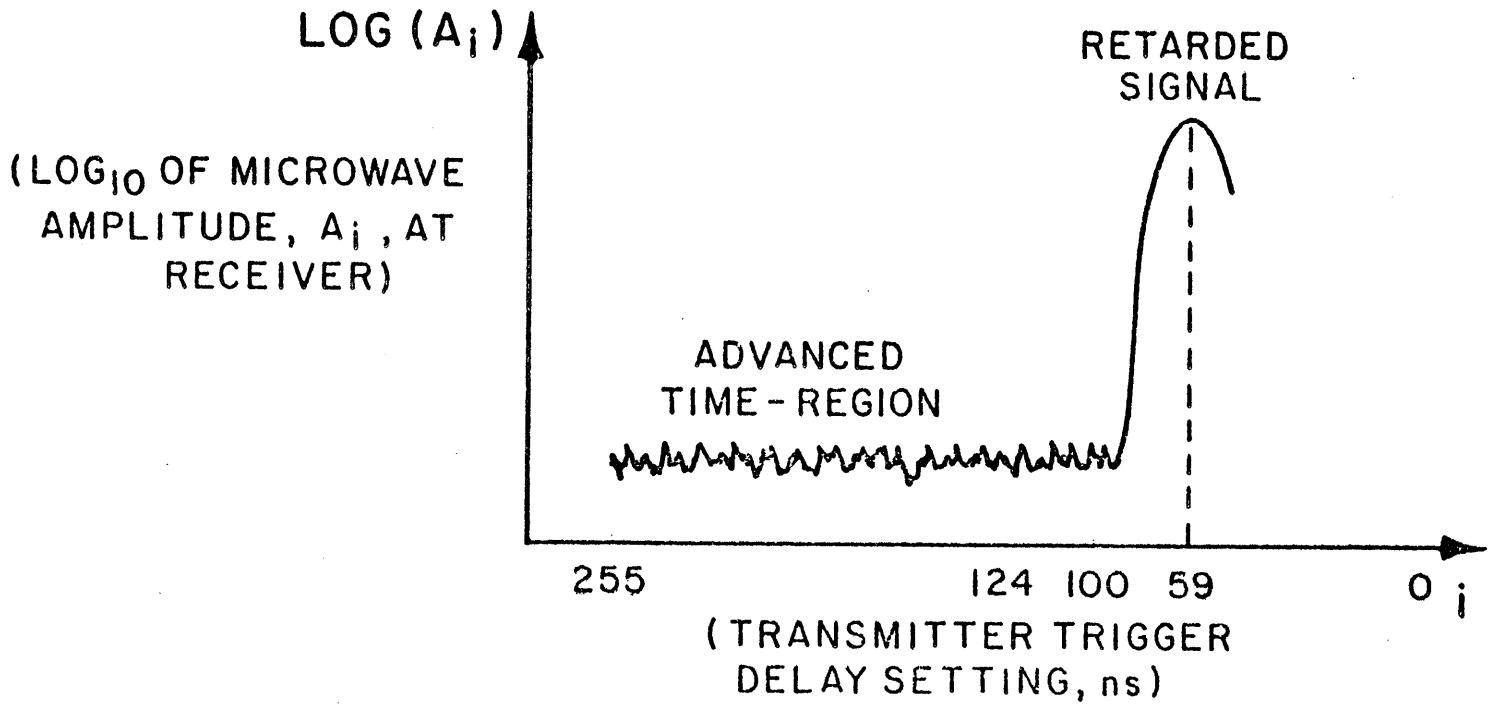
LOG (A_i)
(LOG$_{10}$ OF MICROWAVE AMPLITUDE, A_i, AT RECEIVER)
RETARDED SIGNAL
ADVANCED TIME-REGION
255
124
100
59
0
i
(TRANSMITTER TRIGGER DELAY SETTING, ns)

The 24 resulting difference sets which are labeled $A_i \cos\phi_i$ are summed into one set and the 24 resulting difference sets which are labeled $A_i \sin\phi_i$ are summed into another set. From the 256 elements of each of these two sum sets we subtract the average of each set's own advanced region delay bin contents. The time region i = 100 - 255 (see Figure 17) was used for this purpose. This subtraction is carried out in order to make the average noise amplitude zero and in order to reduce the effect of any drift in the offset, the number of pulses put out by the ADC for zero integrated signal. After the offset subtraction within each of the two sets, the 256 corresponding pairs of elements in the two sets are added in quadrature.

6.3 RESULTS OF THE EXPERIMENT

The final resulting set of 256 numbers again has the form shown in Figure 17. In the advanced time region no peak is seen to stand out above the noise. Therefore we use the advanced time region noise level as an upper limit on the advanced signal level. Specifically we use twice the standard deviation of the 100 ns to 255 ns delay bin contents. This 2σ choice gives a confidence level of about 95%. Our upper limit on the advanced signal power is to be expressed as a fraction of the retarded signal power to which it corresponds.

The retarded peak, however, saturated our receiver. Because of this we made periodic calibration runs during which 30 db attenuation was added to the transmitter output line (see block diagram, Chapter 5, Figure 12), thereby alleviating receiver saturation. These runs consisted of 8 sweeps thru the delay settings instead of the normal 64. Retarded peak amplitudes were determined by taking the average of eight 1 ns delay bin contents around the retarded peak. The retarded peak amplitude finally used was the average result of a number of calibration runs. Before comparison with the advanced amplitude's upper limit this average retarded amplitude was put on an equal basis by scaling it up by a factor of

$$\begin{bmatrix}\text{retarded peak}\\ \text{calibration}\\ \text{scale-up}\\ \text{factor}\end{bmatrix} = \left[\frac{\text{24 quadrature sets of data}}{\text{1 quadrature set for calibration data}} \times \frac{64\ \frac{\text{sweeps}}{\text{run}}}{8\ \frac{\text{sweeps}}{\text{run}}} \times \sqrt{30\ \text{db}}\right] = 6072$$

Then our upper limit on the ratio of advanced power to the retarded power with which it is associated is given by

$$r \equiv \frac{P_{adv}}{P_{ret}} = \left[\frac{2\sigma/\sqrt{8}}{\begin{pmatrix}\text{retarded peak}\\ \text{amplitude from}\\ \text{calibration}\end{pmatrix} \times \begin{pmatrix}\text{retarded peak}\\ \text{calibration}\\ \text{scale-up factor}\end{pmatrix}}\right]^2 \qquad (6.3)$$

$\sigma\sqrt{8}$ is the standard deviation of the average of 8 delay bin contents. (In particular, the group of 8 delay bins which make up the advanced signal time-region.)

24 quadrature sets of data were also accumulated with microwave lenses mounted in a position to focus advanced radiation. These lenses provided a gain of 25.9 db. It must be emphasized that this lens system gain was measured with the lenses mounted in the retarded position. The same gain is expected when the lenses are mounted to focus advanced radiation, although this cannot be measured empirically in the absence of advanced radiation.

Table 1 summarizes the data and their use in Equation 6.3. The final result of our experiment is an upper limit on the amount of advanced electromagnetic radiation associated with normally observed retarded radiation.

Expressed as a fraction of the power of the retarded transmitted signal, we measured

$$(\text{advanced power}) < 10^{-11.5}\ (\text{retarded power})$$

for the lensless experimental configuration, and

$$(\text{advanced power}) < 10^{-14.0}(\text{retarded power})$$

for the experiment with lenses.

The microwave antennas were positioned so as to maximize the possibility, within the absorber theory of radiation, of detecting advanced radiation: earth-based absorber did not intercept the extended line

Table 1. Results of the Experiment.

	without lenses	with lenses
σ_{adv} (standard deviation of noise in advanced time region, delay settings 100 ns - 255 ns) (ADC output counts)	5403	5711
σ_{adv} (standard deviation of noise in section of advanced region where advanced signal would be expected, delay settings 116 ns - 131 ns) (ADC output counts)	2816	4528
retarded peak amplitude from calibration (ADC output counts)	348,900	349,100
$r \equiv \left(\frac{P_{adv}}{P_{ret}}\right)_{\text{upper limit}}$	3.25×10^{-12} $= 10^{-11.5}$	3.63×10^{-12} $= 10^{-11.4}$ Adding in the lens gain of 25.9 db: 9.33×10^{-15} $= 10^{-14.0}$

connecting our antennas. It will be shown in Chapter 9 that absorption by the earth's atmosphere was negligible. Then, within the Wheeler-Feynman theory, our purely retarded result indicates there is eventual absorption elsewhere. Thus if the absorber theory of radiation is valid, the universe must be a complete or very nearly complete absorber (transmission less than about 1 part in 10^{11}) of 10 GHz electromagnetic radiation.

σ for the advanced signal region is smaller than σ for the entire advanced region. If this were of statistical significance it could be interpreted as a "cooling" of the receiving antenna due to advanced action on its side facing the transmitter. ('Inner face' advanced effects remove energy from the absorber as mentioned at the end of Section 2.5.) It is, however, not of clear statistical significance and further examination of the data or further experimentation may be required to resolve this point.

The graphs in Figures 18 and 19 display the results of the final treatment of data for the "without lenses" and "with lenses" series of runs, respectively. Scaled-up calibration run results are shown in the retarded signal time region where the receiver normally saturated.

Figure 18. Graph of the results of the lensless experiment.

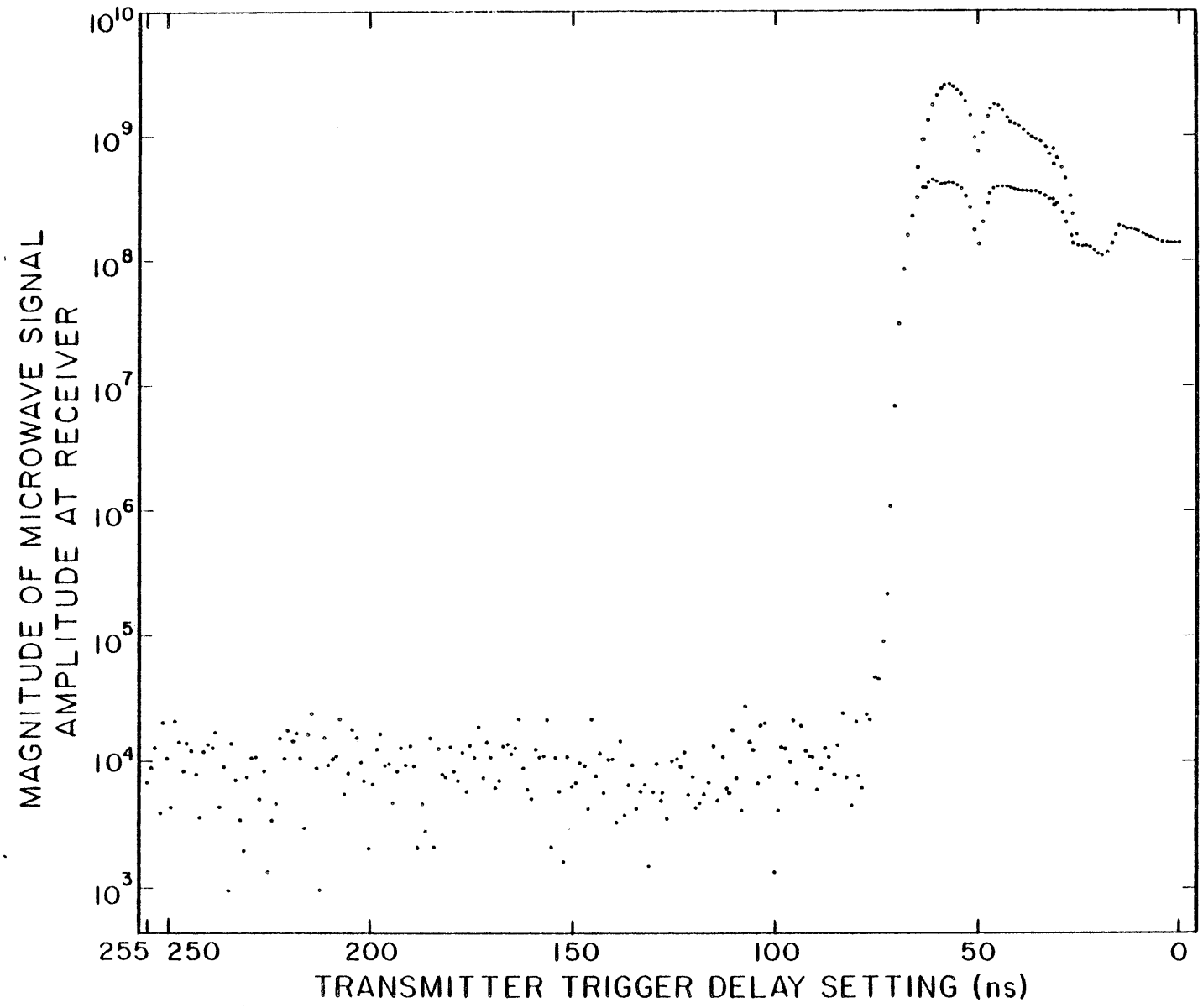
MAGNITUDE OF MICROWAVE SIGNAL
AMPLITUDE AT RECEIVER
10^{10}
10^{9}
10^{8}
10^{7}
10^{6}
10^{5}
10^{4}
10^{3}
255
250
200
150
100
50
0
TRANSMITTER TRIGGER DELAY SETTING (ns)

Figure 19. Graph of the results of the experiment using lenses.

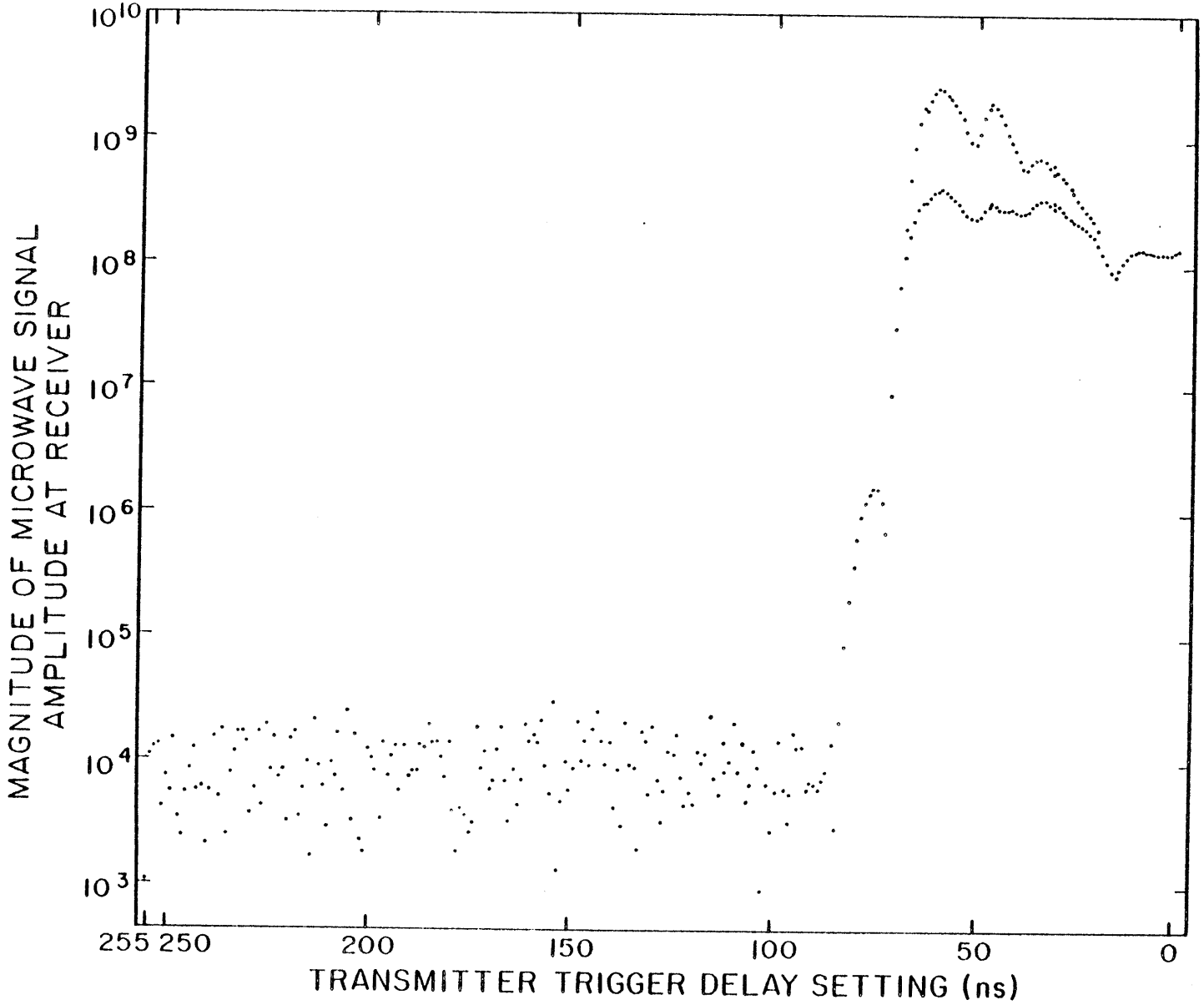
MAGNITUDE OF MICROWAVE SIGNAL
AMPLITUDE AT RECEIVER
10^{10}
10^{9}
10^{8}
10^{7}
10^{6}
10^{5}
10^{4}
10^{3}
255 250
200
150
100
50
0
TRANSMITTER TRIGGER DELAY SETTING (ns)

6.4 STRUCTURE OF THE LOG GRAPHS

It can be seen in the graphs that the retarded peak has a double hump. The mixer-preamplifier has a bandpass of 10 MHz to 200 MHz and therefore an AC response. A monopolar pulse emerges as bipolar. Thus the trailing edge of the retarded pulse generates a mixer-preamplifier output pulse which appears as a second peak after it is made positive by the previously described quadrature calculations. The two peaks are separated by about 12 ns, consistent with the microwave signal pulse width.

The with-lens graph shows a small peak on the leading edge of the retarded peak. This peak is of about 60 db less power than the retarded peak and is the result of microwave leakage from sections of the transmitter between the microwave switch and the TWT amplifier (see block diagram, Chapter 5, Figure 12).

This leakage goes directly to the receiver without delay in the TWT amplifier and thus appears slightly earlier than the full power retarded signal. It was reduced in the runs without lenses by appropriate shielding.

The values of r, the ratio of advanced to retarded signal power given in Table 1, can be roughly determined directly from the graphs by squaring the estimated

ratio of retarded peak amplitude to advanced region amplitude.

Tables 2 and 3 contain the amplitudes and calibrated delay settings which are plotted against each other in Figures 18 and 19.

Table 2. Integrated data for the "without lenses" experimental configuration. (Scaled-up non-saturated data appears in parentheses.)

Delay Setting in ns	Log of Amplitude	Delay Setting in ns	Log of Amplitude	Delay Setting in ns	Log of Amplitude	Delay Setting in ns	Log of Amplitude
0.00	8.1345	63.74	8.5806 (8.9563)	128.16	3.6882	192	4.1151
1.01	8.1343	64.80	8.4967 (8.7383)	129.10	3.9876	193	3.9356
2.22	8.1302	66.10	8.3596	130	3.7637	194	3.6795
3.30	8.1312	67.17	8.1896	131	3.1697	195	3.9867
4.43	8.1428	68.22	7.9265	132	3.8202	196	3.9785
5.52	8.1585	69.30	7.4978	133	3.7672	197	4.2381
6.54	8.1710	70.34	6.8461	134	3.6308	198	4.1116
7.46	8.1796	71.34	6.0440	135	3.9804	199	3.8306
8.37	8.1922	72.34	5.3404	136	3.8210	200	3.3150
9.31	8.2095	73.31	4.9632	137	3.5743	201	3.8527
10.26	8.2257	74.30	4.6584	138	4.1722	202	4.0032
11.17	8.2338	75.23	4.6758	139	3.5238	203	4.1899
12.21	8.2395	76.28	4.3369	140	4.0286	204	4.2690
13.22	8.2512	77.27	4.3808	141	4.0186	205	3.9212
14.32	8.2694	78.32	3.8000	142	3.7517	206	3.7521
15.34	8.2703	79.33	3.8888	143	4.0703	207	4.3533
16.10	8.2041	79.93	4.3211	144	3.8912	208	4.0570
17.11	8.1295	80.99	3.6448	145	4.3427	209	4.0243
18.41	8.0576	82.24	3.8750	146	3.6278	210	3.9853
19.50	8.0386	83.29	4.3947	147	3.9675	211	4.2001
20.52	8.0464	84.37	4.1323	148	3.9916	212	2.9833
21.57	8.0732	85.41	3.3943	149	3.8386	213	3.9566
22.60	8.1053	86.49	4.0405	150	3.8057	214	4.4007
23.54	8.1176	87.47	4.1088	151	4.0411	215	4.2269
24.55	8.1106	88.48	3.9484	152	3.2038	216	3.4765
25.46	8.1053 (8.2026)	89.46	3.7768	153	3.7632	217	4.0343
26.45	8.1258 (8.3647)	90.44	4.0380	154	4.0376	218	4.2366
27.36	8.1912 (8.5096)	91.37	4.0480	155	3.3269	219	4.1728
28.39	8.2964 (8.6460)	92.46	4.0845	156	4.3411	220	4.2588
29.38	8.3819 (8.7347)	93.48	4.2870	157	4.0498	221	4.0364
30.48	8.4489 (8.8073)	94.57	3.8279	158	4.0456	222	4.2042
31.49	8.4877 (8.8842)	95.48	4.3331	159	4.1105	223	3.6767
31.34	8.4301 (8.7642)	95.94	3.9933	160	3.7089	224	3.5371
32.40	8.4780 (8.8410)	96.97	4.1053	161	3.7795	225	3.1256
33.61	8.5120 (8.9009)	98.24	4.1216	162	3.9527	226	3.9348
34.73	8.5314 (8.9462)	99.33	3.6150	163	4.3510	227	3.7078
35.82	8.5433 (8.9703)	100.26	3.1155	164	4.1130	228	4.0483
36.92	8.5473 (8.9801)	101.31	3.8786	165	4.0583	229	4.0452
37.95	8.5470 (9.0038)	102.35	4.3120	166	4.1451	230	3.8915
38.94	8.5482 (9.0357)	103.38	4.2919	167	4.1284	231	3.3035
39.89	8.5546 (9.0678)	104.39	3.8316	168	3.8575	232	3.5516
40.85	8.5645 (9.0809)	105.38	4.0926	169	3.7971	233	3.8642
41.85	8.5736 (9.0938)	106.33	4.1574	170	4.0357	234	4.1527
42.84	8.5786 (9.1333)	107.30	4.4422	171	4.1587	235	2.9796
43.90	8.5816 (9.1897)	108.32	3.6086	172	3.8712	236	3.9693
44.94	8.5839 (9.2346)	109.33	3.8741	173	4.2871	237	3.6505
46.00	8.5722 (9.2397)	110.39	4.2578	174	4.0323	238	4.2434
46.97	8.5342 (9.2078)	111.39	3.7575	175	4.1377	239	4.1227
47.53	8.4569 (9.1461)	111.90	3.7896	176	3.7652	240	4.1550
48.58	8.3068 (9.0137)	112.97	4.0407	177	4.0813	241	4.0923
49.85	8.1237 (8.8580)	114.19	3.6914	178	3.8429	242	3.5685
50.94	8.2455 (8.9728)	115.27	4.1285	179	3.9266	243	3.9164
52.01	8.4239 (9.1594)	116.31	3.8381	180	4.1249	244	4.0968
53.07	8.5169 (9.2664)	117.37	3.7434	181	3.8850	245	4.1622
54.15	8.5698 (9.3249)	118.43	3.6708	182	3.9060	246	3.9355
55.13	8.5969 (9.3577)	119.41	3.6283	183	4.1080	247	4.1695
56.13	8.6120 (9.3790)	120.38	3.8756	184	3.3283	248	4.3324
57.09	8.6164 (9.3944)	121.38	3.7388	185	4.1948	249	3.6447
58.07	8.6115 (9.3919)	122.32	4.0763	186	3.4488	250	4.0383
59.12	8.6091 (9.3679)	123.32	3.9634	187	3.6737	251	4.3247
60.08	8.6214 (9.3089)	124.22	4.0288	188	3.3269	252	3.5980
61.09	8.6349 (9.2299)	125.37	4.0082	189	3.9739	253	4.1165
62.15	8.6234 (9.1084)	126.55	3.5462	190	4.1355	254	3.9628
63.13	8.5758 (8.9516)	127.57	3.7523	191	3.9747	255	3.8445

Table 3. Integrated Data for the "With Lenses" Experimental Configuration. (Scaled-up non-saturated data appears in parentheses.)

Delay Setting in ns	Log of Amplitude	Delay Setting in ns	Log of Amplitude	Delay Setting in ns	Log of Amplitude	Delay Setting in ns	Log of Amplitude
0.00	8.1102	63.74	8.4851 (9.2371)	128.16	3.8428	192	3.7489
1.01	8.0995	64.80	8.4282 (9.1173)	129.10	4.2790	193	4.1083
2.22	8.0855	66.10	8.3342 (8.9209)	130	3.7394	194	4.0253
3.30	8.0762	67.17	8.2180 (8.6588)	131	4.1525	195	3.8683
4.43	8.0724	68.22	8.0542 (8.2770)	132	4.2279	196	4.1362
5.52	8.0756	69.30	7.8158	133	3.2879	197	3.5224
6.54	8.0838	70.34	7.4727	134	3.9427	198	3.9061
7.46	8.0937	71.34	6.9415	135	3.9621	199	4.0118
8.37	8.1028	72.34	5.8254	136	4.3042	200	4.0878
9.31	8.1074	73.31	6.0814	137	3.4772	201	3.2585
10.26	8.1062	74.30	6.1853	138	3.9303	202	3.3503
11.17	8.0992	75.23	6.1889	139	3.6171	203	4.1925
12.21	8.0814	76.28	6.1453	140	4.1405	204	3.5095
13.22	8.0543	77.27	6.0729	141	3.9724	205	4.3875
14.32	8.0123	78.32	5.9579	142	4.1493	206	3.7481
15.34	7.9626	79.33	5.7838	143	4.4029	207	4.2095
16.10	7.9051	79.93	5.5619	144	4.2521	208	3.8617
17.11	7.9334	80.99	5.2942	145	3.9602	209	3.9737
18.41	8.0114	82.24	4.9241	146	4.1588	210	3.4602
19.50	8.0854	83.29	4.3137	147	3.9905	211	3.7808
20.52	8.1542 (8.2754)	84.37	3.4460	148	4.3103	212	3.9493
21.57	8.2061 (8.3417)	85.41	4.1371	149	3.9351	213	4.3202
22.60	8.2449 (8.3787)	86.49	3.9088	150	3.7659	214	3.2178
23.54	8.2727 (8.4154)	87.47	3.8466	151	3.9785	215	3.9824
24.55	8.2978 (8.4611)	88.48	3.7743	152	3.6681	216	3.7761
25.46	8.3206 (8.5163)	89.46	3.8058	153	3.1111	217	3.5331
26.45	8.3414 (8.5681)	90.44	3.8190	154	4.4657	218	4.2158
27.36	8.3618 (8.6075)	91.37	3.7748	155	3.7236	219	4.1724
28.39	8.3905 (8.6447)	92.46	4.1123	156	3.9522	220	3.5087
29.38	8.4220 (8.6932)	93.48	4.0996	157	4.3197	221	3.9185
30.48	8.4588 (8.7394)	94.57	4.2146	158	4.1361	222	3.8516
31.49	8.4868 (8.7851)	95.48	3.7285	159	4.2016	223	4.1809
31.34	8.4431 (8.7216)	95.94	3.4895	160	4.1533	224	3.9125
32.40	8.4773 (8.7672)	96.97	3.7627	161	4.2964	225	4.2775
33.61	8.5027 (8.8085)	98.24	4.1545	162	3.8383	226	3.6218
34.73	8.5068 (8.8277)	99.33	3.7582	163	3.6385	227	4.2196
35.82	8.4891 (8.8271)	100.26	3.4214	164	3.9331	228	3.7673
36.92	8.4544 (8.7980)	101.31	3.8085	165	3.5098	229	3.5623
37.95	8.4181 (8.7527)	102.35	2.9511	166	3.8305	230	4.1353
38.94	8.3978 (8.7582)	103.38	3.9350	167	4.2572	231	4.2219
39.89	8.3986 (8.8211)	104.39	4.0772	168	4.0897	232	4.2191
40.85	8.4106 (8.9016)	105.38	3.8053	169	3.8395	233	4.0591
41.85	8.4493 (8.9638)	106.33	3.6683	170	3.7695	234	3.8995
42.84	8.4199 (9.0281)	107.30	4.1314	171	4.0642	235	3.3858
43.90	8.4194 (9.1120)	108.32	3.9041	172	3.9330	236	4.2337
44.94	8.4328 (9.1885)	109.33	4.3017	173	4.2599	237	3.6891
46.00	8.4571 (9.2478)	110.39	3.9795	174	3.4912	238	4.1752
46.97	8.4696 (9.2630)	111.39	3.9022	175	3.4106	239	3.7488
47.53	8.4597 (9.2375)	111.90	4.1561	176	3.5517	240	3.3069
48.58	8.4206 (9.1635)	112.97	3.7262	177	3.6035	241	3.7737
49.85	8.3742 (9.0378)	114.19	3.8528	178	3.2603	242	3.7582
50.94	8.3561 (8.9483)	115.27	4.3556	179	3.5818	243	4.0888
52.01	8.3641 (8.9679)	116.31	4.0529	180	4.1347	244	3.9225
53.07	8.3885 (9.0631)	117.37	3.9761	181	3.8579	245	3.7284
54.15	8.4219 (9.1549)	118.43	4.0668	182	4.0199	246	3.3793
55.13	8.4624 (9.2185)	119.41	3.6510	183	4.1378	247	3.5259
56.13	8.5042 (9.2682)	120.38	3.7367	184	4.1319	248	4.1650
57.09	8.5415 (9.3118)	121.38	3.6318	185	4.2862	249	3.7411
58.07	8.5662 (9.3489)	122.32	3.8554	186	4.0968	250	3.8652
59.12	8.5787 (9.3783)	123.32	4.2155	187	4.1149	251	3.6112
60.08	8.5748 (9.3866)	124.22	4.0531	188	3.9109	252	4.1126
61.09	8.5547 (9.3644)	125.37	4.0804	189	3.9091	253	4.0959
62.15	8.5222 (9.3106)	126.55	3.7581	190	3.8700	254	4.0345
63.13	8.4821 (9.2283)	127.57	3.5033	191	4.1087	255	3.0165

Chapter 7

THE NOISE CALCULATION

7.1 INTRODUCTION

In our measurement of the upper limit on r, the ratio of advanced to retarded signal power, we saw no signal above the noise level in the time bins where an advanced signal would be expected. This held true even after integration of data. The measured noise in the advanced time region thus constitutes our upper limit on any advanced signal there.

Our intention in the calculations which follow is to compare this measured noise in the advanced region with the noise we would expect to see there from theoretical considerations. For convenience we will make the comparison using equivalent noise temperatures.

7.2 THE THEORETICAL NOISE TEMPERATURE

There are four principle sources of noise in the receiver system: the receiving antenna element, the receiving transmission line, the mixer-preamplifier,

and the amplifier. These are shown schematically in Figure 20. The mixer-preamplifier is the most significant noise source due to its leading position in the amplification sequence.

One can assign a noise temperature to the whole system, T_{system}, to which various system elements contribute. Each element which adds noise to the system can be treated equivalently as adding to the noise temperature of the first element of the system, in our case the receiving antenna.

The system noise temperature of an N-component cascade is given by (Skolnik, 1970, page 2-30, Equation 35)

$$T_{system} = T_a + \sum_{i=1}^{N} \frac{T_{e(i)}}{G_i} \qquad (7.1)$$

where

T_a is the antenna noise temperature, representing the available noise power at the antenna terminals;

$T_{e(i)}$ is the "effective input noise temperature" of cascade element e(i): it is the noise temperature one would have to provide at e(i)'s input terminals, assuming e(i) generates no noise internally, in order to yield at e(i)'s output terminals the noise power which is actually available there in the absence of input noise.

Figure 20. The effective input noise temperature of each element of the receiver system.

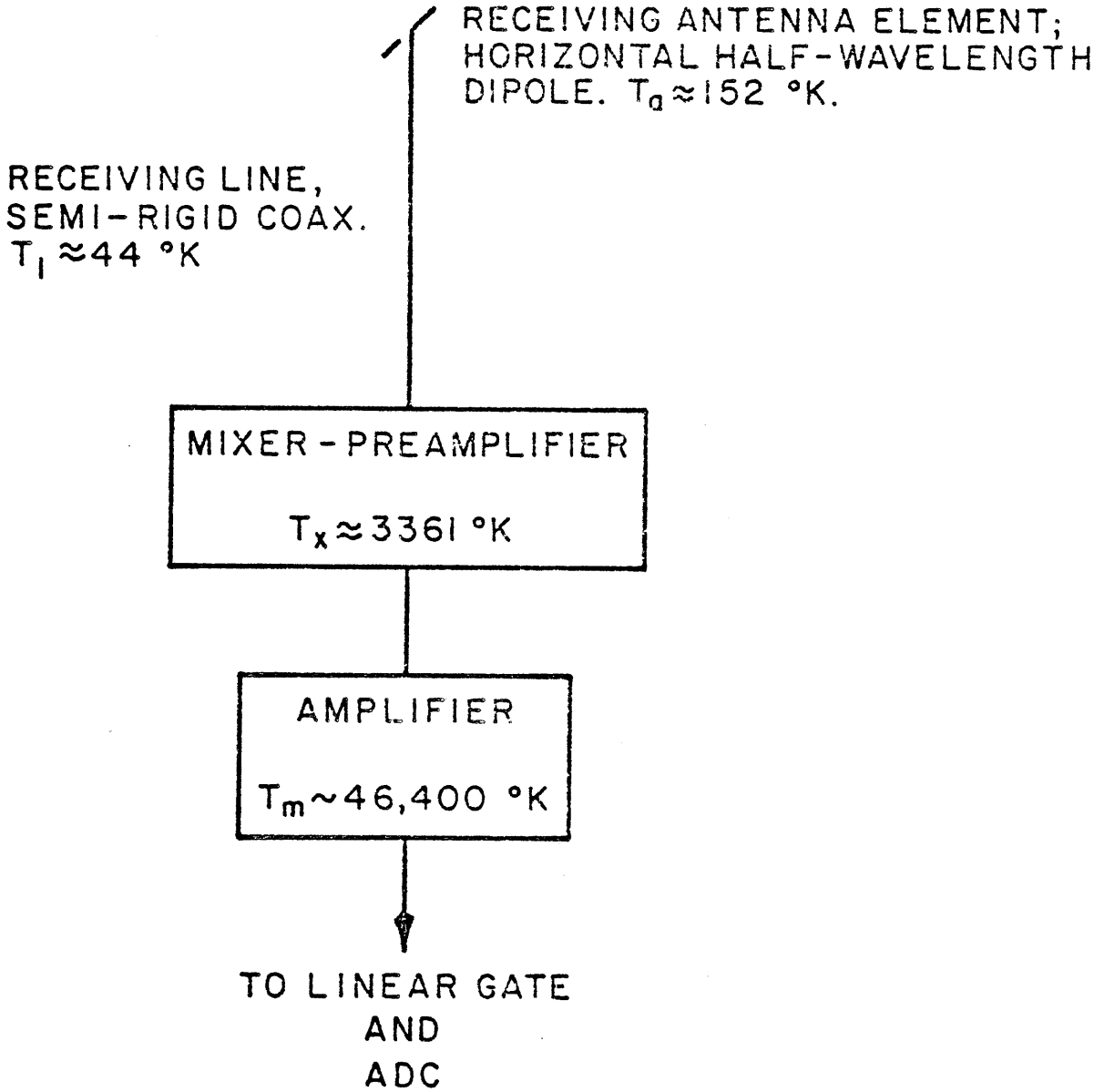
RECEIVING ANTENNA ELEMENT;
HORIZONTAL HALF-WAVELENGTH
DIPOLE. $T_a \approx 152$ °K.
RECEIVING LINE,
SEMI-RIGID COAX.
$T_l \approx 44$ °K
MIXER-PREAMPLIFIER
$T_x \approx 3361$ °K
AMPLIFIER
$T_m \sim 46{,}400$ °K
TO LINEAR GATE
AND
ADC

This "actually available" noise power is that which would result from the circumstance of the noise-free termination of e(i)'s input terminals with the same impedance these terminals see when in the cascade.

G_i is the available gain of the system up to element e(i)'s input terminals. (Thus G_1 is always 1.)

The effective input noise temperature of each element, $T_{e(i)}$, in order to be considered as a contribution to the system <u>input</u> temperature has been divided in our formula by G_i, the power amplification which the noise would experience on its way from the system input to the input of element e(i).

The T values for the four elements in Figure 20 are each calculated in a different way. The calculations follow.

7.3 ANTENNA NOISE

There are many sources of antenna noise including galactic noise, sun noise, atmosphere noise, the 2.7^{o}K cosmic blackbody radiation, and noise from the ground. Grouping all but the last of these under the label "sky noise," we can write for a lossless antenna (Skolnik, 1970, page 2-31, Equation 37):

$$T_a = T_{sky}\left(\frac{\Omega sky}{4\pi}\right)\overline{G_{sky}} + T_{ground}\left(\frac{\Omega ground}{4\pi}\right)\overline{G_{ground}}$$

where Ω_i is the total solid angle of "i" seen by the antenna and $\overline{G_i}$ is the antenna's gain <u>averaged</u> over Ω_i.

Our antenna is a horizontal half wavelength dipole seeing approximately equal solid angles of sky and ground. Although such a dipole has a gain of 2.14 db (Thomas, 1972, page 254) or 1.64 db (Jackson, 1962, Equations 9.57, 9.61) in the forward direction, it is less to the sides so that the average gain over the 2π steradians is 1. Then,

$$T_a = \tfrac{1}{2}T_{sky} + \tfrac{1}{2}T_{ground}.$$

T_{ground}, the effective noise temperature of the ground, will be equal to the actual ground temperature if the earth is perfectly absorptive (blackbody). With this approximation we take $T_{ground} = 290^{o}K$. T_{sky} has been tabulated for typical conditions (Skolnik, 1970, page 2-32, Figure 14). T_{sky} at 10 GHz, averaged over Ω_{sky}, is approximately $14^{o}K$. Thus $T_a \approx 152^{o}K$.

7.4 RECEIVING LINE NOISE

The thermal noise power available at the output of a passive element increases asymptotically (Skolnik, 1970,

page 2-32, Equation 38) with increasing loss factors. The effective input noise temperature of a passive element is given by (Skolnik, 1970, page 2-32, Equation 40) $T_1 = T(L - 1)$. When applied to our receiving antenna transmission line, T represents the thermal temperature of the line and L the line's loss factor, defined in terms of its CW signal transmission characteristics as $L \equiv \frac{\text{signal power in}}{\text{signal power out}} = \frac{1}{G}$.

Our receiving antenna's transmission line was the antenna structure itself—0.46 m of 0.141 inch OD "SMA" size semirigid solid dielectric coax, RG .402U. Its attenuation at 10 GHz is rated (Omni Spectra, Inc., 1979 catalog, "Microwave Coaxial Connectors," pages 192-193) at 40 db/100 ft. so that our receiving line loss factor, L, is 0.60 db or 1.15. Its gain is $G = \frac{1}{L} = 0.87$. Taking $T = 290^{\circ}K$ we have for the effective input noise temperature of the receiving line

$$T_1 \approx 290^{\circ}K\ (1.15-1)$$

$$T_1 \approx 44^{\circ}K$$

7.5 MIXER-PREAMPLIFIER NOISE

The effective input noise temperature of the mixer-preamplifier, T_x, is related to its noise figure (or factor), F_n, by (Skolnik, 1970, page 2-33, Equation 41 or page 2-71,

Figure 45)

$$T_x = T_o(F_n - 1),$$

where T_o is defined to be 290^oK.

Our mixer-preamplifier, an RHG DM1-12/10HH, has a 25 db gain and a noise figure of 11 db as specified by the manufacturer. Its effective input noise temperature is then

$$T_x \approx 3361^oK$$

7.6 AMPLIFIER NOISE

The amplifier's contribution to the system noise is small by virtue of its position at the end of the amplification sequence. We will make a rough estimate of the noise temperature of the amplifier, a Le Croy Model 134, based on an oscilloscope measurement of its noise voltage and on an assumed bandwidth. The amplifier maintains an RMS noise voltage of approximately 4 mV across a 50 ohm load. Assuming a bandwidth greater than 50 MHz and using the relation

$$P_{noise} = \frac{V^2_{noise}}{R} = kTBG,$$

gives an upper estimate on the noise temperature of

$$T_m = \frac{V^2_{noise}}{RkBG}$$

$$= \frac{(4 \times 10^{-3})^2}{(50)(1.38 \times 10^{-23})(5 \times 10^7)(10^4)}$$

$$T_m \sim 46,400^{\circ}K.$$

Table 4 summarizes the above results in terms appropriate for use in Equation 7.1.

Using these results in Equation 7.1 gives our estimate for the system temperature:

$$T_{system} = 152^{\circ}K + \frac{44^{\circ}K}{1} + \frac{3361^{\circ}K}{0.87} + \frac{46,400^{\circ}K}{275}$$

$$T_{system} \approx 4.2 \times 10^3 \ {}^{\circ}K.$$

7.7 THE OBSERVED NOISE TEMPERATURE

This theoretical noise temperature is to be compared with the receiver noise observed before the arrival of the retarded microwave pulse. This noise, which was recorded as analog to digital converter output counts, is to be expressed as a noise temperature for comparison.

Table 4. Power Gain and Noise Temperature of Each Receiver Element.

e(i) element	$T_{e(i)}$ noise temperature	G power gain	G_i gain up to input of element e(i)
receiving antenna	$T_a \approx 152^{\circ}K$	0 db	0 db = 1
receiving transmission-line	$T_1 \approx 44^{\circ}K$	-0.60 db	0 db = 1
mixer-preamplifier	$T_x \approx 3,361^{\circ}K$	25 db	-0.60 db = 0.87
amplifier	$T_m \sim 46,400^{\circ}K$	40 db	24.4 db = 275

We will use the data of two runs taken from a typical 4-run quadrature set. (These are the two 14 minute runs which are combined to form one of the two phase components, 90° apart, to be added in quadrature.) These data were taken in approximately 28 minutes starting at about 3:45 AM on 17 September 1978. The standard deviation of the contents of the time-delay bins in the advanced time region after integration of the data gathered during the 28 minutes is

$$\sigma_{\substack{\text{adv., 1 phase} \\ \text{component, integrated}}} = 1605.$$

(This value of σ is typical of both the "with lenses" and the "without lenses" data.) The standard deviation of a <u>single</u> counter reading is related to this standard deviation of the integrated counter readings by

$$\sigma_{\substack{\text{adv., 1 phase} \\ \text{component, integrated}}} = \sigma_{\text{adv., single}} \sqrt{\left[\frac{\text{no. of sweeps of the delay settings}}{\text{14 min. quad. element run}}\right]\left[\frac{\text{no. of quad. element runs}}{\text{phase component}}\right]\left[\frac{\text{no. of counter readings}}{\text{delay setting}}\right]} .$$

Therefore

$$\sigma_{adv.,single} = \frac{1605 \text{ counts}}{\sqrt{64 \times 2 \times 256}} = 8.9 \text{ counts.}$$

These single counts have what appears to be a gaussian distribution. $\sigma_{adv.,\ single}$ is related to the noise voltage on the input of the analog to digital converter. (When the ADC input is terminated the standard deviation of its output is less than 1 count, thus identifying the ADC input not the ADC gate pulse as the main source of ADC output noise.) This relationship was experimentally found to be

$$\frac{(1 \text{ count})}{(1.1 \text{ mV ADC input})(15 \text{ ns ADC gate width})}$$

or 2.4 mV/count for the 7 ns ADC gate width which was used during data accumulation.

The noise temperature is given by (Skolnik, 1970, page 2-30, Equation 34)

$$T_n = \frac{V_n^2}{RkBG_o}$$

where G_o is the total gain of the system thru the ADC, and B, the ADC bandwidth. The signal passes from the

amplifier thru a linear gate of voltage gain 0.85 and then into the ADC. Thus we have (see Table 4):

$$G_o = (64.4 \text{ db})(0.85)^2 = 63.0 \text{ db} = 1.99 \times 10^6.$$

The 7 ns ADC gating pulse width is its integration time so that $B = \frac{1}{7 \text{ ns}} = 143$ MHz. Then we estimate the observed noise temperature as follows:

$$T_n = \frac{V_n^2}{RkB_nG_o} = \frac{(8.9 \text{ counts} \times 2.4 \text{ mV/count})^2}{(50)(1.38 \times 10^{-23})(143 \times 10^6)(1.99 \times 10^6)}$$

$$T_n \approx 2.3 \times 10^3 \ {}^oK \ .$$

This is the same order of magnitude as our theoretical estimate for the system temperature, 4.2×10^3 ^oK. We should note that there is some uncertainty in the 2.4 mV/count ADC parameter and that the 25 db mixer-preamplifier gain used in our calculation is the manufacturer's specified nominal value. A deviation as small as 2.5 db in the actual gain of our unit would completely account for the above difference.

Chapter 8

PHASE DRIFT DUE TO VARIATIONS IN TEMPERATURE

8.1 INTRODUCTION

Drifts in the phase of the retarded microwave signal relative to the reference signal are caused by temperature drifts within the experimental apparatus. Corresponding drifts in the phase of the advanced signal, if large enough during the total data gathering time, would cancel all or part of any such integrated signal amplitude. This is the case because the signal we integrate is a mixer output, the product of the received signal and a reference signal. Phase drifts between these two signals can affect the magnitude and even the sign of the product. In consideration of these drifts there is an optimum choice for which of the available data to integrate.

In the calculations which follow we make a theoretical upper estimate on the ratio of the advanced phase drift to the retarded phase drift. Then we calculate the theoretical losses in integrated retarded signal and in integrated advanced signal due to phase drifts of the corresponding

amplitudes. Finally, the retarded phase drift, extracted from the data, is used with the results of the first two calculations to estimate the advanced phase drift and the losses in retarded and advanced power. The optimum choice of data to integrate then follows mechanically from the trade-off between the benefits of maximum data usage and the undesirable reduction in the ratio of integrated retarded power to integrated advanced power caused by the associated phase drifts.

8.2 RETARDED AND ADVANCED PHASE DRIFTS

The schematic diagram of the experimental apparatus in Figure 21 is intended to show the principle microwave paths to be considered in a calculation of phase drifts. At the origin, 0, we take the signal amplitude S_o to be

$$S_o = e^{-i\omega t}$$

Then at the mixer

$$S_{ref} = e^{-i(\omega t - k_3 L_3 - k_G L_G - k_4 L_4)}$$

$$S_{ret} = e^{-i(\omega t - k_1 L_1 - k_A L_A - k_2 L_2)}$$

$$S_{adv} = e^{-i(\omega t - k_1 L_1 + k_A L_A - k_2 L_2)}$$

Figure 21. Microwave paths pertinent to phase drifts.

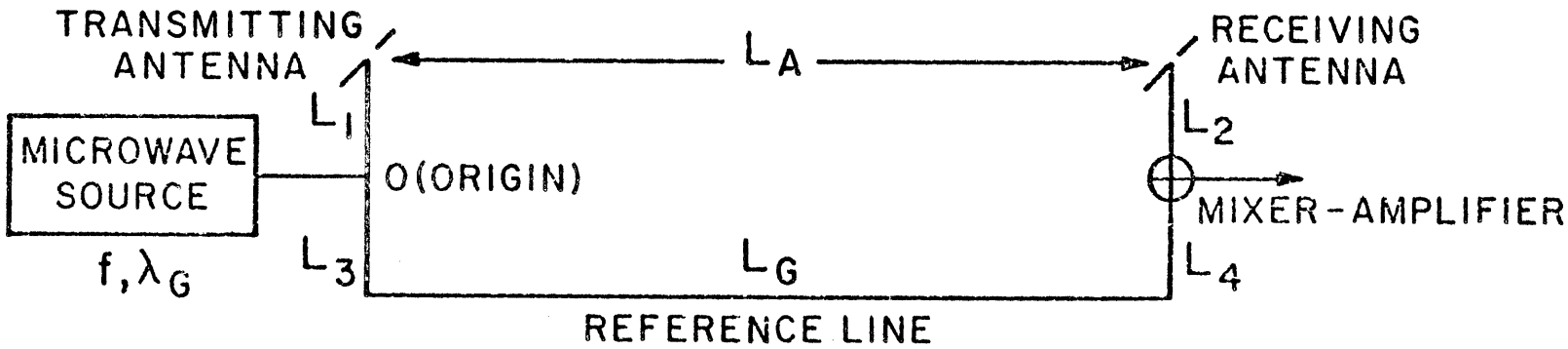
TRANSMITTING ANTENNA
RECEIVING ANTENNA
L_A
L_1
L_2
MICROWAVE SOURCE
O(ORIGIN)
MIXER-AMPLIFIER
f, λ_G
L_3
L_G
L_4
REFERENCE LINE

where the subscripts provide reference as follows:

A : Air path.

G : Rectangular X-band waveguide, RG-52-U.

1,2,3,4 : SMA size semi-flexible waveguide.

ref : Reference.

ret : Retarded.

adv : Advanced.

The signs immediately preceding each wavenumber, k, are negative to indicate waves moving away from the origin or positive to indicate the opposite.

The time average of the retarded signal out of the mixer is

$$S = \overline{(\mathrm{Re}\ S_{ret})(\mathrm{Re}\ S_{ref})}$$

$$= \overline{\tfrac{1}{2}(S_{ret} + S_{ret}^*)\ \tfrac{1}{2}(S_{ref} + S_{ref}^*)}$$

but with ω corresponding to f = 10.24 GHz, we have even for short time intervals

$$\overline{S_{ret}\ S_{ref}} = \overline{S_{ret}^*\ S_{ref}^*} = 0 \text{ because } \overline{e^{\pm 2i\omega t}} = 0.$$

Also,

$$\overline{S_{ret}\ S_{ref}^*} = S_{ret}\ S_{ref}^*$$

and

$$\overline{S_{ret}^* \, S_{ref}} = S_{ret}^* \, S_{ref}$$

because these are not functions of time. Therefore,

$$S = \tfrac{1}{4}\left[(S_{ret} \, S_{ref}^*) + (S_{ret} \, S_{ref}^*)^*\right]$$

$$= \tfrac{1}{2} \, \mathrm{Re}(S_{ret} \, S_{ref}^*)$$

$$= \tfrac{1}{2} \, \mathrm{Re} \, e^{-i(k_1L_1 - k_AL_A - k_2L_2 + k_3L_3 + k_GL_G + k_4L_4)}$$

So that the phase of the retarded signal is

$$\phi_{ret} = -k_1L_1 \quad -k_AL_A \quad -k_2L_2 \quad +k_3L_3 \quad +k_GL_G \; +k_4L_4$$

and, similarly,

$$\phi_{adv} = -k_1L_1 \quad +k_AL_A \quad -k_2L_2 \quad +k_3L_3 \quad +k_GL_G \; +k_4L_4 .$$

Now since L_A and $L_G >> L_1+L_2+L_3+L_4$ we will retain only the terms representing these main contributors to the temperature induced phase drift so that

$$\phi_{ret} = -k_AL_A + k_GL_G$$

$$\phi_{adv} = +k_AL_A + k_GL_G .$$

In a rectangular waveguide of cross-sectional length and width a and b respectively, k_G is a function of a.

$$\lambda_G = \frac{\lambda}{\sqrt{1 - \left(\frac{\lambda}{\lambda_c}\right)^2}} \tag{8.1}$$

where in the TE_{10} mode $\lambda_c = 2a$. Then

$$k_G = k \sqrt{1 - (\lambda/2a)^2}$$

$$k_G = \frac{2\pi f}{c} \sqrt{1 - \left(\frac{c}{2af}\right)^2} .$$

In air

$$k_A = \frac{2\pi f}{c} .$$

Thus we have $\phi = \phi(L,a,f)$ as follows:

$$\phi_{\substack{ret \\ adv}} (L,a,f) = \mp \frac{2\pi f}{c} L_A + \frac{2\pi f}{c} \sqrt{1 - \left(\frac{c}{2af}\right)^2} L_G \tag{8.2}$$

The temperature dependence of the phase is then calculated as follows:

$$\frac{d\phi_{\substack{ret\\adv}}}{dT} = \left[\sum_{i=A,G} \frac{\partial\phi_{\substack{ret\\adv}}}{\partial L_i}\frac{dL_i}{dT}\right] + \left[\frac{\partial\phi_{\substack{ret\\adv}}}{\partial a}\frac{da}{dT}\right] + \left[\frac{\partial\phi_{\substack{ret\\adv}}}{\partial f}\frac{df}{dT}\right]$$

$$= \left[\frac{2\pi}{\lambda_G}(\alpha_G L_G) \mp \frac{2\pi}{\lambda}(\alpha_{bldg} L_A)\right] + \left[\frac{\pi\lambda_G L_G}{2a^3}(\alpha_G a)\right]$$

$$+ \frac{2\pi}{f}\left[\mp\frac{L_A}{\lambda} + \frac{L_G}{\lambda_G}\left(1 + \left[\frac{\lambda_G}{2a}\right]^2\right)\right]\frac{df}{dT}$$

$$= [+\ 2.4\ \text{deg/}\ ^{\circ}\text{C} \mp 1.2\ \text{deg/}\ ^{\circ}\text{C}] + [+1.6\ \text{deg/}\ ^{\circ}\text{C}]$$

$$+ [\pm\ 0.84\ \text{deg/}\ ^{\circ}\text{C} - 1.55\ \text{deg/}\ ^{\circ}\text{C}]$$

$$= +\ 2.09\ \text{degrees/}\ ^{\circ}\text{C and} +\ 2.81\ \text{degrees/}\ ^{\circ}\text{C},$$

where α_G and α_{bldg} are the coefficients of thermal expansion of the brass waveguide and of the building on which the antennas were mounted, respectively.

The following parameters used in the above calculation were obtained from direct measurement:

$$L_G \simeq 14.2\ \text{m}$$
$$L_A \simeq 9.7\ \text{m}$$
$$a = 2.30\ \text{cm}$$
$$f = 10.24\ \text{GHz}$$

from tables or equipment specifications:

$$\alpha_G \simeq 17.5 \times 10^{-6} / {}^{o}C$$

$$\alpha_{bldg} \approx 10^{-5} / {}^{o}C$$

$$\frac{df}{dt} = -70.\ \text{kHz} / {}^{o}C$$

from calculations using the above parameters:

$$\lambda = c/f = 2.92 \text{ cm}$$

$$\lambda_G = 3.78 \text{ cm (see Equation 8.1).}$$

When measured directly with a slotted waveguide section and untuned probe λ_G was 3.76 cm.

The result of our calculation is that the phase drift of the advanced signal can be taken to be

$$K \equiv \left(\frac{d\phi_{adv}}{dT}\right) \Big/ \left(\frac{d\phi_{ret}}{dT}\right) = \frac{2.81}{2.09} = 1.35 \text{ times the}$$

measured phase drift of the retarded signal.

As expected, the retarded phase drift follows a diurnal pattern, the largest changes occurring with the changes in the exposure of the equipment to sunlight in the morning and evening. It is therefore possible that temperature drifts are not uniform throughout the system

as assumed in our calculation, and that the advanced to retarded phase drift ratio, K, is larger than previously indicated. Table 5 summarizes the results of the calculation and shows some other possible drift ratio values. In subsequent calculations we will use K = 3.40, the worst case value of $\left(\frac{d\phi_{adv}}{dT}\right)\Big/\left(\frac{d\phi_{ret}}{dT}\right)$.

8.3 LOSSES IN INTEGRATED RETARDED AND ADVANCED POWER DUE TO PHASE DRIFTS

Due to the temperature caused drifts in its parameters, the phase ϕ, given in Equation (8.2) can be treated as a function of time.

We take S to represent the mixer output integrated over a total running time T (including any number of quadrature sets) and A_o to represent the unmixed signal amplitude of any component of a quadrature set multiplied by the number of components per quadrature set and by the number of quadrature sets taken during the time T.

In the absence of phase drifts from one quadrature set run to another we expect that $S = \frac{1}{2}A_o$. The factor of $\frac{1}{2}$ reflects the nature of the quadrature data gathering process whereby the transmitter's signal wave was set to spend equal time in essentially two phase relationships, 90° apart, with the mixer's reference input.

Table 5. Results of Phase Drift Calculations.

Phase change caused by an increase in temperature and the associated...	$\frac{d\phi_{ret}}{dT}$ (degrees/^{o}C)	$\frac{d\phi_{adv}}{dT}$ (degrees/^{o}C)	$K \equiv \frac{\left(\frac{d\phi_{adv}}{dT}\right)}{\left(\frac{d\phi_{ret}}{dT}\right)}$
expansion of waveguide (L_G and a)	L_G: + 2.40 a: + 1.60	+ 2.40 + 1.60	
decrease in frequency of microwave source (and therefore along waveguide and air paths)	G: - 1.55 A: + 0.84	- 1.55 - 0.84	
expansion of the air path (building)	- 1.20	+ 1.20	
all three effects	+ 2.09	+ 2.81	1.35
waveguide expansion and frequency decrease only	+ 3.29	+ 1.61	0.49
waveguide expansion and air path expansion only	+ 2.80	+ 5.20	1.86
frequency decrease only	- 0.71	- 2.39	3.40
	"+" in this column indicates that retarded signal peaks arrive sooner relative to retarded reference peaks	"+" in this column indicates advanced peaks arrive sooner relative to retarded reference peaks	

With the presence of phase drifts, however, S is less than $\frac{1}{2}A_o$ and is given by the quadrature equation:

$$S^2 = A_o^{\,2}\left[\frac{1}{T}\int_o^T \sin(\omega t)\sin\left[\omega t + \phi(t)\right]\,dt\right]^2 + A_o^{\,2}\left[\frac{1}{T}\int_o^T \sin(\omega t + 90^o)\,\sin\left[\omega t + \phi(t)\right]\right]^2,$$

where the first sin factor in each integrand represents the transmitter's signal as received in each of its two basic quadrature run phase settings, and the second sin factor represents the reference signal, also as received by the mixer. Upon expansion we have

$$S^2 = A_o^{\,2}\left[\frac{1}{T}\int_o^T \sin\omega t\,(\sin\omega t\,\cos\phi + \sin\phi\,\cos\omega t)\,dt\right]^2 + A_o^{\,2}\left[\frac{1}{T}\int_o^T \cos\omega t\,(\sin\omega t\,\cos\phi + \sin\phi\,\cos\omega t)\,dt\right]^2.$$

If ϕ varies slowly with time

$$S^2 = \tfrac{1}{4}A_o^{\,2}\left[(\overline{\cos\phi})^2 + (\overline{\sin\phi})^2\right],$$

where the indicated time averages cover the interval 0 to T.

Representing the phase drift with time as $\phi(t) = \phi_o + \Delta\phi_o(t)$ leads to

$$S^2 = \tfrac{1}{4}A_o^{\,2}\left[\left(\overline{\sin\Delta\phi_o(t)}\right)^2 + \left(\overline{\cos\Delta\phi_o(t)}\right)^2\right].$$

If $\Delta\phi_o(t)$ is identically 0 the factor in brackets is 1. We therefore define this factor to be the <u>Phase Drift Retarded Power Factor</u>. The <u>Phase Drift Advanced Power Factor</u> is then

$$\text{(Advanced Power Factor)} = \left(\overline{\sin\left[K\Delta\phi_o(t)\right]}\right)^2 + \left(\overline{\cos\left[K\Delta\phi_o(t)\right]}\right)^2$$

where K is the ratio of advanced phase drift to retarded phase drift.

The final result of our experiment, the ratio of the corresponding measured powers in the advanced and retarded regions, is dependent on the above power factors and on n, the number of quadrature sets we choose to integrate:

$$r_{\text{power}} = \frac{\text{measured noise power in advanced time region}}{\text{measured signal power in retarded time region}}$$

$$\propto \frac{\text{(Retarded Power Factor)}}{\text{(Advanced Power Factor)}} \cdot \left[\frac{\sqrt{n}}{n \cdot S_1}\right]^2 ,$$

where S_1 is the typical one-quadrature-set retarded signal amplitude. The amplitude given in the final parentheses has the same form as those discussed in Section 5.3 because n is directly proportional to the integrating time.

It follows that

$$r_{power} \propto \frac{(\text{Retarded Power Factor})}{n \cdot (\text{Advanced Power Factor})} \tag{8.3}$$

Thus we can achieve smaller values of r by using larger values of n. Doing so, however, requires using quadrature sets with larger $\Delta\phi_o$, leading to a decreased advanced power factor and therefore a tendency to increase r (the Retarded Power Factor remains close to 1). Thus we seek the value of n which minimizes r.

8.4 CONSIDERATION OF THE PHASE DATA AND DETERMINATION OF THE OPTIMAL CHOICE OF DATA TO INTEGRATE

Retarded phase data from the "with lenses" experimental configuration were considered first. Assuming a drift ratio factor K = 3.40, we calculated as a function of n the retarded and advanced power loss factors and the term (Equation 8.3) to which r_{power} is proportional. In our calculations we took the zero of phase to be midway between the phases of two relatively phase-stable nighttime periods of data collection (see Figures 22 and 23).

Figure 22. Phase (of 77 ns delay bin) versus starting time of run. With lenses.

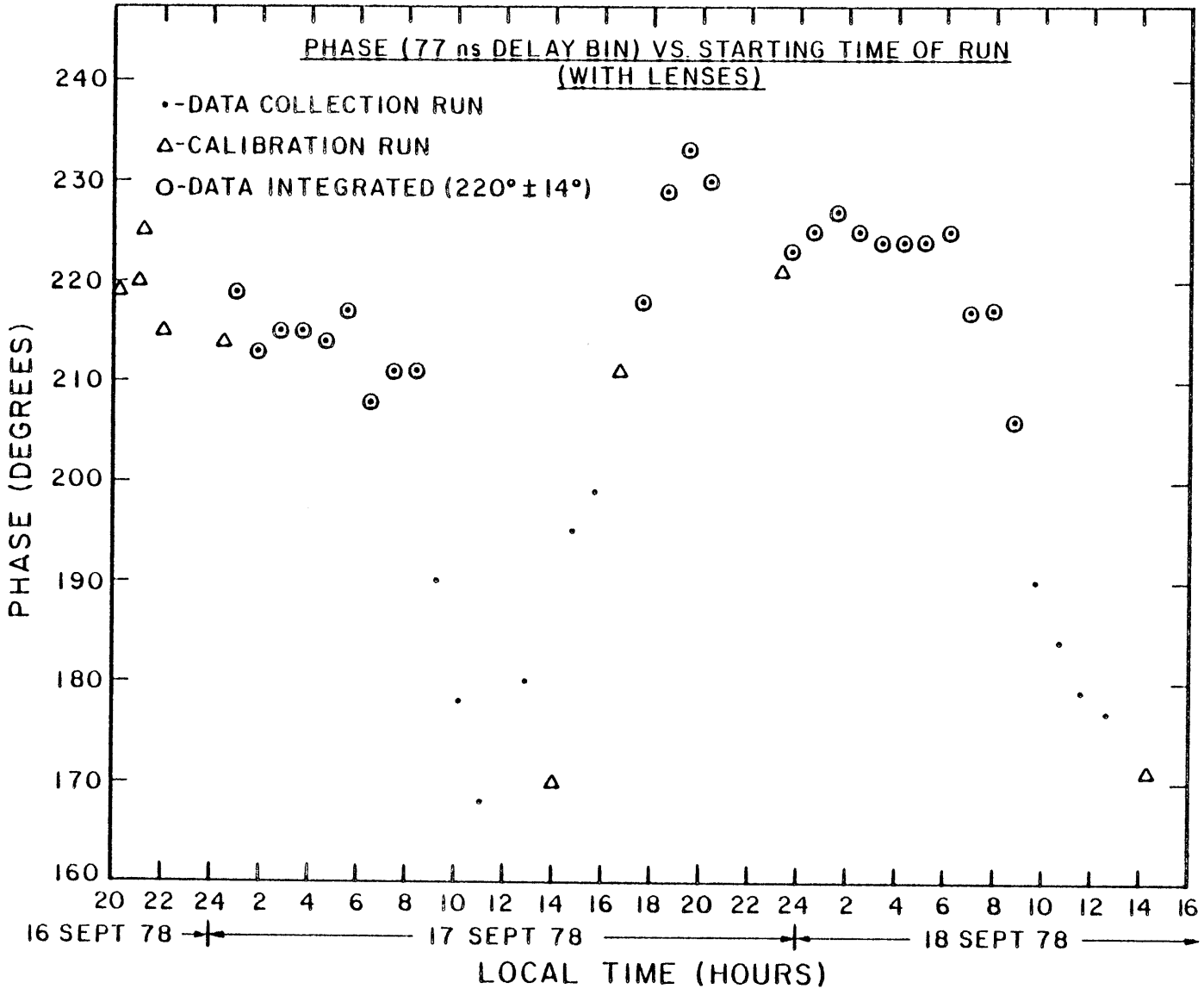
PHASE (77 ns DELAY BIN) VS. STARTING TIME OF RUN
(WITH LENSES)
•-DATA COLLECTION RUN
Δ-CALIBRATION RUN
O-DATA INTEGRATED (220° ± 14°)
PHASE (DEGREES)
240
230
220
210
200
190
180
170
160
20 22 24 2 4 6 8 10 12 14 16 18 20 22 24 2 4 6 8 10 12 14 16
16 SEPT 78
17 SEPT 78
18 SEPT 78
LOCAL TIME (HOURS)

Figure 23. Phase (of 69 ns delay bin) versus starting time of run. Without lenses.

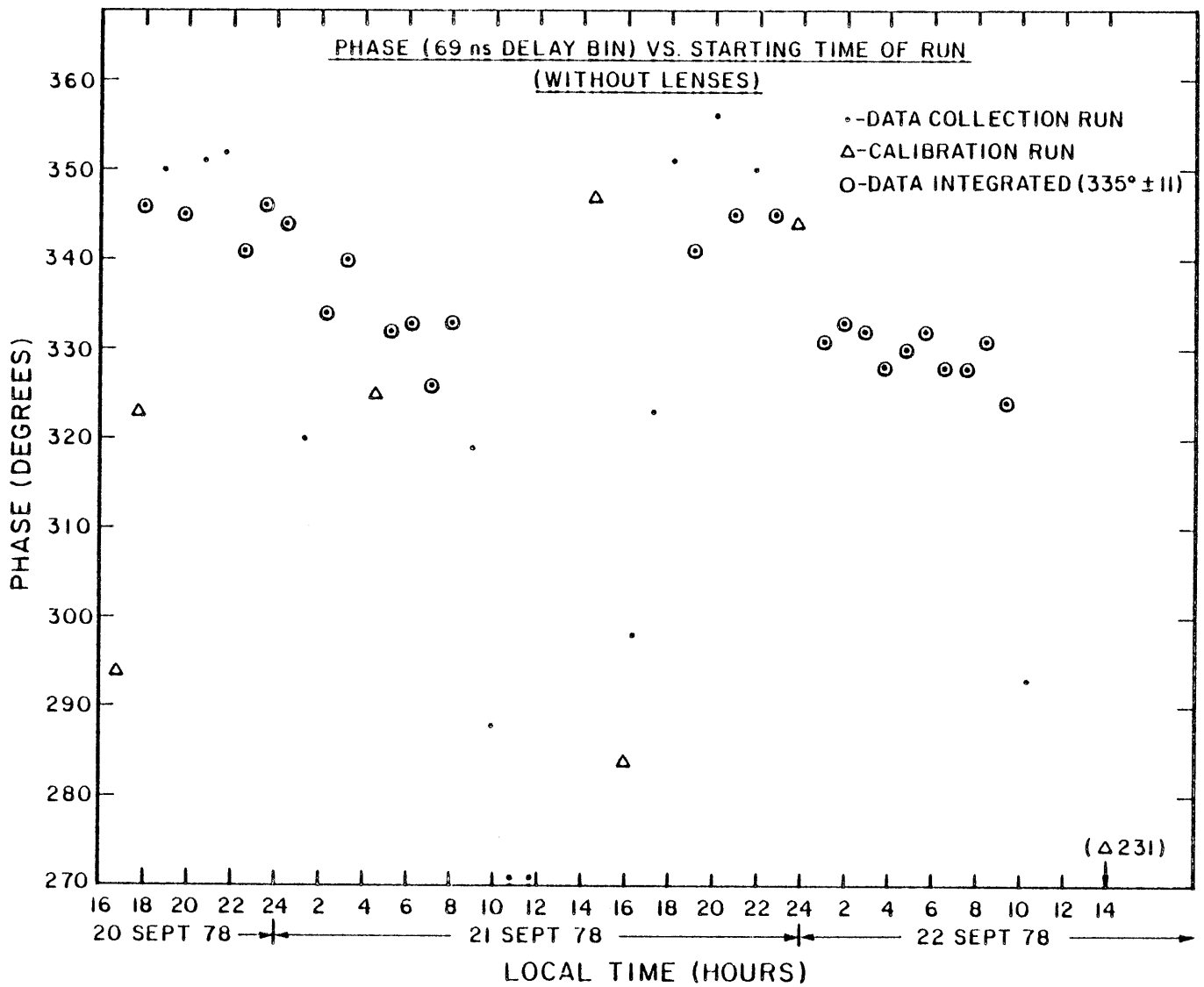
PHASE (69 ns DELAY BIN) VS. STARTING TIME OF RUN
(WITHOUT LENSES)
•-DATA COLLECTION RUN
Δ-CALIBRATION RUN
O-DATA INTEGRATED (335° ± 11)
PHASE (DEGREES)
360
350
340
330
320
310
300
290
280
270
(Δ231)
16 18 20 22 24 2 4 6 8 10 12 14 16 18 20 22 24 2 4 6 8 10 12 14
20 SEPT 78
21 SEPT 78
22 SEPT 78
LOCAL TIME (HOURS)

The results, given in Table 6 for the "with lenses" arrangement, show that it is optimal to use 24 of the 34 available quadrature sets of data.

The power factor quotient corresponding to n = 24 is 85% (see Table 6) indicating that the phase drifts require us to make an undesired correctional increase of 0.7 db in our final calculated value of r.

We used this 85% figure as the minimum tolerable power factor quotient on the "without lenses" data. As a result 24 of those 38 quadrature sets were integrated.

If we use our most likely value of K, 1.35 (see Table 5), on the same 24 data sets, instead of the worst case value, 3.40, the power factor quotient is 98.8% with or without lenses. This, together with the smallness of the worst case correction itself, 0.7 db, leads us to forego phase drift correction of our final value of r.

8.5 THE EXTRACTION OF PHASE INFORMATION FROM THE DATA

The single retarded phase value of the microwave pulse assigned to each quadrature set and used in the above calculations was determined from the data in the quadrature sets themselves. We will describe here how this was accomplished.

During data collection two basic phase settings, 90° apart, were used on the transmitter's signal line.

Table 6. Results Which Indicate the Choice of Data to Minimize r.

$\Delta\phi_o$, Drift from "0°" (deg)	n, number of quad. sets with phase $0° \pm \Delta\phi_o$	$(\overline{\sin\Delta\phi_o})^2 + (\overline{\cos\Delta\phi_o})^2$, Retarded Power Factor	$\overline{\sin(K\Delta\phi_o)}^2 + \overline{\cos(K\Delta\phi_o)}^2$, Advanced Power Factor K = 1.35	Advanced Power Factor K = 3.40	Advanced Power Factor / Retarded Power Factor K = 3.40	Retarded Power Factor / n· Advanced Power Factor K = 3.40
1	1	1.00000	1.00000	1.00000	1.0000	1.0000
2	2	0.99992	0.99986	0.99912	0.9992	0.5004
3	6	0.99860	0.99746	0.98400	0.9854	0.1691
4	9	0.99702	0.99458	0.96598	0.9689	0.1147
5	14	0.99545	0.99172	0.94831	0.9526	0.07498
6	15	0.99494	0.99079	0.94260	0.9474	0.07037
7	17	0.99378	0.98869	0.92986	0.9357	0.06287
9	20	0.99107	0.98377	0.90049	0.9086	0.05503
10	21	0.99002	0.98188	0.88939	0.8984	0.05301
12	22	0.98854	0.97920	0.87394	0.8841	0.05141
13	23	0.98679	0.97603	0.85593	0.8674	0.05013
14	24	0.98492	0.97266	0.83710	0.8499	0.04902*
21	25	0.98065	0.96501	0.79708	0.8128	0.04921
25	26	0.97518	0.95524	0.74851	0.7676	0.05010
30	28	0.96175	0.93140	0.63912	0.6645	0.05374
36	29	0.95318	0.91633	0.57792	0.6063	0.05688
40	30	0.94344	0.89933	0.51507	0.5459	0.06106
41	31	0.93444	0.88364	0.45880	0.4910	0.06570
42	32	0.92608	0.86912	0.40836	0.4410	0.07086
43	33	0.91829	0.85561	0.36309	0.3954	0.07644
52	34	0.90623	0.83513	0.31205	0.3443	0.08541

(*: minimizes r)

Using $A_i \sin\phi_i$ to represent one set of data and $A_i \cos\phi_i$ for the other yields the quadrature set's 256 values of $\phi_i = \tan^{-1} \frac{A_i \sin\phi_i}{A_i \cos\phi_i}$, one for each of the 256 time relationships (programmable delay settings) between microwave pulse transmission and receiver monitoring.

In the advanced time region the ϕ_i appear random over the 0° - 360° range, averaging 180° as expected. In the time region of the retarded peak the values of the numerator and denominator on the argument of the above $\tan^{-1}$ are each nonlinearly restricted according to their amplitudes because of receiver saturation. Thus the ϕ_i in the saturated region are unreliable measures of the phase of the retarded microwave pulse.

We chose to determine our phase from the leading edge of the retarded peak at an amplitude well below saturation but well above the noise amplitude. For the "with lenses" quadrature sets this was the 77 ns delay setting. For the "without lenses" runs it was the 69 ns setting.

Figures 22 and 23 display the drifting of the phases of these delay settings as a function of time.

Chapter 9

THE ATMOSPHERIC TRAJECTORY AND ATTENUATION OF THE MICROWAVE SIGNAL

9.1 THE TRAJECTORY AND ATMOSPHERIC ATTENUATION OF A MICROWAVE SIGNAL PROJECTED FROM A MOUNTAIN TOP

The trajectory of our microwave beam in the atmosphere is to be calculated for two purposes. First, to verify that the path of the microwave signal is free of encounters with local (earth based) absorber and, second, to estimate the total attenuation of the signal by the atmosphere.

Such a beam, although projected horizontally, will deviate downward from a straight line path due to the decrease in the atmospheric index of refraction with increasing altitude.

In the calculations which follow we determine in polar coordinates the index of refraction as a function of height and the differential equation satisfied by the beam's trajectory. After conversion to rectagular

coordinates this equation is solved numerically. Then the absorption of microwaves by the atmosphere as a function of height is estimated and integrated along the calculated trajectory to find the total absorption.

9.2 THE INDEX OF REFRACTION AS A FUNCTION OF POSITION IN THE ATMOSPHERE

For purposes of calculating the index of refraction of air we use a simple model of the atmosphere: an ideal gas at constant temperature, 273 K, in a constant gravitational field. We write the ideal gas equation, $PV = nRT$, as $PV = mKT$, where K is given by $K = nR/m$. For air

$$K = \frac{(1 \text{ mole})(8.314 \text{ J/mole}\cdot{}^{\circ}\text{K})}{0.0290 \text{ kg}} = 287 \frac{\text{J}}{\text{kg}\cdot{}^{\circ}\text{K}} .$$

Then the density $\rho = m/V = P/(KT)$, where P is a function of h, the height above the surface of the earth. Consideration of the increment in pressure with height in a column of air of cross-section A leads to

$$dP = -\frac{g\ dm}{A}$$

$$= -\frac{g}{A}\rho A\ dh$$

so that

$$\frac{dP}{P} = -\frac{g}{KT}dh$$

and

$$\rho(h) = \rho_o e^{-h/h_s} ,$$

where h_s, the "scale height" of the atmosphere is

$$h_s \equiv \frac{KT}{g} = \frac{(287\ J/kg\cdot{}^oK)(273^oK)}{9.8\ N/kg} = 7980\ m.$$

The index of refraction, n, of dry air is related to its density ρ by (Battan, 1973, page 18):

$$n = 1 + K_1\rho.$$

Then

$$n(h) = 1 + \varepsilon_o e^{-h/h_s} ,$$

where (Battan, 1973, page 19, Equation 3.11)

$$\varepsilon_o \equiv K_1\rho_o \approx .00030.$$

In rectangular coordinates with origin at the surface of the earth this is

$$n(x,y) = 1 + \varepsilon_o\ e^{-\frac{1}{h_s}(\sqrt{x^2 + (y+R)^2} - R)} \qquad (9.1)$$

9.3 THE TRAJECTORY OF THE MICROWAVE BEAM THRU THE ATMOSPHERE

The path of a light beam in a medium in which its speed is a function of position is given by Fermat's principle: the trajectory will be the path of extremal time.

In the general case the speed, v, is a function of the general coordinates x and y so that

$$T = \int_{P_1}^{P_2} \frac{ds}{v}$$

$$= \int_{P_1}^{P_2} \frac{\sqrt{1 + (dy/dx)^2}\, dx}{v(x,y)}$$

$$= \int_{P_1}^{P_2} f(y,\dot{y},x)dx$$

where

$$\dot{y} \equiv \frac{dy}{dx}$$

and

$$f = \frac{\sqrt{1 + \dot{y}^2}}{v(x,y)} .$$

The desired trajectory obtains from imposing the requirement that $\delta T = 0$.

General conditions under which $\int_{P_1}^{P_2} f(y,\dot{y},x)\,dx$ is extremal will be determined and then applied to our particular integrand, f. We require

$$\delta \int_{P_1}^{P_2} f(y,\dot{y},x)dx = 0$$

where δ is defined implicitly by $\delta w = \frac{\partial w}{\partial x}\,dx$.

Then

$$\int_{P_1}^{P_2} \left[\frac{\partial f}{\partial y}\,\delta y + \frac{\partial f}{\partial \dot{y}}\,\delta\dot{y}\right] dx = 0$$

$$\int_{P_1}^{P_2} \left[\frac{\partial f}{\partial y}\,\delta y + \frac{\partial f}{\partial \dot{y}}\,\frac{d}{dx}\,(\delta y)\right] dx = 0.$$

But

$$\frac{d}{dx}\left[\left(\frac{\partial f}{\partial \dot{y}}\right)\left(\delta y\right)\right] = \frac{\partial f}{\partial \dot{y}}\,\frac{d}{dx}\,(\delta y) + \left[\frac{d}{dx}\left(\frac{\partial f}{\partial \dot{y}}\right)\right](\delta y).$$

Therefore

$$\int_{P_1}^{P_2} \left(\frac{\partial f}{\partial y}\,\delta y + \frac{d}{dx}\left[\left(\frac{\partial f}{\partial \dot{y}}\right)\left(\delta y\right)\right] - \left[\frac{d}{dx}\left(\frac{\partial f}{\partial \dot{y}}\right)\right](\delta y)\right) dx = 0$$

$$\left(\frac{\partial f}{\partial \dot{y}}\right)(\delta y)\Bigg|_{P_1}^{P_2} + \int_{P_1}^{P_2} \left[\frac{\partial f}{\partial y} - \frac{d}{dx}\,\frac{\partial f}{\partial \dot{y}}\right](\delta y)dx = 0.$$

Since y is fixed at the endpoints (δy) is zero there and the first term vanishes. (δy) is otherwise arbitrary, reducing the second term to

$$\frac{d}{dx}\frac{\partial f}{\partial \dot{y}} - \frac{\partial f}{\partial y} = 0,$$

the Euler-Lagrange equation. From this, another form of the Euler-Lagrange equation, more useful for our purposes, can be derived. Multiplying thru by $\dot{y}$ and using the fact that

$$\frac{d}{dx}\left[\dot{y}\,\frac{\partial f}{\partial \dot{y}}\right] = \frac{d\dot{y}}{dx}\frac{\partial f}{\partial \dot{y}} + \dot{y}\,\frac{d}{dx}\frac{\partial f}{\partial \dot{y}}\ ,$$

leads to

$$\frac{d}{dx}\left[\dot{y}\,\frac{\partial f}{\partial \dot{y}}\right] - \frac{d\dot{y}}{dx}\frac{\partial f}{\partial \dot{y}} - \frac{dy}{dx}\frac{\partial f}{\partial y} = 0.$$

But

$$\frac{df}{dx} = \frac{\partial f}{\partial y}\frac{dy}{dx} + \frac{\partial f}{\partial \dot{y}}\frac{d\dot{y}}{dx} + \frac{\partial f}{\partial x}$$

so that

$$\frac{d}{dx}\left[\dot{y}\,\frac{\partial f}{\partial \dot{y}}\right] - \left[\frac{df}{dx} - \frac{\partial f}{\partial x}\right] = 0$$

and finally

$$\frac{\partial f}{\partial x} - \frac{d}{dx}\left[f - \dot{y}\,\frac{\partial f}{\partial \dot{y}}\right] = 0,$$

a form of the Euler-Lagrange equation particularly useful when f is not a function of x. In polar coordinates our integrand, f, will not be a function of Θ since the index of refraction of the atmosphere and therefore the velocity of microwaves therein is independent of Θ (see Figure 24a). In polar coordinates

$$T = \int_{P_1}^{P_2} \frac{ds}{v} = \int_{P_1}^{P_2} \frac{\sqrt{(dr)^2 + (rd\Theta)^2}}{v(r)}$$

$$= \int_{P_1}^{P_2} \frac{\sqrt{r^2 + \dot{r}^2}}{v(r)}\, d\Theta = \int_{P_1}^{P_2} f(r,\dot{r},\Theta)d\Theta,$$

where $\dot{r} \equiv \frac{dr}{d\Theta}$ and $f = \frac{1}{v(r)}\sqrt{r^2 + \dot{r}^2}$. With f independent of Θ the Euler-Lagrange equation in polar coordinates, $\frac{\partial f}{\partial \Theta} - \frac{d}{d\Theta}\left(f - \dot{r}\,\frac{\partial f}{\partial \dot{r}}\right) = 0$, reduces to

$$\left[f - \dot{r}\,\frac{\partial f}{\partial \dot{r}}\right] = c_1.$$

The constant c_1 can be determined from the initial condition

Figure 24. Definition of parameters for various calculations.

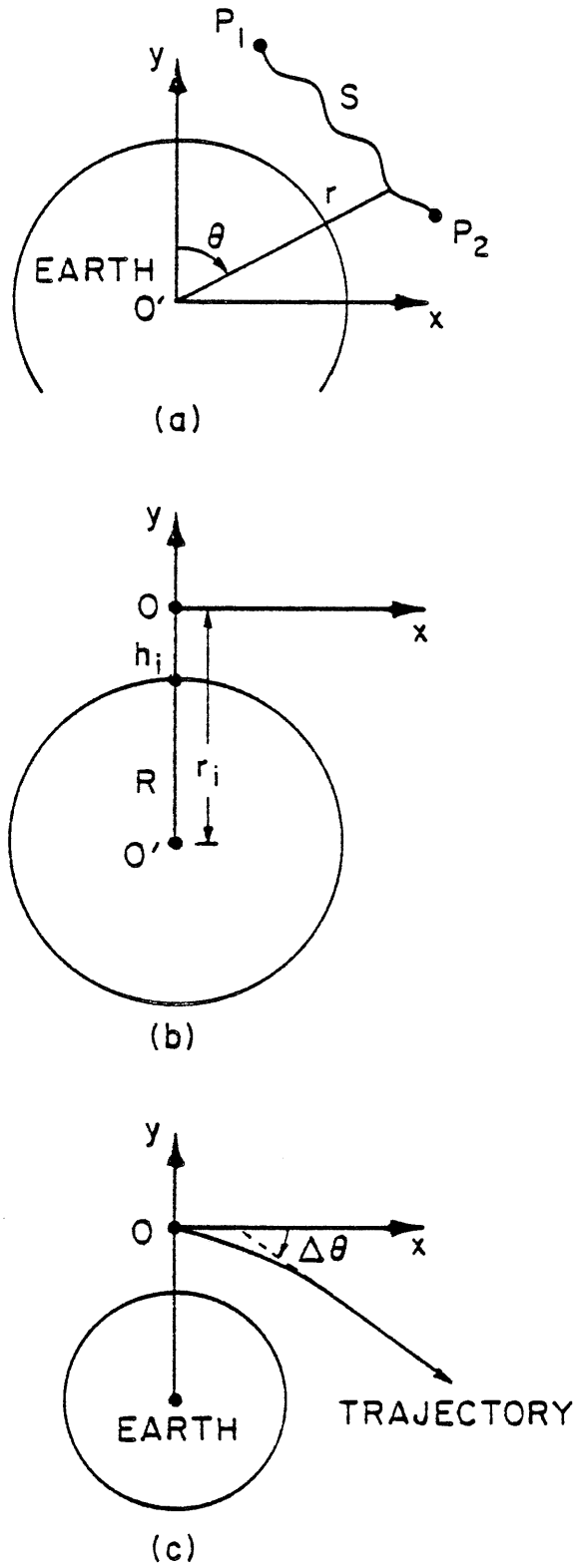
P1
S
y
r
θ
P2
EARTH
O′
x
(a)
y
O
x
hi
R
ri
O′
(b)
y
O
x
Δθ
EARTH
TRAJECTORY
(c)

of horizontal projection (tangential to the surface of the earth) for which $\dot{r}\Big|_i = 0$. Thus

$$c_1 = \left[f - \dot{r}\,\frac{\partial f}{\partial \dot{r}}\right]_i = f_i = \frac{r_i}{v(r_i)} ,$$

and our equation

$$\left[f - \dot{r}\,\frac{\partial f}{\partial \dot{r}}\right] = c_1$$

becomes

$$\frac{\sqrt{r^2 + \dot{r}^2}}{v(r)} - \dot{r}\,\frac{\partial}{\partial \dot{r}}\left(\frac{\sqrt{r^2 + \dot{r}^2}}{v(r)}\right) = \frac{r_i}{v(r_i)} .$$

solving for $\dot{r}$ yields

$$\dot{r} = r\sqrt{\left(\frac{r\ v(r_i)}{r_i v(r)}\right)^2 - 1} .$$

But

$$\frac{v(r_i)}{v(r)} = \frac{n(r)}{n(r_i)} .$$

Therefore

$$\frac{dr}{d\Theta} = r\sqrt{\left(\frac{r\ n(r)}{r_i n(r_i)}\right)^2 - 1} \qquad (9.2)$$

is the differential equation for the trajectory of a microwave beam horizontally projected from an altitude h_i, where $r_i = R_{earth} + h_i$. Henceforth $n(r_i)$ will be written as n_i.

In order to most easily find the trajectory's total deviation from the horizontal, $\Delta\Theta$, and to most easily interpret the solution, we rewrite the differential equation in rectangular coordinates and then translate the origin from the center of the earth to the mountain top.

With reference to Figure 24a, r, Θ, and $dr/d\theta$ can be written in terms of x, y, and dy/dx as follows:

$$r = (x^2 + y^2)^{\frac{1}{2}}$$

$$\Theta = \tan^{-1}(x/y)$$

$$\frac{dr}{d\Theta} = \frac{\frac{\partial r}{\partial x}dx + \frac{\partial r}{\partial y}dy}{\frac{\partial \Theta}{\partial x}dx + \frac{\partial \Theta}{\partial y}dy} = (x^2+y^2)^{\frac{1}{2}}\left(\frac{x + y\dot{y}}{y - x\dot{y}}\right),$$

where $\dot{y} \equiv dy/dx$.

Using this in Equation (9.2) leads to

$$\frac{dy}{dx} = \frac{-xy + \frac{n_i}{n}r_i\sqrt{x^2 + y^2 - \left[\frac{n_i}{n}r_i\right]^2}}{\left[\frac{n_i}{n}r_i\right]^2 - x^2}$$

where the sign of the square root was chosen to yield the solution $y = r_i$ in the case $n = n_i$.

Translation of the origin from 0' at the center of the earth to 0 at the mountain top of altitude h_i, (see Figure 24 b) is accomplished by the substitution

$$x \rightarrow x$$

$$y \rightarrow y + R + h_i$$

so that our final differential equation for the trajectory of a microwave beam horizontally projected in the atmosphere from an altitude h_i, in rectangular coordinates with origin at 0, is

$$\frac{dy}{dx} = \frac{-x(y+R+h_i) + \frac{n_i}{n}(R+h_i)\sqrt{x^2 + (y+R+h_i)^2 - \left[\frac{n_i}{n}(R+h_i)\right]^2}}{\left[\frac{n_i}{n}(R+h_i)\right]^2 - x^2}$$

where from equation (9.1)

$$n(x,y) = 1 + \varepsilon_o e^{-\frac{1}{h_s}\left[\sqrt{x^2 + (y+R+h_i)^2} - R\right]} .$$

The equation was solved numerically with a computer program based on a fourth order Runge-Kutta integration used on a recursive basis. An x-axis incremental step size of 10 meters was used yielding the corresponding y coordinates of the trajectory.

The following parameters were used:

$$\varepsilon_o = .00030$$
$$h_s = 7980 \text{ m}$$
$$R = 6{,}371{,}000 \text{ m}$$
$$h_i = 1290 \text{ m}$$
$$n_i = n(0,0) = 1.00025522.$$

The program gave the total deviation of the microwave beam from the horizontal (see Figure 24c) due to the earth's atmosphere as $\Delta\Theta = 0.57$ degrees. Comparison with the sea level value of 0.53 degrees as given by Tricker (1970, page 16) indicates that our model provides an upper bound on the microwave bending.

Nevertheless, because of the curvature of the earth, this bending is not great enough to direct the signal into any earth based absorber. As an example, 100 km away from the transmitter the beam is only 158 m below the horizontal x-axis.

9.4 ABSORPTION OF THE MICROWAVE SIGNAL BY THE ATMOSPHERE

One-way attenuation by the ionosphere for "low elevation" angles of projection and high frequencies ($f \gtrsim 100$ MHz) is given by (Skolnik, 1970, page 2-59)

$$L = \frac{A}{2f^2} \text{ db}$$

with f in MHz, and A at most 1.3×10^4. For f = 10 GHz, $L \approx 7 \times 10^{-5}$ db, indicating that absorption by the ionosphere is insignificant.

Atmospheric absorption at 10.24 GHz is primarily due to absorption by oxygen and water-vapor:

$$ABS_{atm} = ABS_{O_2} + ABS_{H_2O} .$$

Each of these two terms, usually expressed in db/km, decrease exponentially with height, each with its own scale height. The scale height for oxygen in the atmosphere is (Skolnik, 1970, page 24-16):

$$h_{s(O_2)} \cong \frac{T_o}{68.6^oK/km - 2.75\alpha} ,$$

where T_o is the surface air temperature in ^oK and α is the atmospheric temperature lapse rate with height in $^oK/km$. Using $T_o = 293\ ^oK$ and $\alpha = 6.2\ ^oK/km$ yields $h_{s(O_2)}$ = 5.7 km. $h_{s(H_2O)}$ is found (Skolnik, 1970, page 24-19) to be less than $h_{s(O_2)}$ in spite of theoretical arguments to the contrary (Feynman, 1963, page 40-2). So as to make an upper estimate on the total atmospheric attenuation we will take $h_{s(H_2O)}$ to be $h_{s(O_2)}$. Then

$$ABS_{atm} = ABS_{atm}(h=0)\ e^{-h/h_{s(O_2)}},$$

where

$$ABS_{atm}(h=0) = ABS_{O_2}(h=0) + ABS_{H_2O}(h=0).$$

The first term on the right is due principally to oxygen's absorption lines centered around 0.5 cm. The second term arises from water's 1.35 cm line and from its higher absorption bands. Each of these two terms can be calculated as follows (Skolnik, 1970, Section 24-8):

$$ABS_{O_2}(h=0)$$

$$= \frac{0.34}{\lambda^2}\left[\frac{\Delta v_1}{\frac{1}{\lambda^2} + (\Delta v_1)^2} + \frac{\Delta v_2}{(2+\frac{1}{\lambda})^2 + (\Delta v_2)^2} + \frac{\Delta v_2}{(2-\frac{1}{\lambda})^2 + (\Delta v_2)^2}\right]$$

$$ABS_{H_2O}(h=0)$$

$$= \frac{3.5 \times 10^{-3}\rho_o(\Delta v_3)}{\lambda^2}\left[\frac{1}{(\frac{1}{\lambda} - \frac{1}{1.35})^2 + (\Delta v_3)^2}\right.$$

$$\left. + \frac{1}{(\frac{1}{\lambda} + \frac{1}{1.35})^2 + (\Delta v_3)^2}\right] + \frac{0.05\rho_o(\Delta v_4)}{\lambda^2}$$

where

$$\rho_o = \text{the absolute humidity at } h=0 \text{ in gm/m}^3$$

$$\lambda = \text{the wavelength in cm}$$

and

$$\Delta v_i = \text{absorption line-width factors.}$$

Taking

$$\rho_o = 7.75 \text{ gm/m}^3,$$

$$T = 293^oK$$

and

$$P = 1013.25 \text{ mb}$$

we have (Skolnik, 1970, Page 24-14, Tables 3 and 4)

$$\Delta v_1 = 0.018$$

$$\Delta v_2 = 0.050$$

$$\Delta v_3 = 0.094$$

$$\Delta v_4 = 0.094.$$

The resulting absorption rates are

$$ABS_{O_2}(h=0) = 0.00718 \text{ db/km}$$

$$ABS_{H_2O}(h=0) = 0.00626 \text{ db/km}$$

so that

$$ABS_{atm}(h=0) = 0.013 \text{ db/km},$$

a result consistent with measurement elsewhere (Skolnik, 1970, page 24-18, Figure 8). Thus the absorption of

10.24 GHz microwave radiation by atmospheric oxygen and water vapor as a function of altitude above the earth's surface is given by

$$ABS_{atm}(h) \simeq 1.3 \times 10^{-5}\ e^{-h/5700m}\ db/m.$$

Integrating this absorption factor numerically along the beam trajectory gives the total attenuation due to the atmosphere:

$$\text{Total Attenuation} = \int_{\text{Trajectory}} ABS_{atm}(h)\ dl = 2.7\ db.$$

This is 10.% greater than would be the case for a straight line trajectory ($\varepsilon_o = 0$).

Chapter 10

REVIEW

We have described an experiment in which a search for an advanced component in electromagnetic radiation resulted in establishment of an upper limit on the relative power of such a component.

In Chapter 1 we saw the strongest theoretical argument for the existence of such backwards-in-time fields, the time-symmetry of Maxwell's equations, come into conflict with their absence in normal experience. In Chapter 2, Wheeler and Feynman's time-symmetric absorber theory of radiation was seen to provide self-consistent solutions in accord with this normal experience. While succeeding at this in the case of complete absorption of radiation, their theory reopened the possibility of advanced activity in the case of incomplete absorption.

Our experiment looked directly for the advanced fields predicted by Maxwell's equations but did so in such a way as to optimize the possibility of their measurement within

Wheeler-Feynman theory. This involved placement of source and detector (pictured in Chapter 2) such that the line connecting them, if extended in either direction, encounters no local (earth-based) absorber.

Because of this the absence of an advanced signal in our measurements has cosmological implications within the absorber theory of radiation as explained in Chapter 1: having avoided local absorption, our fields must have been headed for future absorption elsewhere. This future absorption occurs within certain cosmological models which are also described in Chapter 1.

In Chapter 3 we presented an argument due to Wheeler and Feynman that advanced effects do not lead to logical paradoxes. The argument is based on the assumption that in nature effects vary in a continuous way with causes. Systems designed to be discontinuous may require further analysis.

Our choice of 10 GHz microwave radiation was seen to have certain advantages over other frequencies. These include convenient detection without the need to block the beam path with absorbing material, and small absorption by gases in space.

The absence of an advanced signal left noise as the limiting factor in our measurement. Various steps were taken to minimize the effects of noise. The phase

sensitive receiving system, built around a mixer, gave a high signal to noise ratio as described in Chapter 5. The sources of noise are analyzed quantitatively in Chapter 7.

In Chapter 5 we described what we considered to be a second experiment. Here two microwave lenses were mounted to focus the advanced radiation and thereby increase the strength of any advanced signal present. Their gain, measured with the lenses in the retarded position, was 25.9 db.

Our transmitter emitted 7 ns bursts of 4 W microwave radiation. The receiver, 9.7 m away, would be expected to see any associated advanced radiation about 65 ns before the retarded, as is explained in Chapter 6. Data was collected over a period of about one day. During this period the receiver was monitored about 10^7 times in the time region which precedes the arrival of the retarded microwave signal by about 65 ns. Other times regions were also monitored for comparison.

In Chapter 6 we discussed the analysis of the data and reported the result—an upper limit on the power of an advanced microwave signal, expressed as a fraction of the power of the associated retarded microwave signal:

$$\frac{P_{adv}}{P_{ret}} < 10^{-11.5} \qquad \text{(lensless experiment)}$$

$$\frac{P_{adv}}{P_{ret}} < 10^{-14.0}$$ (experiment with lenses; 25.9 db lens gain assumed (see section 6.3) for advanced radiation and calculated in).

Strictly speaking these limits apply to "outer face" advanced effects, as discussed in Section 2.6. Such advanced effects deposit energy into the absorber (in this case, our receiving antenna) in a way which is locally indistinguishable from the absorption of retarded radiation. The validity of our results as limits on "inner face" advanced effects is less clear because our apparatus was designed to detect signal power above noise power in the advanced signal time region: "inner face" advanced effects remove energy from the absorber as noted at the ends of Sections 2.5 and 6.3. In Section 2.6 we noted, with a strong caveat, that the Partrige experiment may have been particularly sensitive to such "inner face" advanced effects.

In Chapter 8 we took note of the effect of drifts in the phase of the microwaves during data collection. These phase drifts are associated with temperature drifts in the apparatus. Such drifts in the phase of a microwave signal whose amplitude is being integrated (a property of our mixer-based detection system described in Section 5.3), if large enough, are harmful because they can change the

sign of the signal being integrated. If this happens, signal integrated before the phase drift will be totally or partially cancelled by signal added-in after the phase drift. In our analysis, detailed in Chapter 8, we reconstructed from the data the phase of the signal as it drifted during integration. This enabled us to optimize the choice of data to be included in the final integration. Thus in our analysis we used data with phase constant within limits. Optimal limits allowed use of two-thirds of the total data.

Finally, as described in Chapter 9, the trajectory of our microwave beam in the atmosphere was calculated. The result, confirmed by optical sighting, showed that the atmospheric refraction was too small to direct the signal into earth-based absorber. Atmospheric attenuation along the trajectory of the signal was also calculated and found to be small at our frequency.

REFERENCES

Battan, L. J., 1973. Radar Observation of the Atmosphere, The University of Chicago Press, Chicago.

Davies, P. C. W., 1974. The Physics of Time Asymmetry, University of California Press, Berkeley.

Davies, P. C. W., 1975. J. Phys. A, 8, 272-280.

Feynman, R. P., 1963. The Feynman Lectures on Physics, Volume 1, Addison-Wesley Publishing Company, Reading, Massachusetts.

Feynman, R. P., 1966. Physics Today, 19, no. 8, 31-44.

Fokker, A. D., 1929a. Zeitschrift für Physik, 58, 386-393.

Fokker, A. C., 1929b. Physica, 9, 33.

Fokker, A. D., 1932. Physica, 12, 145.

Hogarth, J. E., 1962. Proc. Roy. Soc. A, 267, 365-383.

Hoyle, F. and Narlikar, J. V., 1974. Action at a Distance in Physics and Cosmology, W. H. Freeman, San Francisco.

Jackson, J. D., 1962. Classical Electrodynamics, John Wiley & Sons, Inc., New York.

Jackson, J. D., 1975. Classical Electrodynamics, Second Edition, John Wiley & Sons, Inc., New York.

Kuhn, T. S., 1970. The Structure of Scientific Revolutions, The University of Chicago Press, Chicago.

Marion, J. B., 1965. Classical Electromagnetic Radiation, Academic Press Inc., New York.

Partridge, R. B., 1973. Nature, 244, 263-265.

Pegg, D. T., 1975. Reports on Progress in Physics, 38, 1339-1383.

Sagan, C., editor, 1973. Communication With Extra-terrestrial Intelligence, M.I.T. Press, Cambridge.

Shklovskii, I. S. and Sagan, C., 1966. Intelligent Life in the Universe, Holden-Day, Inc., San Francisco.

Skolnik, M. I., editor, 1970, Radar Handbook, McGraw-Hill, New York.

Thomas, H. E., 1972. Handbook of Microwave Techniques and Equipment, Prentice-Hall, Inc., Englewood Cliffs, New Jersey.

Tricker, R. A. R., 1970. Introduction to Meteorological Optics, American Elsevier Pub. Co., New York.

Wheeler, J. A. and Feynman, R. P., 1945. Reviews of Modern Physics, 17, 157-181.

Wheeler, J. A. and Feynman, R. P., 1949. Reviews of Modern Physics 21, 425-433.

Appendix A

SOME CALCULATIONS IN THE ABSORBER THEORY OF RADIATION

A.1 INTRODUCTION

We have performed some calculations in the absorber theory of radiation using as a source an oscillating charge sheet (a current sheet) of infinite extent. These calculations were motivated by a desire to illustrate the essential features of the theory in a simple one-dimensional model and to possibly gain insight into the spatial distribution of advanced effects in the case of incomplete absorption. Additionally, we want to explore any influence by the particular nature of the absorbing material on the nature of the resulting self-consistent solutions.

Assuming retarded and advanced fields to be emitted in equal amplitude by the source as well as by responding charges in the absorber, we sought the net fields everywhere for two absorber configurations. See Figure A-1.

Figure A-1. Absorber placement for two calculations.

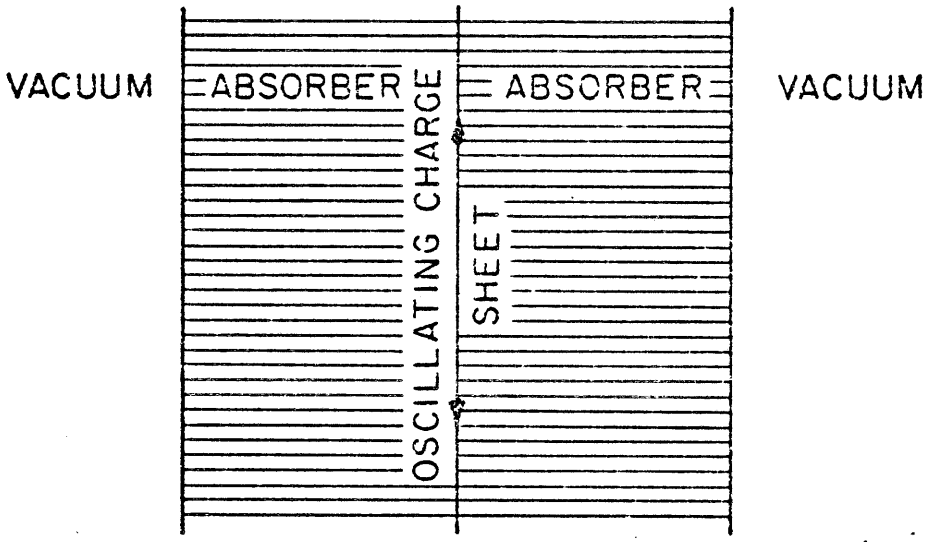
VACUUM
ABSORBER
ABSORBER
VACUUM
OSCILLATING CHARGE
SHEET

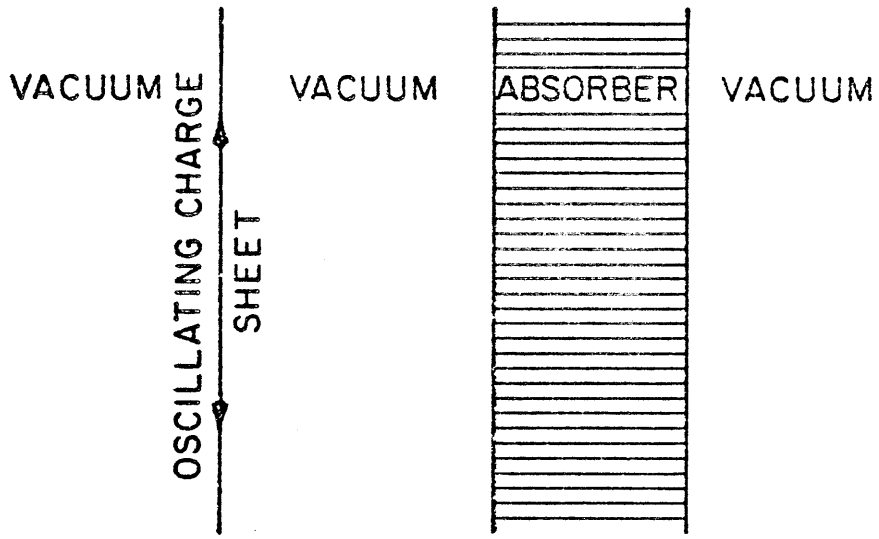
VACUUM
VACUUM
ABSORBER
VACUUM
OSCILLATING CHARGE
SHEET

First, with the source sheet placed in the $z = 0$ plane, absorbing material filled the space between $z = -a$ and $z = a$ (Figure A-4). Second, with the oscillating charge sheet again at $z = 0$, absorbing material was placed to one side, filling the space between $z = a$ and $z = b$ (Figure A-6).

The absorber in our calculations is characterized by a conductivity σ; it has no dielectric or magnetic properties different from free space: $\varepsilon = 1$, $\mu = 1$.

A.2 FIELDS FROM AN OSCILLATING SHEET OF CHARGE

A vector potential, $\vec{A}(\vec{x},t)$, was derived for the current sheet and used to calculate the fields. Recall from Chapter 1 that the components of $\vec{A}_{\substack{ret\\adv}}(\vec{x},t)$ are given by

$$A_{\substack{\mu\\ret\\adv}}(\vec{x},t) = \frac{1}{c}\int_t\int_\tau \frac{J_\mu(\vec{x}',t')}{R'}\,\delta(t' \pm \frac{R'}{c} - t)\,d^3x'dt',$$

where

$$\vec{R}' = \vec{x} - \vec{x}'.$$

For our current sheet $\vec{J}(\vec{x},t) = j_o e^{i\omega t}\hat{y}\delta(z)$, where j_o is the current/unit length measured across any length parallel to the x-axis and in the $z = 0$ plane (See Figure A-2).

Figure A-2. Assignment of variables in the integration to find the vector potential of an oscillating sheet of charge. Charge is in the x-y plane.

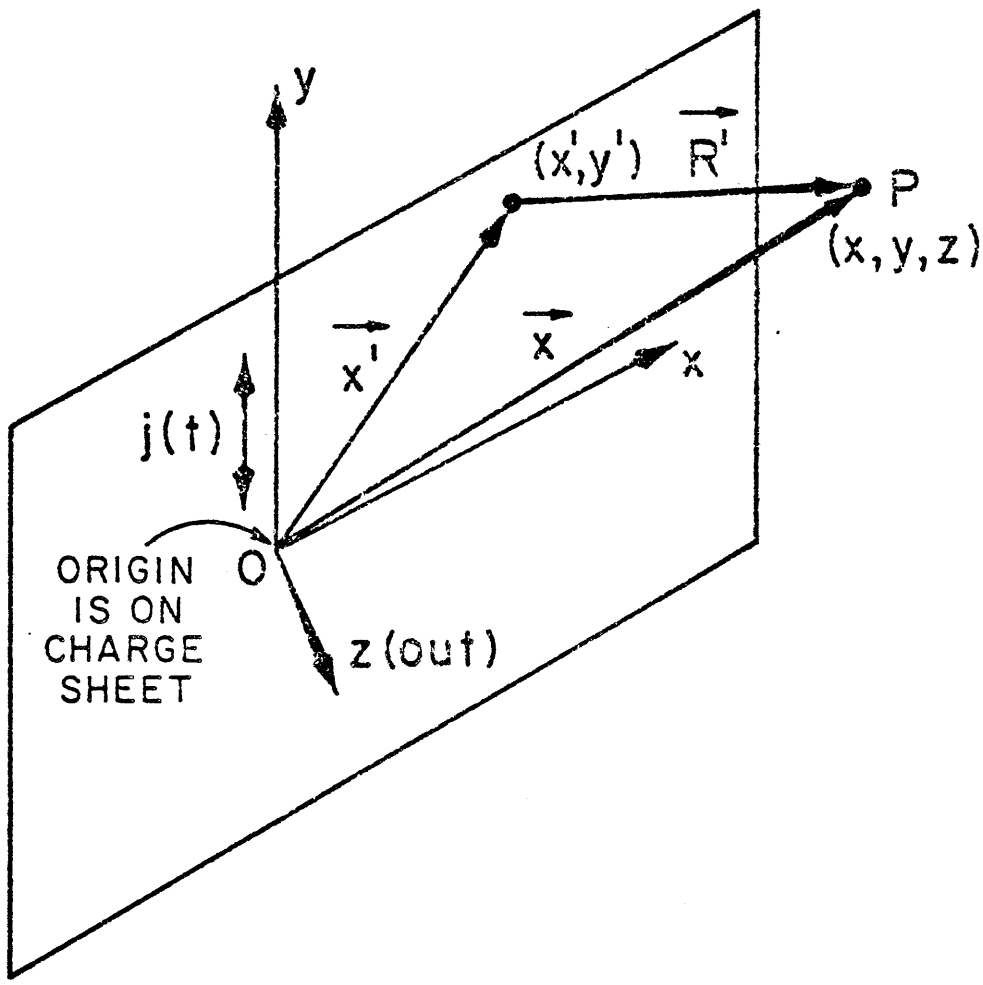
y
(x',y')
$\vec{R'}$
P
(x, y, z)
$\vec{x'}$
$\vec{x}$
x
j(t)
ORIGIN IS ON CHARGE SHEET
O
z (out)

The only non-zero component of $\vec{A}$ is

$$A_{\substack{y\\ret\\adv}}(\vec{x},t) = \frac{1}{c}\int_t\int_{x,y}\frac{j_o e^{i\omega t'}}{R'}\,\delta(t' \pm \frac{R'}{c} - t)dx'dy'dt'.$$

Since the sheet is infinite the result will be independent of x and y and the calculation can be simplified by placing the origin under the field point P. See Figure A-3. The delta function is zero unless $t' = t \mp \frac{R'}{c}$. The result is

$$\vec{A}_{\substack{ret\\adv}}(\vec{x},t) = \mp\frac{2\pi j_o i}{\omega}\, e^{i\omega(t \mp \frac{|z|}{c})}\,\hat{y}$$

which leads to the fields

$$\vec{E}_{\substack{ret\\adv}} = \mp\frac{2\pi j_o}{c}\, e^{i\omega(t \mp \frac{|z|}{c})}\,\hat{y}$$

and

$$\vec{B}_{\substack{ret\\adv}} = (\varepsilon)\frac{2\pi j_o}{c}\, e^{i\omega(t \mp \frac{|z|}{c})}\,\hat{x},$$

where

$$\varepsilon \equiv \begin{cases} +1, & z > 0 \\ -1, & z < 0. \end{cases}$$

Figure A-3. Simplification of the vector potential integral as made possible by symmetry.

$$\rho = \sqrt{R'^2 - z^2}$$

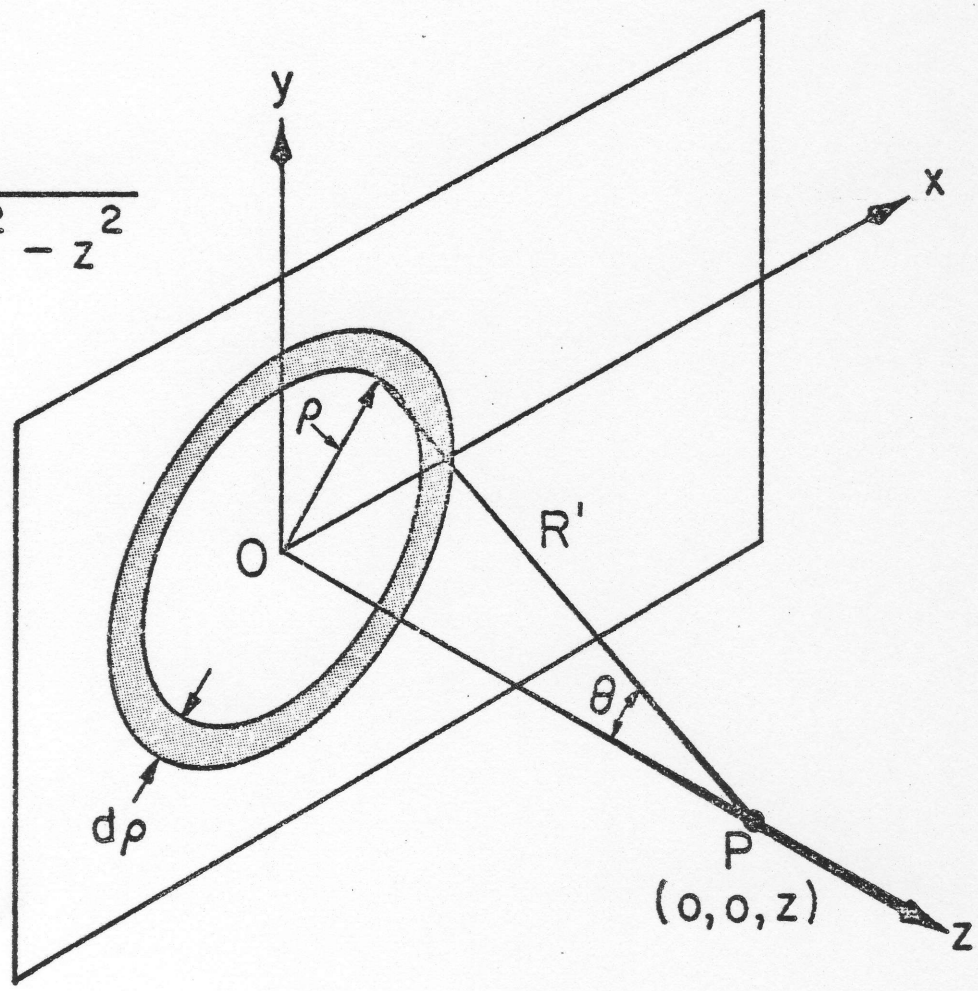

The direction of the energy flow is the direction of $(\vec{E} \times \vec{B})$. For the above two equations, then, retarded radiation carries energy away from the source and advanced radiation carries energy toward the source. In the presence of absorber the retarded or advanced nature of the net radiation present will depend in part on fields from stimulated charges in the absorber. Hence we must consider in detail the nature and placement of the absorbing material.

A.3 SYMMETRIC ABSORBER PLACEMENT

First we will consider the symmetric absorber configuration mentioned above and illustrated in Figure A-4. E(z), the net electric field, is given by

$$E(z) = \tfrac{1}{2}E_{\substack{i\\ret}}(z) + \tfrac{1}{2}E_{\substack{i\\adv}}(z)$$

$$+ \text{(retarded response of absorber charges)}$$

$$+ \text{(advanced response of absorber charges)}, \tag{A.1}$$

where $\tfrac{1}{2}E_{\substack{i\\ret}}(z)$ and $\tfrac{1}{2}E_{\substack{i\\adv}}(z)$ are the initial fields emanating from the current sheet source. These are

$$E_{\substack{i\\ret\\adv}}(z) = \mp \frac{2\pi j_o}{c} e^{i(\omega t \mp k|z|)}, \text{ where } k = \frac{2\pi}{\lambda} \text{ and } \omega = ck.$$

Figure A-4. Symmetric placement of absorber material

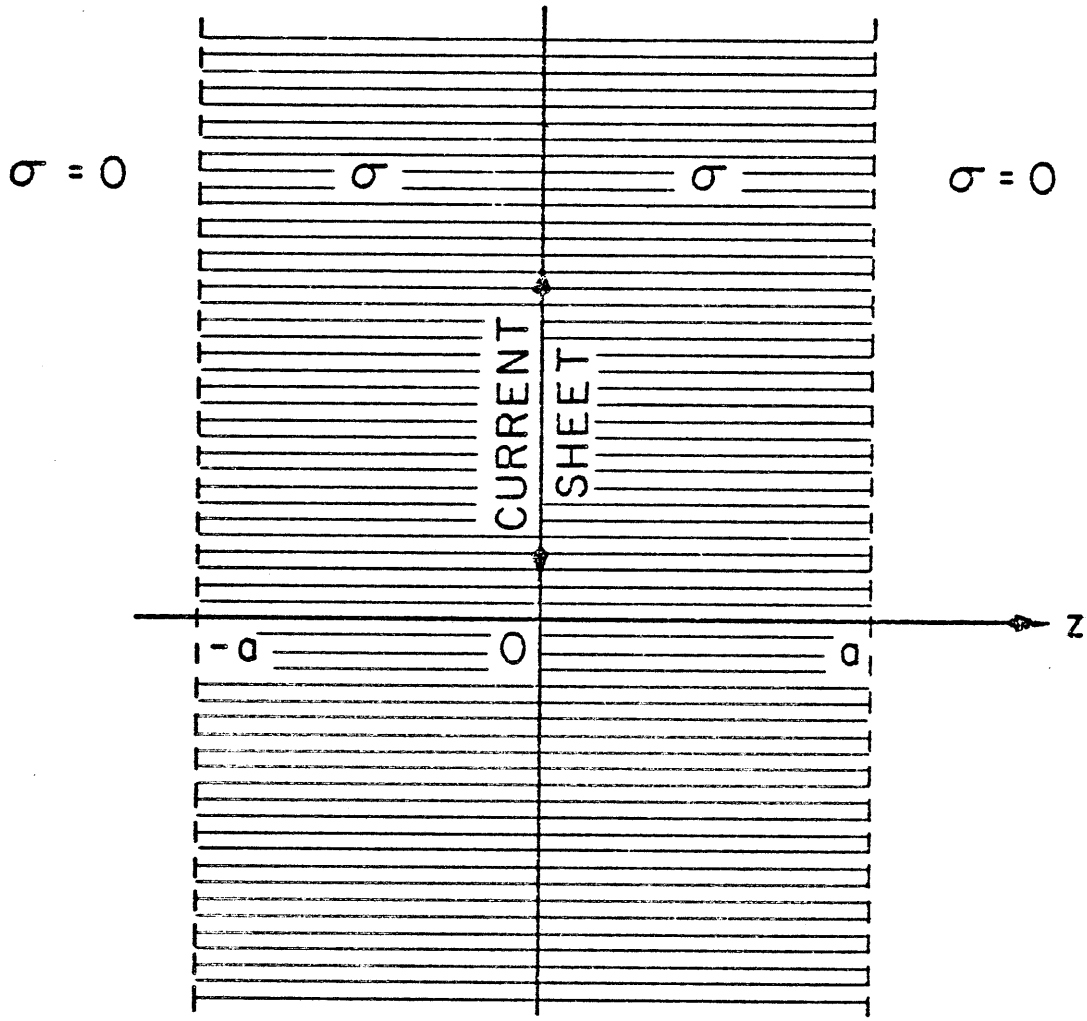
σ = 0
σ
σ
σ = 0
CURRENT
SHEET
z
-a
0
a

Retarded and advanced contributions to E(z), the field at z, each come from induced currents in three absorber regions: (-a,0), (0,z), and (z,a). See Figure A-5. Thus

$$\begin{bmatrix}\text{contribution to } E(z) \text{ from} \\ \text{retarded response of absorber}\end{bmatrix}$$

$$= \begin{bmatrix}\text{rightward moving retarded wave from } (-a,0)\end{bmatrix}$$
$$+ \begin{bmatrix}\text{rightward moving retarded wave from } (0,z)\end{bmatrix}$$
$$+ \begin{bmatrix}\text{leftward moving retarded wave from } (z,a)\end{bmatrix},$$

and

$$\begin{bmatrix}\text{contribution to } E(z) \text{ from} \\ \text{advanced response of absorber}\end{bmatrix}$$

$$= \begin{bmatrix}\text{leftward moving advanced wave from } (-a,0)\end{bmatrix}$$
$$+ \begin{bmatrix}\text{leftward moving advanced wave from } (0,z)\end{bmatrix}$$
$$+ \begin{bmatrix}\text{rightward moving advanced wave from } (z,a)\end{bmatrix}.$$

Then,

$$E(z) = \tfrac{1}{2}E_{\substack{i\\ret}}(z) + \tfrac{1}{2}\left[\int_{z'=-a}^{0} -\frac{2\pi}{c}\, j(z')e^{-ik(z-z')}dz'\right.$$

$$+ \int_{z'=0}^{z} -\frac{2\pi}{c} j(z')e^{-ik(z-z')}dz'$$

$$\left. + \int_{z'=z}^{a} -\frac{2\pi}{c} j(z')e^{+ik(z-z')}dz'\right]$$

Figure A-5. Induced current sheets such as dz contribute to E(z), the field at z.

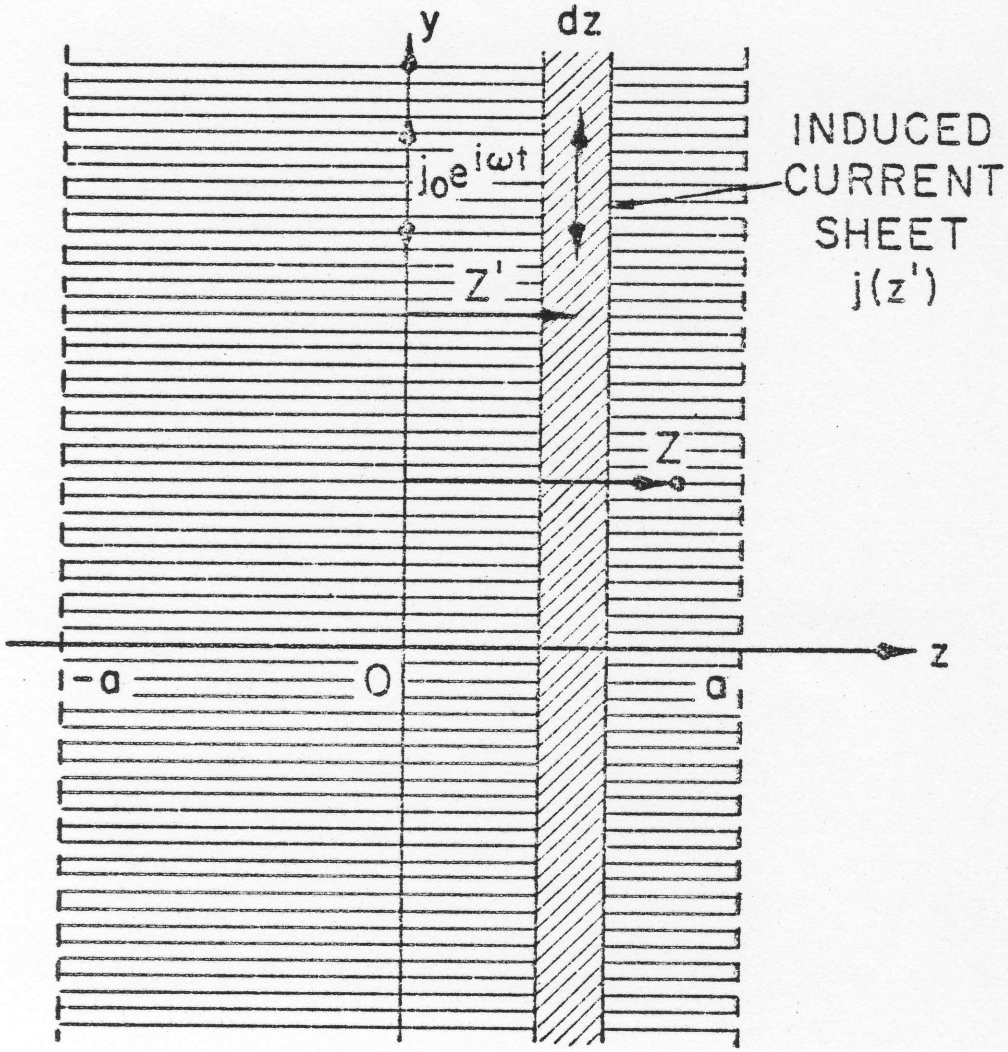
y
dz
$j_0 e^{i\omega t}$
INDUCED
CURRENT
SHEET
j(z')
Z'
Z
z
-a
0
a

$$+ \tfrac{1}{2}E_{\substack{i\\ adv}}(z) + \tfrac{1}{2}\left[\int_{z'=-a}^{o} + \frac{2\pi}{c}j(z')e^{+ik(z-z')}dz'\right.$$

$$+\int_{z'=0}^{z} + \frac{2\pi}{c}\, j(z')e^{+ik(z-z')}dz'$$

$$\left. +\int_{z'=z}^{a} + \frac{2\pi}{c}j(z')e^{-ik(z-z')}dz'\right].$$

We set $j(z) = \sigma E(z)$ and assume a solution of the form $E(z) = (Ae^{-\gamma|z|} + Be^{+\gamma|z|})e^{i\omega t}$, $|z| \leq a$.

The result can be written as a homogeneous equation with terms in $e^{-\gamma z}$, $e^{+\gamma z}$, e^{-ikz}, and e^{+ikz}. If this equation is to hold for all z, then the coefficients of each of these terms must vanish separately. This yields values of γ, A, and B as follows:

$$\gamma = \pm\, \gamma', \text{ where } \gamma' \equiv + \sqrt{\frac{4\pi i\sigma k}{c} - k^2}\,,$$ "+" indicating the root with $\mathrm{Re}\gamma' > 0$;

$$A = -\frac{2\pi j_o}{c}\,\frac{ik}{\gamma}\,\frac{e^{2\gamma a}\left(\dfrac{1 - \frac{\gamma}{k}\tan ka}{1 + \frac{\gamma}{k}\tan ka}\right)}{1 + e^{2\gamma a}\left(\dfrac{1 - \frac{\gamma}{k}\tan ka}{1 + \frac{\gamma}{k}\tan ka}\right)}\,;$$

$$B = + \frac{2\pi j_o}{c} \frac{ik}{\gamma} \frac{1}{1 + e^{2\gamma a}\left(\frac{1 - \frac{\gamma}{k}\tan ka}{1 + \frac{\gamma}{k}\tan ka}\right)} .$$

Thus we have found $E(z) = (Ae^{-\gamma|z|} + Be^{+\gamma|z|})e^{i\omega t}$ for $|z| \leq a$. We note that $B = A_{\gamma\to-\gamma}$ so that $E(z)_{\gamma=+\gamma'} = E(z)_{\gamma=-\gamma'}$; the choice of sign in γ' is unimportant.

We can find $E(z)$ for $|z| > a$ from the continuity of the parallel components of E and H across the boundary at $z = \pm a$. The result is

$$E(z) = \left[\frac{2e^{\gamma a}}{(\cos ka + \frac{\gamma}{k}\sin ka) + e^{2\gamma a}(\cos ka - \frac{\gamma}{k}\sin ka)}\right]$$

$$\times \left[\tfrac{1}{2}E_{i_{ret}}(z) + \tfrac{1}{2}E_{i_{adv}}(z)\right], \quad |z| \geq a.$$

The quantity in the first brackets can be viewed as an attenuation and phase shift factor which, as $\overset{\alpha}{A} \to 0$, approaches 1. For large a it is proportional to $e^{-\gamma a}$. Since the retarded and advanced fields have the same coefficients here, there is no net energy flow into empty space beyond the absorber. This is an expected result. Again $\left[E(z)\right]_{\gamma=+\gamma'} = \left[E(z)\right]_{\gamma=-\gamma'}$.

These results for $|z| \leq a$ and $|z| > a$ indicate that in the case of complete absorption ($a \to \infty$) the solution for all z is $E(z) = -\frac{2\pi j_o}{c} \frac{ik}{\gamma'} e^{-\gamma'|z|} e^{i\omega t}$. Since $\sigma > 0$ and $\gamma' = +\sqrt{\frac{4\pi i\sigma k}{c} - k^2}$ where $\mathrm{Re}\gamma' > 0$, we must have $\mathrm{Im}\gamma' > 0$. This root is illustrated in the diagram.

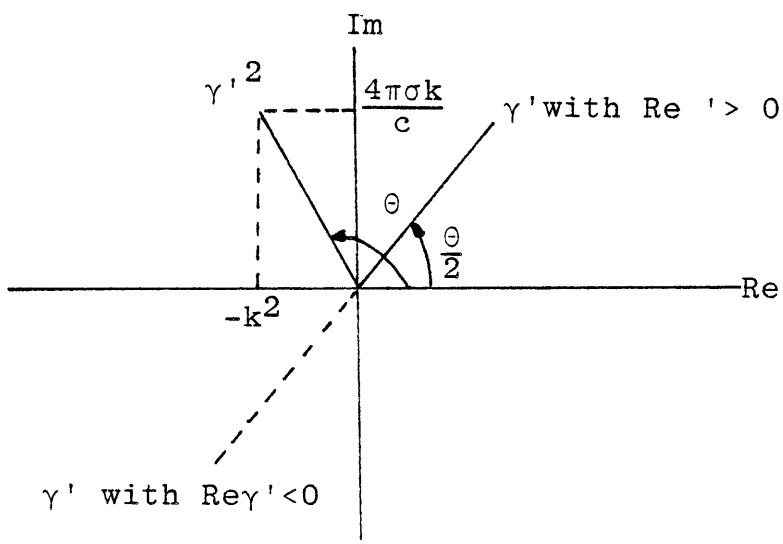

$\mathrm{Im}\gamma' > 0$ corresponds to a wave moving away from the charge sheet, a characteristic of a retarded wave. This is the same solution one would get from the purely retarded theory. Thus the absorber theory of radiation, in the circumstance of complete absorption, reproduces the result of the purely retarded theory as is expected.

However in this absorber configuration ($a \to \infty$) the absorber theory of radiation was equally expected to lead to a mathematically valid purely advanced solution, a solution which Wheeler and Feynman throw out on thermodynamic grounds (rather than on grounds of causality violation, as in conventional retarded theory). Then, how is it we were led to just one solution, $E(z) = -\frac{2\pi j_o}{c}\frac{ik}{\gamma'}e^{-\gamma'|z|}e^{i\omega t}$, a solution with retarded characteristics? Evidently our choice of $\sigma > 0$ in our model of an absorber is responsible. Positive resistivity characterizes a thermodynamic process where energy is dissipated in time.

Thus in this model of an absorber we expect a solution with advanced characteristics when $\sigma < 0$. With $\sigma < 0$ and $\mathrm{Re}\gamma' > 0$ we must have $\mathrm{Im}\gamma' < 0$ as is illustrated in the diagram:

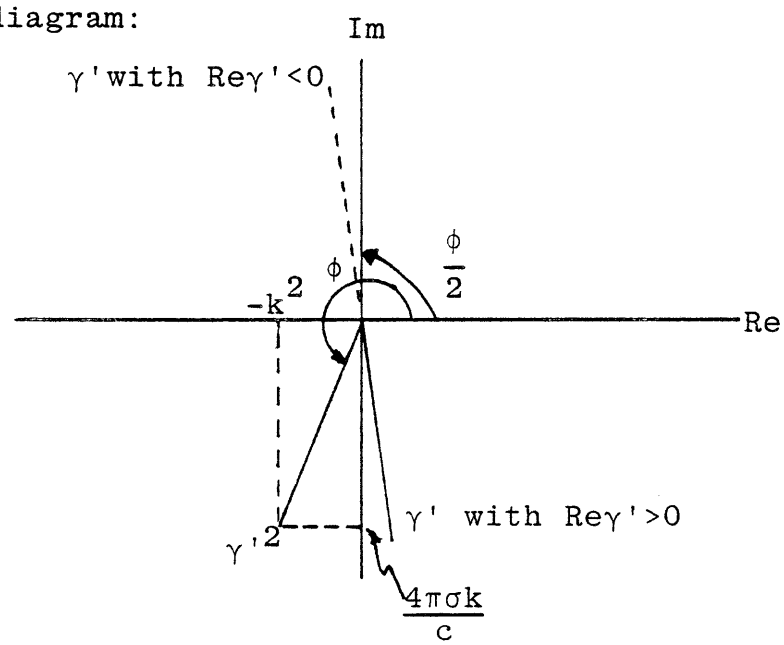

$\mathrm{Im}\gamma' < 0$ gives an incoming wave, a characteristic of an advanced field, as expected.

We have seen, then, that in our model of an absorber the electromagnetic arrow of time follows the sign of the conductivity of the absorber (the thermodynamic arrow of time).

A.4 ENERGY FLOW

Energy flow was calculated in the case $a \to \infty$, an infinitely thick absorbing medium. In this case $A = -\frac{2\pi j_o}{c}\frac{ik}{\gamma}$ and $B = 0$ so that $E(z) = -\frac{2\pi j_o}{c}\frac{ik}{\gamma'}e^{-\gamma'|z|}e^{i\omega t}$.

We calculate the power per unit area of current sheet in three different ways, all with the same result: the total joule heating throughout the absorbing medium; the energy flow thru a cross-sectional area at the current sheet (Poynting vector); and the rate at which work must be done against the radiation reaction force.

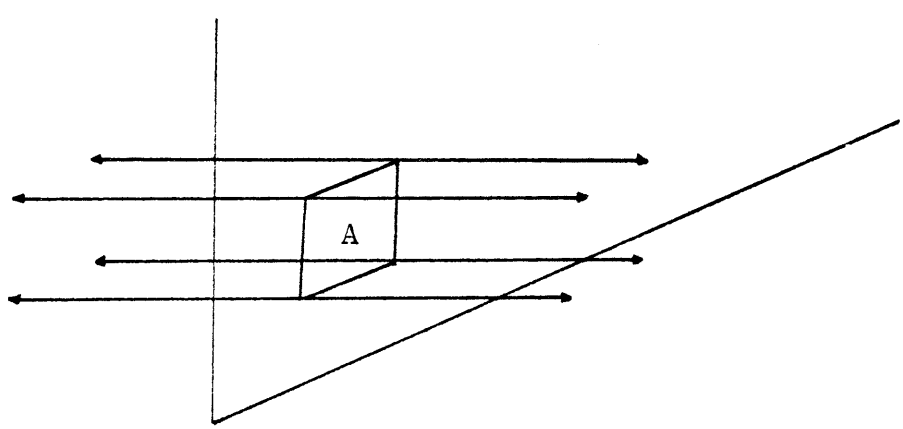

The joule heating is

$$P = \int_{vol} \vec{j}\cdot\vec{E}\, d\tau$$

$$= \int_{vol} \sigma E^2\, d\tau.$$

The time-average power emitted in the $\pm$ z direction from a unit area is

$$\frac{\overline{P}}{A} = \int_{z=-\infty}^{\infty} \sigma \overline{E^2}\, dz$$

$$= 2\,\sigma \int_{z=0}^{\infty} \overline{(\mathrm{Re}E)^2} dz.$$

But $\overline{(\mathrm{Re}E)^2} = \frac{1}{2}EE^*$ so that $\frac{\overline{P}}{A} = \sigma \int_{z=0}^{\infty} EE^*\, dz$. The result is

$$\frac{\overline{P}}{A} = \frac{\sqrt{2}\pi j_o^{\,2}}{2c} \frac{\sqrt{1 + \left[1 + (\frac{4\pi\sigma}{kc})^2\right]^{\frac{1}{2}}}}{\left[1 + (\frac{4\pi\sigma}{kc})^2\right]^{\frac{1}{2}}} .$$

The energy flow is given by

$$\vec{S} = \frac{c}{4\pi} (\vec{E} \times \vec{H})_{z=0}.$$

The time average is $\vec{S} = \frac{c}{8\pi} \mathrm{Re}(\vec{E} \times \vec{B}^*)_{z=0}$. According to Jackson (1975, Equation 7.75),

$$\vec{H} = \sqrt{\frac{\varepsilon}{\mu}} \left[1 + (\frac{4\pi\sigma}{\omega\varepsilon})^2\right]^{\frac{1}{4}} e^{i\phi} \hat{n} \times \vec{E},$$

where

$$\phi = \tfrac{1}{2}\tan^{-1}(\frac{4\pi\sigma}{\omega\varepsilon}).$$

Since a plane wave in a conducting medium is transverse (Marion, 1965, page 143),

$$\hat{n} \times \vec{E} = - E\hat{x}$$

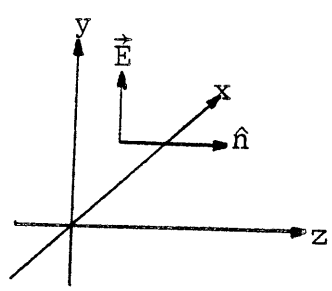

We have $\varepsilon = 1$, $\mu = 1$, and $k = \sqrt{\mu\varepsilon}\,\frac{\omega}{c}$, therefore $\vec{B} = - \left[1 + (\frac{4\pi\sigma}{kc})^2\right]^{\frac{1}{4}} e^{i\phi} E\hat{x}$ where $\phi = \frac{1}{2}\tan^{-1}(\frac{4\pi\sigma}{kc})$. This leads to a value of $\vec{S}$ which represents the energy flow in only one direction. Energy flows in both directions (+z and -z). The result is

$$\vec{S}_{z=0} = \frac{\sqrt{2}\pi j_o^{\,2}}{4c} \frac{\sqrt{1 + \left[1 + (\frac{4\pi\sigma}{kc})^2\right]^{\frac{1}{2}}}}{\left[1 + (\frac{4\pi\sigma}{kc})^2\right]^{\frac{1}{2}}} (\hat{z})$$

with an equal power flowing in the $-\hat{z}$ direction.

In the Wheeler-Feynman formulation fields of radiation reaction which act on a given particle arise only from other particles. Thus, in the steady state situation, we let

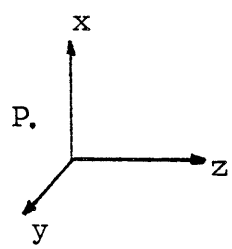

$E_{RR} \equiv$ field at a charge P on the charge sheet due to all other charges (on the sheet and in the absorber).

$$E_{RR} = \left[\left(\tfrac{1}{2} E_{i_{adv}} \right)_{\substack{\text{at P, due to} \\ \text{all other} \\ \text{charges on} \\ \text{source} \\ \text{sheet}}} + \left(\tfrac{1}{2} E_{\substack{\text{advanced} \\ \text{response} \\ \text{of absorber}}} \right)_{\text{at P}} \right]$$

$$+ [\text{same for retarded}].$$

But P is infinitesimal, so the field at P is the field anywhere on the z = 0 plane.

Thus

$$E_{RR} = \left[\left(\tfrac{1}{2}E_{i\,adv} \right)_{\substack{\text{at } z=0 \text{ plane} \\ \text{due to all} \\ \text{charges on} \\ \text{source sheet}}} + \left(\tfrac{1}{2}E_{\substack{adv \\ response \\ of\ absorber}} \right)_{z=0} \right]$$

$$+ \left[\text{same for retarded} \right]$$

$$= \left[(\tfrac{1}{2}E_{ret})_{z=0} \right] + \left[(\tfrac{1}{2}E_{ret})_{z=0} \right]$$

$$= - \frac{2\pi j_o}{c} \frac{ik}{\gamma'} e^{-\gamma'|z|} e^{i\omega t} \Big|_{z=0}$$

$$= - \frac{2\pi j_o}{c} \frac{ik}{\gamma'} e^{i\omega t}.$$

The power required to overcome this radiation reaction field is

$$\frac{P}{A} = (j_o e^{i\omega t}) E_{RR}.$$

Then

$$\frac{\overline{P}}{A} = \tfrac{1}{2}\mathrm{Re} \left[(j_o e^{i\omega t})(E_{RR}^*) \right] \qquad (A.2)$$

which leads to

$$\frac{\overline{P}}{A} = \frac{\sqrt{2}\pi j_o^2}{2c} \frac{\sqrt{1 + \left[1 + (\frac{4\pi\sigma}{ck})^2\right]^{\frac{1}{2}}}}{\left[1 + (\frac{4\pi\sigma}{ck})^2\right]^{\frac{1}{2}}}, \text{ as before.}$$

For small σ, $\frac{\overline{P}}{A} = \frac{\pi j_o^2}{c}$, a result independent of σ. This represents absorption within the charge sheet itself: the power required to move charges through the fields ($E_i(z=0)$) of other charges on the sheet. This result can be obtained from Equation A.2 by using $E_i(z=0)$ as E_{rr}.

For large σ, however, $\frac{\overline{P}}{A} = \frac{1}{4}(\frac{\pi j_o^2}{c}) \sqrt{\frac{2kc}{\pi\sigma}}$. The $\frac{1}{\sqrt{\sigma}}$ dependence of energy flow may be associated with the large reflectivity of a medium characterized by large σ. In fact, it can be shown (Jackson, 1975, problem 7.4) that for large σ the fractional transmission, T, into a conducting medium (and therefore absorption by the medium) is given by

$$T = \sqrt{\frac{2kc}{\pi\sigma}} \quad , \text{ large } \sigma.$$

A.5 ASYMMETRIC ABSORBER PLACEMENT

Finally, we consider the asymmetric absorber configuration mentioned earlier and illustrated in Figure A-6.

We use the same procedure (Equation A.1) as in our first example to find E(z) within the absorber:

Figure A-6. Induced current sheet dz contributes to the field at z.

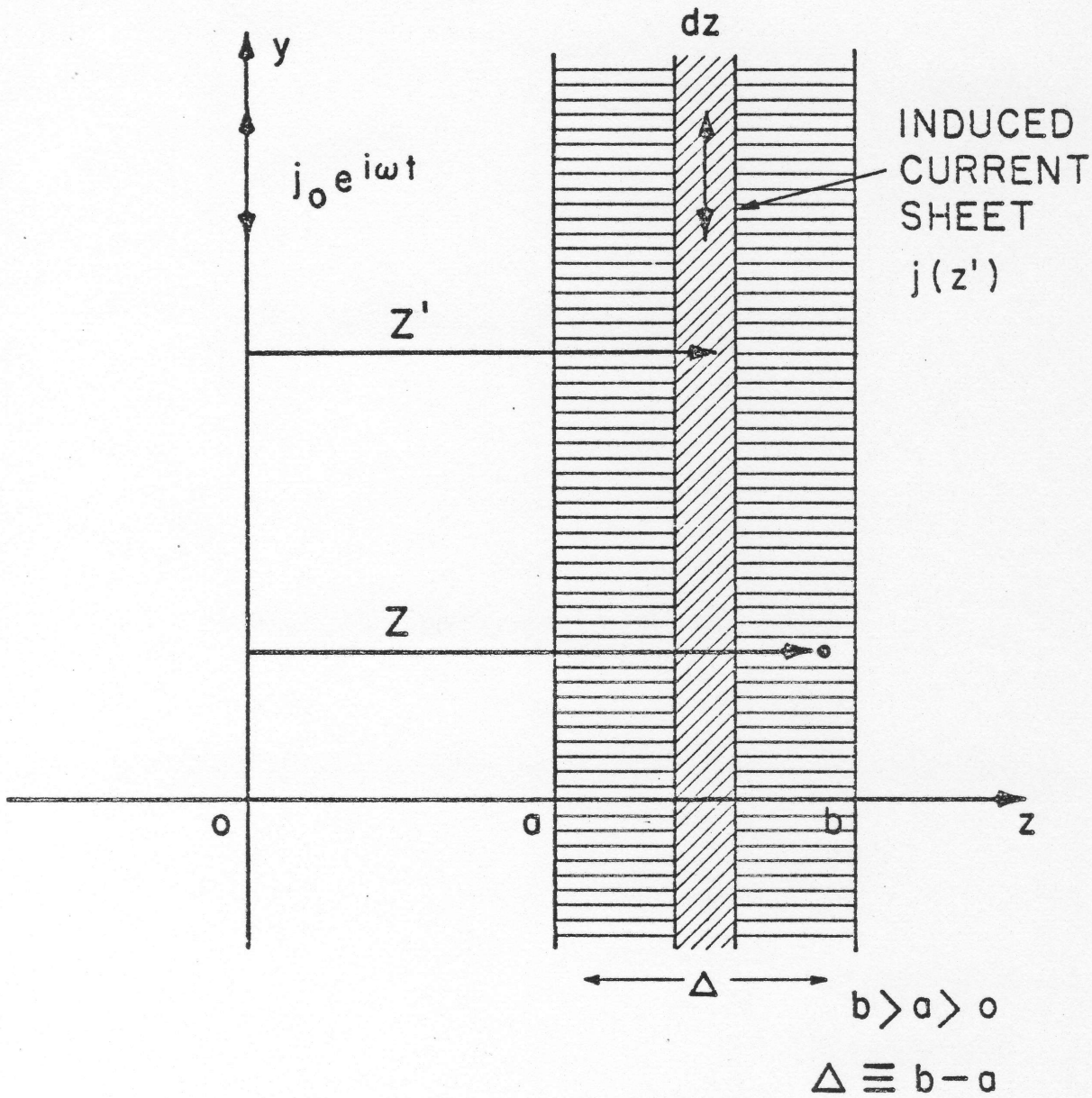
dz
y
$j_o e^{i\omega t}$
INDUCED
CURRENT
SHEET
j(z')
Z'
Z
o
a
b
z
Δ
b > a > o
Δ ≡ b − a

$$E(z) = \tfrac{1}{2}E_{\substack{i\\ret}}(z) + \tfrac{1}{2}\left[\int_{z'=a}^{z} - \frac{2\pi}{c}\, j(z')e^{-ik(z-z')}dz' + \int_{z'=z}^{b} - \frac{2\pi}{c}\, j(z')e^{+ik(z-z')}dz'\right]$$

$$+ \tfrac{1}{2}E_{\substack{i\\adv}}(z) + \tfrac{1}{2}\left[\int_{z'=a}^{z} + \frac{2\pi}{c}\, j(z')e^{+ik(z-z')}dz' + \int_{z'=z}^{b} + \frac{2\pi}{c}\, j(z')e^{-ik(z-z')}dz'\right].$$

Again, we set $j(z) = \sigma E(z)$ and $E(z) = (Ae^{-\gamma z} + Be^{+\gamma z})e^{i\omega t}$, $a \leq z \leq b$. This leads to $\gamma = \pm\gamma'$, where $\gamma' \equiv +\sqrt{\frac{4\pi i\sigma k}{c} - k^2}$, "+" indicating the root with Re $\gamma' > 0$,

$$A = \frac{-2\pi j_o i e^{\gamma a}\left[e^{-\gamma\Delta}(k\cos ka - \gamma\sin ka) + k\cos k(a+\Delta) - \gamma\sin k(a+\Delta)\right]}{c\gamma\left[2e^{-\gamma\Delta} + (1+e^{-2\gamma\Delta})\cos k\Delta - (1-e^{-2\gamma\Delta})\left(\frac{\gamma^2-k^2}{2\gamma k}\right)\sin k\Delta\right]},$$

and

$$B = \frac{+2\pi j_o i e^{-\gamma a}e^{-2\gamma\Delta}\left[e^{+\gamma\Delta}(k\cos ka + \gamma\sin ka) + k\cos k(a+\Delta) + \gamma\sin k(a+\Delta)\right]}{c\gamma\left[2e^{-\gamma\Delta} + (1+e^{-2\gamma\Delta})\cos k\Delta - (1-e^{-2\gamma\Delta})\left(\frac{\gamma^2-k^2}{2\gamma k}\right)\sin k\Delta\right]},$$

where $\Delta \equiv (b-a)$.

Thus we have found $E(z) = (Ae^{-\gamma z} + Be^{+\gamma z})e^{i\omega t}$ for $a \leq z \leq b$. We note, as in the case of symmetric absorber distribution, that $B = A_{\gamma \to -\gamma}$ so that $\left[E(z)\right]_{\gamma = +\gamma'} = \left[E(z)\right]_{\gamma = -\gamma'}$.

If Δ is large and $\mathrm{Re}\gamma > 0$, we have, for $a \leq z \leq b$,

$$E(z) = 2\pi j_o i e^{i\omega t}$$

$$\times \frac{\left(\left[\gamma \sin k(a+\Delta) - k \cos k(a+\Delta)\right]e^{-\gamma(z-a)} + \left[\gamma \sin ka + k \cos ka\right]e^{-\gamma(b-z)}\right)}{c\gamma\left[\cos k\Delta - \frac{\gamma^2 - k^2}{2\gamma k} \sin k\Delta\right]}.$$

This is small except within the skin depth of the inner and outer faces, at $z = a$ and $z = b$ respectively. The amplitudes at these faces seem to vary trigonometrically with the number of free-space wavelengths (modulo 1) separating the faces from the source sheet and from each other. Near the absorber's inner and outer faces the expression for $E(z)$ is dominated respectively by its terms in $e^{i\omega t - \gamma z}$ and $e^{i\omega t + \gamma z}$, outgoing and incoming waves. Although these waves move in directions respectively associated with retarded and advanced radiation their steady state nature does not allow their immediate identification as such.

We are, however, in a position to calculate the distribution of steady state effects on the outer and

inner faces of the absorber. As in Section 2.6 we are interested in the energy. The distribution of effects within the absorber, in terms of energy, is proportional to $E(z)E^*(z)$, $a \leq z \leq b$. In our case, that of large Δ,

$$E(z)E^*(z) = \frac{(2\pi j_o \sin kR)^2}{c^2[1-\cos^2 kR \cos^2 k(b-a-R)]} \times$$

$$\left([\sin^2 kb + \sin^2 k(b-R)]\, e^{-2(\mathrm{Re}\gamma)(z-a)} + [\sin^2 ka + \sin^2 k(a+R)]\, e^{-2(\mathrm{Re}\gamma)(b-z)} \right),$$

where $kR \equiv \tan^{-1} \sqrt{\frac{2}{\alpha-1}}$ with $\alpha \equiv \left[(\frac{4\pi\sigma}{kc})^2 + 1\right]^{\frac{1}{2}}$ so that $\gamma\gamma^* = \alpha k^2$ and $\mathrm{Re}\,\gamma = k\sqrt{\frac{\alpha-1}{2}}$. It can be seen that the skin depth is the same at the two faces, $z = a$ and $z = b$. Then, outer face effects represent a fraction of total inner and outer face effects given by

$$f_{\substack{\text{steady}\\ \text{state}}} = \frac{E(b)E^*(b)}{E(a)E^*(a) + E(b)E^*(b)} ;$$

$$f_{\substack{\text{steady}\\ \text{state}}} = \frac{\sin^2 ka + \sin^2 k(a+R)}{\sin^2 ka + \sin^2 k(a+R) + \sin^2 k(a+\Delta) + \sin^2 k(a+\Delta-R)}.$$

This expression for f applies to the absorber geometry of Figure A-6, with large Δ, and in the steady state. $f = \frac{1}{2}$ when $k\Delta = n\pi - 2ka$ and when $k\Delta = m\pi + kR$, for integral n and m.

The curves in Figures A-7 and A-8 display f as a function of $k\Delta$ for five values of ka. α is 4 in Figure A-7 and 50 in Figure A-8. f has a period of π radians in ka and in $k\Delta$.

Thus instead of the range of solutions (as discussed in Section 2.6) differing in spatial distribution of effects, our specific absorber model leads to a definite distribution of effects for each specific geometry.

Figure A-7. Fraction, f, of outer face effect versus absorber thickness, $k\Delta$ ($k\Delta$ is the number of radians corresponding to the number of free-space wavelengths in the thickness, modulo π radians), for large absorber thickness. Curves are shown for five source sheet-absorber separations. $\alpha = 4$.

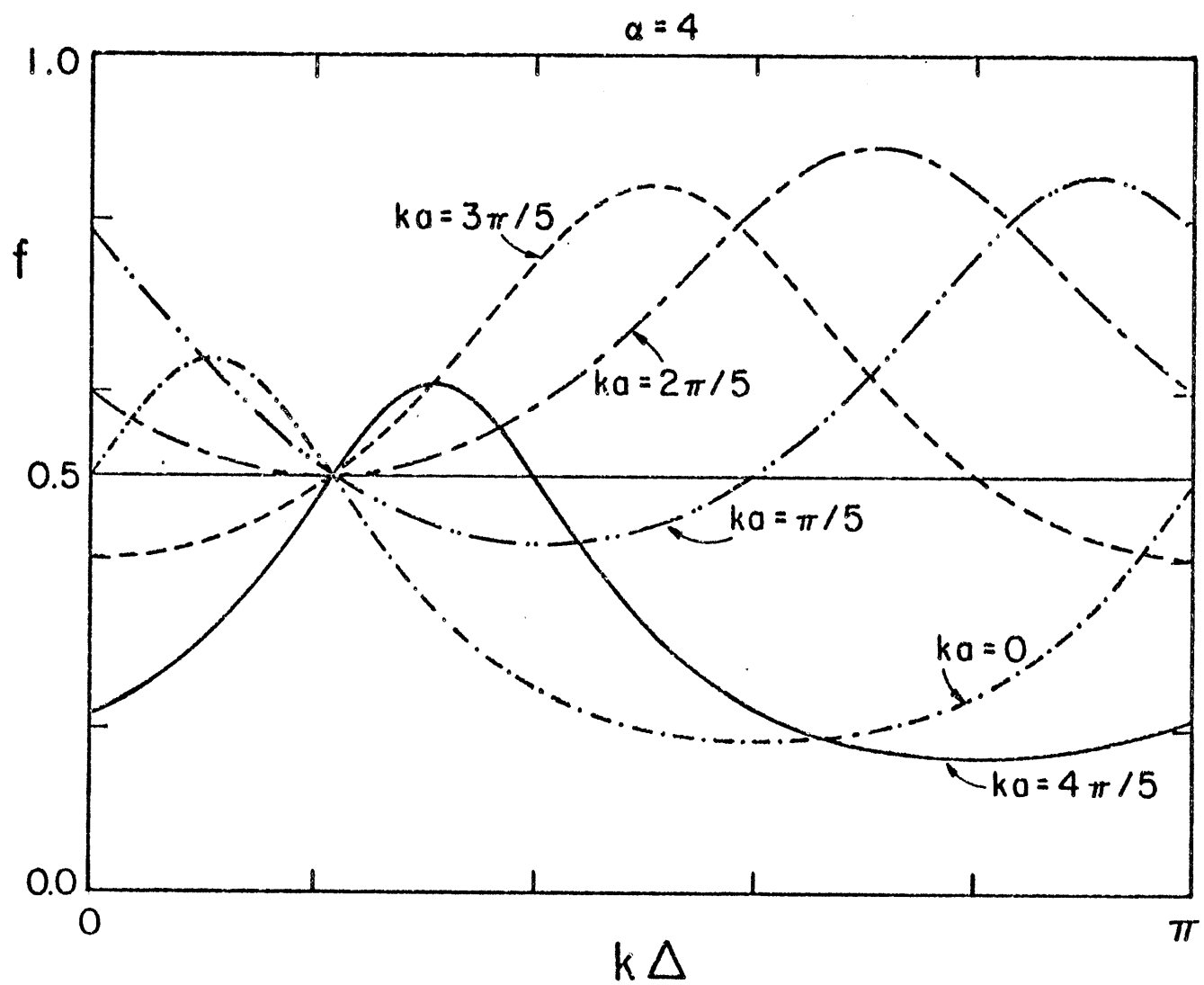
α = 4
1.0
0.5
0.0
f
0
π
kΔ
ka = 3π/5
ka = 2π/5
ka = π/5
ka = 0
ka = 4π/5

Figure A-8. Fraction, f, of outer face effect versus absorber thickness, $k\Delta$ ($k\Delta$ is the number of radians corresponding to the number of free-space wavelengths in the thickness, modulo π radians), for large absorber thickness. Curves are shown for five source sheet-absorber separations. $\alpha = 50$.

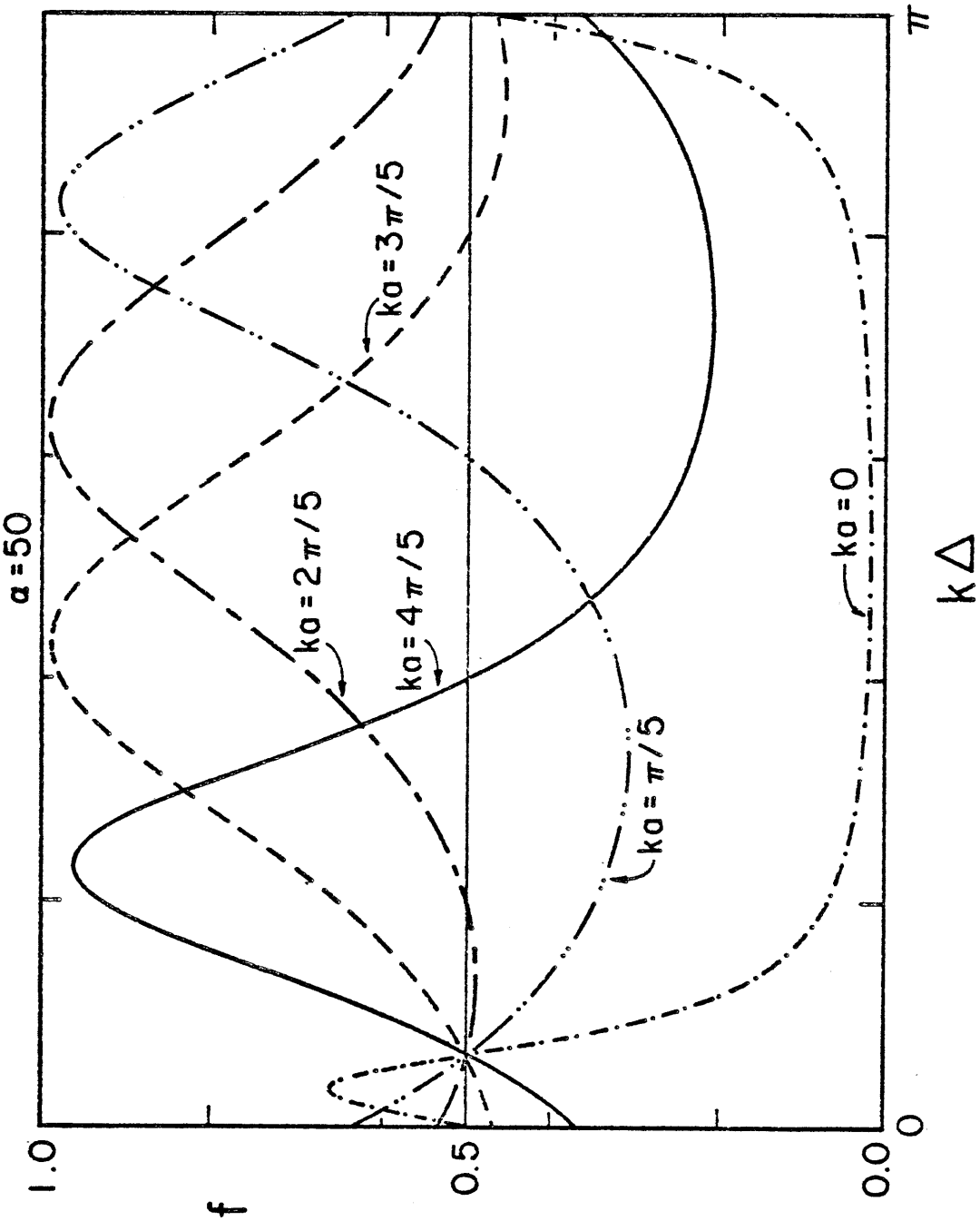
a=50
ka=3π/5
ka=2π/5
ka=4π/5
ka=π/5
ka=0
1.0
0.5
0.0
f
0
π
kΔ

Appendix B

A NOTE IN THE ABSORBER THEORY OF RADIATION

In the case of complete absorption we saw (in Chapter 2) that the "full retarded" self-consistent solution is composed of equal parts of retarded radiation from "source" charges and advanced radiation from "absorber" charges. This full retarded solution is said to correspond to experience because the electromagnetic activity at the "source" occurs before the electromagnetic activity at the "absorber." Wheeler and Feynman rule out the mathematically equally valid full advanced solution on the basis of its small statistical mechanical probability. Thus we are left with retarded radiation as the mechanism by which "sources" lose energy to "absorbers."

We note that in a given system thermodynamics specifies the direction in which the electromagnetic energy flows. We need not, however, allow thermodynamics to dictate whether we describe that radiation as retarded or advanced.

It is conventional to designate the relatively hot object as "source" and the relatively cool object as "absorber." Retarded radiation then flows from "source" to "absorber."

However, there is no electrodynamic basis for these designations. We could equally call the cool object the "source" and the hot object the "absorber" and describe the same flow of energy in terms of advanced radiation. (Here statistical mechanics would rule out retarded radiation from the (cool) "source".)

From this viewpoint it is probably most convenient to describe normally observed radiation as an equally retarded and advanced electromagnetic interaction between charges in which energy flows from hot to cold. (A more precise definition of relatively hot and cold objects might come with use of the concept of "brightness temperature." The brightness temperature of an object is the temperature a blackbody must have in order to match, at the frequency of interest, the power radiated by the object.)